50272-101

REPORT DOCUMENTATION PAGE	1. REPORT NO. GRI 91/0219	2.	3. Recipient's Accession No.

4. Title and Subtitle

LNG Vapor Barrier and Obstacle Evaluation:
Wind Tunnel Simulation of 1987 Falcon Spill Series, Final Report

5. Report Date March, 1991

6.

7. Author(s)

Seong-Hee Shin, Robert N. Meroney and David E. Neff

8. Performing Organization Rept. No. CER90-91SHS-RNM-DEN-1

9. Performing Organization Name and Address

Fluid Mechanics and Wind Engineering Program
Civil Engineering Department
Colorado State University
Fort Collins, Colorado 80523

10. Project/Task/Work Unit No. N00014-88-K-0029

11. Contract(C) or Grant(G) No.

(C)

(G)

12. Sponsoring Organization Name and Address

Gas Research Institute
8600 West Bryn Mawr Avenue
Chicago, Illinois 60613

13. Type of Report & Period Covered Final Report

14.

15. Supplementary Notes

16. Abstract (Limit: 200 words)

Measurements of the behavior of simulated liquefied natural gas clouds dispersing over small-scale model placed in environmental wind tunnels permits evaluations of the fluid physics of dense cloud movement and dispersion in a controlled environments. A large data base on the interaction of simulated LNG plumes with the Falcon test configuration of vapor barrier fences and vortex generators was obtained.

The purpose of the reported test program is to provide post-field-spill wind tunnel experiments to augment the LNG Vapor Fence Field Program data obtained during the Falcon Test Series in 1987. The goal of the program is to determine the probable response of a dense LNG Vapor cloud to vortex inducer obstacles and fences, examine the sensitivity of results to various scaling arguments which might augment limit, or extend the value of the field and wind-tunnel tests, and identify important details of the spill behavior which were not predicted during the pretest planning phase.

17. Document Analysis a. Descriptors

b. Identifiers/Open-Ended Terms

c. COSATI Field/Group

18. Availability Statement:	19. Security Class (This Report)	21. No. of Pages
Distribution Unlimited	Unclassified	138
	20. Security Class (This Page) Unclassified	22. Price

(See ANSI-Z39.18) *See Instructions on Reverse*

OPTIONAL FORM 272 (4-77)
(Formerly NTIS-35)
Department of Commerce

GRI-91/0219

LNG VAPOR BARRIER AND OBSTACLE EVALUATION: WIND-TUNNEL SIMULATION OF 1987 FALCON SPILL SERIES

FINAL REPORT
(July 1987 - February 1991)

Prepared by

SEONG-HEE SHIN
ROBERT N. MERONEY
DAVID E. NEFF

GRI-91/0219

LNG VAPOR BARRIER AND OBSTACLE EVALUATION: WIND-TUNNEL SIMULATION OF 1987 FALCON SPILL SERIES

FINAL REPORT
(July 1987 - February 1991)

Prepared by

Seong-Hee Shin, Robert N. Meroney, and David Neff

Fluid Mechanics and Wind Engineering Program
Department of Civil Engineering
Colorado State University
Fort Collins, Colorado 80523

CER90-91SHS-RNM-DEN-11

for

GAS RESEARCH INSTITUTE

Contract No. N00014-88-K-0029

GRI Project Manager
Ted Williams
Environment and Safety Research

March, 1991

GRI DISCLAIMER

LEGAL NOTICE This report was prepared by Colorado State University as an account of work sponsored by the Gas Research Institute (GRI). Neither GRI, members of GRI, nor any person acting on behalf of either:

a. Makes any warranty or representation, express or implied, with respect to the accuracy, completeness, or usefulness of the information contained in this report, or that the use of any apparatus, method or process disclosed in this report may not infringe privately owned rights; or
b. Assumes any liability with respect to the use of, or for damages resulting from the use of, any information, apparatus, method, or process disclosed in this report.

RESEARCH SUMMARY

Title	LNG Vapor Barrier and Obstacle Evaluation: Wind-Tunnel Simulation of 1987 Falcon Spill Series, Final Report
	Accession Code: GRI-91/0219
Contractor	Civil Engineering Department Colorado State University Fort Collins, Colorado 80523
Principal Investigator	Robert N. Meroney
Report Period	July 1987 - February 1991 Final Report
Objective	The purpose of the reported test program is to provide post-field-spill wind-tunnel experiments to augment the LNG Vapor Fence Field Program data obtained during the Falcon Test Series in 1987. The goal of the program is to determine the probable response of a dense LNG vapor cloud to vortex inducer obstacles and fences, examine the sensitivity of results to various scaling arguments which might augment, limit, or extend the value of the field and wind-tunnel tests, and identify important details of the spill behavior which were not predicted during the pretest planning phase.
Technical Perspective	A liquefied natural gas (LNG) spill would result in a cold LNG vapor plume, remaining negatively buoyant for a long period of time. The LNG plume could be diluted utilizing passive systems such as a vapor barrier fence or a vortex generator at or near the LNG spill location. Measurements of the behavior of simulated liquefied natural clouds dispersing over small-scale models placed in environmental wind tunnels permits evaluations of the fluid physics of dense cloud movement and dispersion in a controlled environment. An evaluation of scaling arguments and limitations to laboratory testing may be obtained by pre- and post-simulation of a documented field scale spill of LNG such as the 1987 Falcon LNG Spill Tests.
Results	The wind-tunnel experiments included replication of Falcon 2 through 5 at simulated scales of 1:50, 1:100, 1:150 and 1:250. In addition some tests were performed with exaggerated density for the simulation gases, additional wind approach angles, and source release conditions. Data were analyzed statistically using surface pattern comparisons, performance measures, and direct comparison methods. Results showed wind-tunnel model predictions of gas dispersion well within the accuracy required for hazard site evaluation. Model accuracies improved as the model size increased and distorted density simulant gas was used. Comparisons of field data and wind-tunnel data agreed well within ± 20 percent.

Technical Approach

Wind-tunnel tests were performed in the Environmental Wind-Tunnel at Colorado State University to simulate the micrometeorological and source conditions that occurred at the Nevada test site during Falcon Tests 2, 3, 4, and 5. Approach wind flow conditions were carefully adjusted to simulate the characteristic surface roughness and consequent wind and turbulence profiles observed at the Nevada test site. The fences and vortex generator of various sized were constructed from sheet metal, the model source-spider and spill-pond-plenum were designed to reproduce concentration time histories measured within the vapor fence. Each test was replicated up to five times while concentration time series were measured over a distributed grid within and outside the vapor barrier fence. Flow visualization was also used to document model spill behavior on TV tape. Data from wind-tunnel tests were analyzed using surface pattern comparisons, performance measures and direct comparison methods.

Project Implications

This study demonstrates, once again, the potential of wind-tunnel modelling methods for LNG vapor dispersion simulation and hazard evaluation. As with earlier research sponsored by GRI at Colorado State University, this study shows that wind-tunnel simulations can account for vapor dilution and detention effects from a wide variety of structures and site configurations. Also, wind-tunnel approaches can be used to cost-effectively examine design alternatives such as installation of vapor fences and other hazard mitigation approaches. While some uncertainties persist about the full range of application of wind-tunnels to LNG vapor dispersion (e.g., very low wind speed cases), it is clear that wind-tunnel approaches should receive greater attention by regulators and safety personnel in evaluating heavy gas dispersion hazards.

GRI Project Manager
Ted Williams
Environment and Safety Research

ACKNOWLEDGEMENTS

The authors acknowledge the financial support and management guidance provided by the Gas Research Institute. Mr. Ted Williams and the GRI safety committee were ever helpful in maintaining perspective concerning the needs of the public and the gas industry.

TABLE OF CONTENTS

LIST OF TABLES

LIST OF FIGURES

LIST OF SYMBOLS

Dimensions are given in terms of mass (m), length (L), time (t), moles (n) and temperature (T).

Symbol	Definition	Units
A	Area $[L^2]$	
C_p	Specific heat capacity at constant pressure $[L^2t^{-2}T^{-1}]$	
C_p^*	Molar specific heat capacity at constant pressure	$[L^2mt^{-2}T^{-1}n^{-1}]$
g	Gravitational acceleration	$[Lt^{-2}]$
g'	$(=g(\rho_s-\rho_a)/\rho_a)$ gravitational parameter	$[Lt^{-2}]$
κ	Thermal conductivity	$[mLT^{-1}t^{-3}]$
ℓ_b	Buoyancy length scale	$[L]$
L	Length $[L]$	
M	Molecular weight	$[mn^{-1}]$
$\overline{M}$	Equivalent molecular weight	$[mn^{-1}]$
n	Mole or frequency	$[n]$, $[t^{-1}]$
P	Pressure $[mL^{-1}t^{-2}]$	
p	Velocity power law exponent	-
Q	Volumetric rate of gas flow	$[L^3t^{-1}]$
$\overline{R}$	Universal gas constant	$[mL^2n^{-1}t^{-2}T^{-1}]$
$S_u(n)$	Spectral power density	$[L^2t^{-1}]$
T	Temperature $[T]$	
ΔT	Temperature difference across some reference layer	$[T]$

t	Time [t]	
u_*	Friction velocity	$[Lt^{-1}]$
u_e	Entrainment velocity	$[Lt^{-1}]$
U	Mean velocity	$[Lt^{-1}]$
$\forall$	Volume [L^3]	
W,w	Plume vertical velocity	$[Lt^{-1}]$
x,y,z	Downwind, lateral, & vertical coordinate	$[L]$
z_o	Surface roughness parameter	$[L]$
α	Temperature ratio	-
∇	Gradient of quantity	$[L^{-1}]$
γ	Heat capacity ratio	-
δ	Boundary layer thickness	$[L]$
λ_p	Peak wavelength	$[L]$
ν	Kinematic viscosity	$[L^2t^{-1}]$
ρ	Density [mL^{-3}]	
σ	Standard deviation or plume surface area	- , $[L^2]$
χ	Mole fraction of gas component	-
Ω	Angular velocity of earth = $0.726*10^{-4}$ (radian/sec)	$[t^{-1}]$

Subscripts

$_a$	air
$_{bg}$	Background
$_{cal}$	Calibration value
$_g$	Gas
$_H$	Evaluated at height H
$_{iso}$	Isothermal
$_{\text{℄}}$	On centerline

$_{LNG}$ Liquefied Natural Gas

$_{m}$ Model

$_{mea}$ Measured

$_{p}$ Prototype, peak

$_{r}$ Reference conditions

$_{s}$ Source gas

$_{u}$ Upwind

Superscripts

$\overline{(\ )}$ Mean of a quantity

$(\ )'$ Fluctuating part of a quantity

Dimensionless Parameters

Re Reynolds number

Ri Bulk Richardson number

Ro Rossby number

Pr Prandtl number

Ec Eckert number

Ma Mach number

M Mass flux ratio

F Momentum flux ratio

Fr Densimetric Froude number

Fr_s Densimetric Froude number relative to inertia of the plume

$\hat{F}r$ Flux Froude number

V Volume flux ratio

SG Specific gravity

K Dimensionless concentration

f Dimensionless plume parameter

ϕ_ϵ Dimensionless dissipation rate for turbulent energy

1 INTRODUCTION

In recent years the demand for liquid natural gas has increased because it is convenient to store and transport. Since liquefied natural gas (LNG) is cooled to -162°C for transportation and storage, the cold flammable vapor cloud which results from an accidental spill may remain negatively buoyant for the majority of its flammable life time [American Gas Association, 1974; Neff et al., 1976]. Hazards associated with the flammable gas cloud will extend downwind until the atmosphere has diluted the vapor cloud below the lower flammability level (LFL; the maximum local concentration below which the gas is not flammable; 5 percent by volume for methane). Thus safety at LNG facilities is of utmost importance to the gas industry and the public.

Experiments and numerical investigations have been performed to develop accurate predictive models for LNG vapor cloud formation and dispersion, so that the associated hazards of transportation and storage may be evaluated. Industrial and governmental agencies have sponsored field experiments, and analytical, numerical, and physical modeling studies to analyze the behavior of dense gas dispersion. Field experiments on the dispersion of heavy gases started around 1970, but they have included a very limited set of data on the mitigating effects of vapor barrier fences, obstacles, and water or steam spray curtains. Thus new field experiments were planned by the Lawrence Livermore National Laboratory (LLNL) for the Department of Transportation (DOT) and the Gas Research Institute (GRI) as part of a joint government/industry study in 1987 [Brown et al., 1988] to evaluate the effectiveness of vapor fences as a mitigation technique for accidental releases of LNG. The objective of this study was to

evaluate the rate of dispersion and extent of downwind hazards associated with the spill of LNG particularly when surrounded by diked storage areas or vapor barriers.

Wind-tunnel pre-field tests were performed to provide data to define the relative influence of wind velocity, vortex inducers, spill rate, spill volume, and impoundment volume on dispersion during the design of the field experiments [Neff et al., 1986]. A series of five large scale pressurized LNG spill tests called the Falcon Series field tests were conducted with the assistance of the pre-field wind-tunnel test data. The field tests were performed over flat terrain at the Department of Energy (DOE) Liquefied Gaseous Fuels Spill Test Facility (LGFSTF) in the Frenchman Flat Area of the Nevada Test Site (NTS) which is under the jurisdiction of the DOE Nevada Operations Office (DOE/NV).

Large scale field experiments have a limited ability to control flow conditions. Measurements of the behavior of simulated LNG clouds dispersing over small-scale models placed in wind-tunnels permit evaluations of the fluid physics of dense gas cloud movement and dispersion in a controlled environment. This report describes post-field-spill wind-tunnel experiments designed to augment the LNG Vapor Fence Program data obtained during the Falcon Test Series in 1987. The purpose of this post-field-spill program is to (1) provide a basis for the analysis of the simulation of physical modeling tests using proper physical modeling techniques and (2) to assist in the development and verification of analytical or numerical models.

Additional objectives of this study are to determine the probable response of a dense LNG vapor cloud to vortex inducer obstacles and fences, examine the sensitivity of results to various scaling arguments, and identify important details of the spill behavior which were not predicted during the pre-test

planning phase. This study will present statistically reduced results of field/model data comparisons.

The modeling criteria necessary for physical modeling of atmospheric and plume motion are discussed in Chapter 2. The details of the model construction and the experimental measurements are described in Chapter 3. Chapter 4 examines the reproduction of atmospheric flow by physical model tests, and Chapter 5 analyzes the laboratory data and presents comparisons of data between field scale LNG releases and laboratory scale models. Chapter 6 presents the conclusions derived from this study.

All data from wind-tunnel simulations for the Falcon Spill Series were published separately [Shin et al., 1989]. Data are also available on magnetic tape.

2 SIMULATION OF ATMOSPHERIC BOUNDARY LAYER AND PLUME MOTION

Similitude of two systems at different geometric scales will be achieved if a one-to-one correspondence between the pertinent parameters (space, time, velocity, pressure, concentration, temperature, density, etc.) of both systems exists. However, this similarity is not easy to accomplish, and the specification of parameters which assure similarity has been discussed [Meroney, 1986]. To achieve this similarity, the conservation equations of mass, momentum and energy are formulated in the atmospheric boundary layer, normalized with characteristic scales, and dimensionless parameters are derived as the following.

Eckert number = $Ec = [U^2/C_p(\Delta T)]_r$

Peclet number = $Pe = [(UL)/D]_r$ = $\frac{\text{Advection}}{\text{Diffusion}}$

Prandtl number = $Pr = [\nu/(\kappa/\rho C_p)]_r$ = $\frac{\text{Viscous Diffusivity}}{\text{Thermal Diffusivity}}$

Reynolds number = $Re = (UL/\nu)_r$ = $\frac{\text{Inertial Force}}{\text{Viscous Force}}$

Bulk Richardson number = $Ri = [(\Delta T)/T)(L/U^2)g]_r$ = $\frac{\text{Gravitational Force}}{\text{Inertial Force}}$

Rossby number = $Ro = (U/L\Omega)$ = $\frac{\text{Inertial Force}}{\text{Coriolis Force}}$

To achieve exact similarity, all dimensionless parameters mentioned above should be equal for the physical model and the prototype situation. Also, surface-boundary conditions governing the flow domain of interest must be similar for the model and prototype in the following features:

a. Topographic relief,

b. Surface roughness distribution,

c. Surface-temperature distribution, and

d. Reproduction of associated obstacles, buildings, fences, source areas, etc.

Similarity of the approach-flow characteristics requires similarity of the following features:

a. Distribution of mean and turbulent velocities,

b. Distribution of mean fluctuating temperatures and humidities, and

c. Distributions of turbulent scales and energies.

However, all similarity requirements can not be satisfied simultaneously ;thus model conditions must be chosen to simulate most accurately those scales of motion which are of greatest significance for the application [Cermak, 1975].

2.1 PHYSICAL MODELING OF THE ATMOSPHERIC BOUNDARY LAYER

The atmospheric boundary layer is that portion of the atmosphere where the major exchanges of mass, momentum, and heat occur due to surface interaction of the air with the ground. The depth of the boundary layer is variable (50 m ~ 2000 m) and highly dependent upon atmospheric stratification. To accomplish model similitude to the atmosphere, one should reproduce the important features of the atmospheric surface layer. The following section 2.1.1 reviews the characteristics of the atmosphere. Methods to reproduce these characteristics at model scales are discussed in Section 2.1.2.

2.1.1 Similarity of Mean Wind and Turbulence Characteristics

To accomplish accurate extrapolation from model to field values, similarity in the distribution of upwind turbulent velocities is required. The turbulent velocity at one spatial point is described by probabilistic[1] or a spectral[2] methods assuming statistical stationarity of upwind turbulent velocities. To assure the similarity of the approach wind fields of model and prototype, it is considered sufficient to compare the profiles of vertical mean velocity, root-mean-square (rms) velocity, and spectral energy.

Representation of Mean Wind Velocity Profiles

The lowest 10 percent of the atmospheric boundary layer is called the surface layer, and it is characterized by the sharpest variations of wind speed, temperature, humidity, and turbulence characteristics with height. Within the surface layer the mean wind-speed profile is commonly described by either a logarithmic expression (1) or a power-law representation (2) as follows:

$$U(z)/u_* = 2.5 \ln[(z-d)/z_0], \quad (1)$$

where u_* = friction velocity at the wall and,

d = displacement thickness,

z_0 = roughness length,

$$U(z)/U_H = (z/H)^p. \quad (2)$$

The displacement thickness, d, is important for tall roughness element, and d = 0 for short roughness thickness, i.e. $z_0 < 0.2$ m [Snyder, 1981]. The exponent, p, in the power-law description and the roughness length, z_0, in the log

---

[1]A probabilistic description of a turbulent velocity includes the probability of occurrence of a velocity of a certain magnitude. The most probable velocity is the mean velocity.

[2]A spectral description of a turbulent velocity is the harmonic description of the turbulent velocities magnitude or, more commonly, turbulent energy.

description are functions of surface roughness. Rougher boundary conditions (z_0 and p larger) increase the momentum deficit in the mean shear flow.

Turbulent Intensity Profiles

The turbulent intensity of a boundary layer is a ratio of the rms of the fluctuating component of the velocity, σ_u, to the local mean velocity, $\overline{U}$. By correlating strong wind atmospheric data over a large variety of different roughness conditions ESDU [1974] derived the variation of longitudinal turbulent intensity with height up to 100 meters as:

$$\frac{\sigma_u}{\overline{U}} = \frac{[0.867 + 0.556 \log_{10} z - 0.246(\log_{10} z)^2]B}{\log_e(z/z_0)}$$

where $B = 1.0$ for $z_0 \leq 0.02$ m

$B = 0.76/z_0^{0.07}$ for $0.02 \text{ m} < z_0 \leq 1.0$ m, and

$B = 0.76$ for $z_0 > 1.0$ m.

Power Spectrum of Turbulent Velocity Fluctuations

The kinetic energy associated with the fluctuating velocity component, u′ is measured as $\overline{u'^2}$, and the random variation of this measure is harmonically decomposed as the sum of cosine and sine waves of varying amplitudes and frequencies using Fourier integral transformations. This energy measure at frequency n (Hz) is presented as the integral of power over an incrementally small frequency range, dn, and this is described mathematically as:

$$S_u(n) = \frac{\overline{du'^2}(n)}{dn}$$

where $S_u(n)$ = longitudinal power spectral density,

$\overline{u'^2}$ = energy density at frequency n.

Integration of $S_u(n)$ over all frequencies produce the total mean square velocity fluctuations, $\sigma_u^2 = \overline{u'^2}$.

Spectral data is commonly presented in a normalized form such that equal areas on a graph are equal to the fractional energies. By presenting $nS_u(n)/\overline{u'^2}$ versus $n/\overline{U}$, the magnitude of the ratio of the turbulent energy at a specific wave number to the total turbulent energy of the flow is represented. The wavelength, λ_p, characteristic of the eddies of largest energy will be at the peak of the curve.

2.1.2 Partial Simulation of the Atmospheric Boundary Layer

Kline [1965] commented that it is often impossible to model all aspects of the behavior of the prototype, hence it is necessary to determine conditions for which some parameters can be neglected. Under those conditions several of the dimensionless parameters mentioned above may be relaxed without causing a significant effect on the modeled flow field.

Eckert Number

The Eckert number is the ratio of kinetic to internal energy and is also expressed as $Ec = 0.4Ma^2(T/\Delta T)_r$ for air [Hinze, 1975] which is generally smaller than unity for both laboratory and atmospheric flows. Thus, the requirement for Eckert number similarity is waived.

Peclet Number

The Peclet number is a ratio of the ability of the fluid to advect heat or mass to the ability to disperse heat or mass by molecular transport. When the Reynolds number independence does not exist, the relative ability of the fluid to transport heat or mass by molecular collision and the rate of transport by

turbulent motions become comparable. This situation can result in incorrectly simulated plume entrainment and transport rates (See section 6.2.3 for further discussion).

Prandtl Number

Prandtl number indicates the relative ability of the fluid to transport momentum as compared to heat via molecular processes. Since it is dependent on the molecular properties of the working fluid which is air for both the atmosphere and the laboratory, Prandtl number equality is always maintained.

Reynolds Number

The Reynolds number (Re) is the ratio of inertial forces to viscous forces. Reynolds number equality implies $U_m = (L_p/L_m)U_p$ and this imposes very strict limitations on simulation. If a model scale ratio L_p/L_m of 100 is introduced then the model flow velocity required would be two orders of magnitude larger than the flow velocity of the prototype. This is generally impractical to produce, hence, Reynolds number equality must be distorted. However, the larger scale motions dominate momentum and mass transfer within a boundary layer and a range of Reynolds numbers exist for which flow characteristics are invariant [Hinze, 1968]. Thus, it is possible to use reduced scale physical modeling of atmospheric flows. It should be noted that there is a minimum Reynolds number to guarantee invariant flow characteristics within the boundary layer which is:

$$Re = u_* z_0/\nu < 2.5,$$

where

u_* = friction velocity,

z_0 = roughness length.

The value of 2.5 is an empirically determined constant in turbulent pipe flow measurement [Schlichting, 1968]. Hence, extrapolation of this result to flat

plate boundary layers may shift the value of the minimum Reynolds number, but it is generally felt that this shift is small [Schlichting, 1968]. However, Re > 2.5 is not applicable for flow over complex terrain or building clusters.

Richardson number

A very large value of Richardson number implies that fluid buoyancy forces are very large compared to inertial forces. As the Richardson number decreases, thermal effects or density differences become less important. Non-neutral conditions in wind-tunnel facilities are obtained by controlling air and floor temperature. However, all model tests performed for this study were neutrally stable cases.

Rossby number

The Rossby number measures the relative magnitude of the advective or local acceleration to Coriolis acceleration, and this number controls the extent to which the mean wind direction changes with the height. Since the Coriolis acceleration is relatively small this only becomes important when the plume height is the same order of magnitude as the boundary layer height. Thus, Coriolis effects would be extremely small for plumes near ground level. A nearly infinite model Rossby number exists in most laboratory wind tunnels.

Quite often during the modeling of a specific flow phenomenon it is sufficient to model only a portion of a boundary layer or a portion of the spectral energy distribution. This relaxation allows more flexibility in the choice of the length scale that is to be used in a model study. When this technique is employed it is common to scale the flow by any combination of the following length scales, δ, the portion of the boundary layer to be simulated; z_o, the aerodynamic roughness; Λ_i, the integral length scale of the velocity

fluctuations, or λ_p, the wavelength at which the peak spectral energy is observed.

Unfortunately, many of the scaling parameters and characteristic profiles are difficult to obtain in the atmosphere. They are infrequently known for many of the sites at which a model study is to be performed. To help alleviate this problem Counihan [1975] has summarized measured values of some of these different parametric descriptions for many different atmospheric flow conditions.

2.2 PHYSICAL MODELING OF PLUME DISPERSION

Proper scaling of the plume source conditions is also required to accomplish the similarity of plume dispersion between model and prototype. Normalization of the conservation equations produces scaling parameters by reasoning that the mass ratios, force ratios, energy ratios, and property ratios should be equal in both model and prototype [Kline, 1965]. When one considers the dynamics of gaseous plume behavior the following nondimensional parameters of importance are identified [Halitsky, 1969; Hall, 1977; Hoot et al., 1974; Skinner and Ludwig, 1978; Snyder, 1981; Davis and Inman, 1986; Meroney, 1986][3,4]

$$\text{Length Scale Ratio} = \frac{D}{L}$$

$$\text{Excess Density Ratio} = \frac{(\rho_g - \rho_a)}{\rho_a}$$

---

[3]It has been assumed that the dominant transfer mechanism is that of turbulent entrainment. Thus the transfer processes of heat conduction, convection, and radiation are negligible.

[4]The scaling of plume Reynolds number is also a significant parameter. Its effects are invariant over a large range; thus it is possible to scale the distribution of mean and turbulent velocities and relax exact parameter equality.

Volume Flux Ratio $= \dfrac{(WA)_g}{(UA)_a} = \dfrac{Q}{U_a L^2}$

Mass Flux Ratio $= \dfrac{(\rho WA)_g}{(\rho UA)_a} = \dfrac{\rho_g Q}{\rho_a U_a L^2}$

Momentum Flux Ratio $= \dfrac{(\rho W^2 A)_g}{(\rho U^2 A)_a} = \dfrac{\rho_g Q^2}{\rho_a U_a{}^2 L^4}$

Densimetric Froude No. relative to the inertia of air $= \dfrac{(\rho U^2 A)_a}{g(\rho_g - \rho_a)\forall_g} = \dfrac{U_a{}^2}{Lg(\rho_g - \rho_a)/\rho_a}$

Densimetric Froude No. relative to inertia of the plume $= \dfrac{(\rho W^2 A)_g}{g(\rho_g - \rho_a)\forall_g} = \dfrac{Q^2}{L^5 g(\rho_g - \rho_a)/\rho_g}$

Flux Froude No. $= \dfrac{(\rho U^2 A)_a}{Qg(\rho_g - \rho_a)(L/U_a)} = \dfrac{U_a{}^3 L}{Qg(\rho_g - \rho_a)/\rho_a}$

Plume Reynolds No. $= \dfrac{W_g D}{\nu_g}$

Peclet No./Richardson No. $= \dfrac{\rho_a U^3}{g(\rho_g - \rho_a)D}$

Ideally these parameters must be equal at equivalent scaled locations and times over the entire lifetime of a dispersion episode. Usually it is argued that if the initial values of these parameters are equal, and if the surrounding flow fields are similar, then all subsequent plume motions and dilution must remain identical. This equality is restricted, of course, to the normal variance expectations that each atmospheric flow is a single realization from larger ensembles.

It is important to examine each modeling situation and decide if an approximation to complete plume behavior may be employed without a significant loss in the similarity of the modeled plume structure. Section 2.2.1 discusses several different approximation methodologies which help formulate a physical model, and it addresses the errors incurred by such approximations.

2.2.1 Partial Simulation of Plume Dispersion

Specific Gravity Ratio

The equality of the plume specific gravity ratio, ρ_g/ρ_a, over the plume's entire lifetime needs to be maintained to obtain the simultaneous simulations of all parameters mentioned above. However, the equality of the plums gas specific gravity ratio results in several complications in practice. When the equality of the source gas specific gravity of model and prototype is satisfied, it implies a wind speed scaling of $U_m = (L_m/L_p)^{1/2}U_p$. Thus, a typical length scale reduction of 1:100 in the model would require that the flow velocity decrease by at least an order of magnitude which conflicts with the need for Reynolds number similitude. A reasonably complete simulation may be obtained in some situations even when a modified density ratio ρ_s/ρ_a is stipulated [Schatzmann, 1985]. The advantage of such a procedure is demonstrated most clearly by the statement of equality of Froude numbers.

$$\left[\frac{U_a^2}{\left[\frac{\rho_s}{\rho_a} - 1\right]L_g}\right]_m = \left[\frac{U_a^2}{\left[\frac{\rho_s}{\rho_a} - 1\right]L_g}\right]_p$$

Solving this equation to find the relationship between model velocity and prototype velocity yields:

$$(U_a)_m = \left[\frac{S.G._m - 1}{S.G._p - 1}\right]^{1/2} \left[\frac{1}{L.S.}\right]^{1/2} (U_a)_p$$

where S.G. is the specific gravity, (ρ_s/ρ_a), and L.S. is the length scale, (L_p/L_m) By increasing the specific gravity of the model gas compared to that of the prototype gas, for a given length scale, one increases the reference velocity used in the model. It is difficult to generate a flow which is similar to that of the atmospheric boundary layer in a wind tunnel run at very low wind speeds.

Thus, the effect of modifying the model specific gravity extends the range of flow situations which can be modeled accurately.

Exact duplication of the density ratio for the entire life of a plume is difficult to accomplish for LNG plumes which simultaneously vary in molecular weight and temperature. To clarify this point consider the mixing of two volumes of gas, one being the source gas, $\forall_s$, the other being ambient air, $\forall_a$. Consideration of the conservation equations of mass and energy for this system produces [Skinner and Ludwig, 1978][5]:

$$\frac{\rho_g}{\rho_a} = \frac{(\rho_s/\rho_a)\forall_s + \forall_a}{\left[\frac{T_a}{T_s}\forall_s + \forall_a\right]\left[\frac{(C_p^*)_s}{(C_p^*)_a}\forall_s + \forall_a\right]\left[\frac{(C_p^*)_s\ T_a}{(C_p^*)_a\ T_s}\forall_s + \forall_a\right]^{-1}}$$

Given equality of the temperature of the air, T_a, and the temperature of the source gas, T_s, or equality of the molar specific heat capacity, C_p^* for both source gas and air simplifies the equation to:

$$\frac{\rho_g}{\rho_a} = \frac{(\rho_s/\rho_a)\forall_s + \forall_a}{\forall_s + \forall_a}$$

Thus one can model the density ratio variation isothermally as long as the initial density ratio is equal for both model and prototype and if the prototype plume is either isothermal or composed of mostly air. Figure 3 displays the variation in the density history behavior for the isothermal simulation of an LNG vapor plume. Figure 1 displays the variation in the plume cross sectional area as the plume mixes with air for this same situation. These two figures suggest that, although an isothermal simulation of an adiabatic LNG vapor cloud as it entrains dry air is not exact, it is a good approximation to actual behavior.

---

[5]The pertinent assumption in this derivation is that the gases are ideal and properties are constant.

Heat transfer across plume boundaries is often small [Neff et al., 1981] even in the case of an LNG vapor plume so that this will not affect the plume buoyancy significantly. But the release of latent heat through the entrainment of humid air can have a very significant effect on the density history of a thermal plume. Figure 2 displays the variation of specific gravity from a spill of liquefied natural gas in atmospheres of different humidities. Humidity effects are thus shown to reduce the extent in space and time of plume buoyancy dominance on plume motion. Hence a dry adiabatic model condition should be conservative.

Unfortunately, during the adjustment of the specific gravity of the model gases, several of the similarity parameters listed previously must be neglected. The options as to which parameters to retain, if any, depends upon the physical situations being modeled.

(1) Froude No. Equality
Momentum Ratio Equality
Mass Ratio Inequality
Velocity Ratio Inequality[6]

(2) Froude No. Equality
Momentum Ratio Inequality
Mass Ratio Inequality
Velocity Ratio Equality

Both of these schemes have been used to model plume dispersion downwind of an electric power plant complex by Isyumov [1976] and Meroney [1974] respectively.

---

[6]When this technique is employed distortion in velocity scales or similarity volume flow rates requires that a correction be applied to the measured concentration field.

Plume Reynolds Number

The modeling of the plume Reynolds number is relaxed in all physical model studies. This parameter is thought to be of small importance since the plume character will be dominated by background atmospheric turbulence soon after its emission. But, if one was interested in plume behavior near the source, then steps should be taken to assure that the plume in the model is fully turbulent.

Halitsky [1969] reported that for dispersion in the vicinity of a cube placed in a near uniform flow field the Reynolds number required for invariance of the concentration distribution over the cube surface and downwind must exceed 11,000. Because of this invariance exact similarity of Reynolds parameter is neglected when physically modeling the atmosphere.

Peclet/Richardson Number Ratio

This parameter measures the ratio of turbulent entrainment to molecular diffusion. In the full scale prototype, the turbulent entrainment is far larger than molecular diffusion; thus, molecular effects can be ignored. However, small value of Pe/Ri which may occur for a model situation implies that the molecular diffusion rate is large compared to the rate of turbulent entrainment, and this would result in smaller concentrations for the model than field concentrations. A critical value of Pe/Ri based on the approach wind speed at a 10 m reference height is about 1500 [Meroney, 1986].

An alternative way to define Pe/Ri is to include the frictional velocity, u_*. Laboratory wind-tunnel data from Neff and Meroney [1982] for which the Pe_*/Ri_* ratio varies from 0.05 to 0.5 were evaluated [Meroney, 1986], and the result showed a systematic deviation of concentrations only when $Pe_*/Ri_* < 0.2$. The depth-integrated numerical model DENS20 also reproduced such concentration deviations as the Pe_*/Ri_* parameter decreased [Meroney, 1986]. The criterion Pe_*/Ri_*

< 0.2 may be overly conservative in the presence of large initial mixing caused by fences, explosions, water spray curtains, or collapse of a tall dense-cloud.

Modeling of Heat Transfer

Scaling the effects of heat transfer by conduction, convection, or radiation cannot be reproduced when the model source gas and environment are isothermal. Fortunately in a large majority of industrial plumes the effects of heat transfer by conduction, convection, and radiation from the environment are small enough that the plume buoyancy essentially remains unchanged. In the specific case of a cryogenic liquid spill the influence of heat transfer on cold dense gas dispersion can be divided into two phases. First the temperature (and hence specific gravity) of the plume as it exits from a containment tank and surrounding dike area is dependent on the thermal diffusivity of the tank-dike-spill surface materials, the volume of the tank-dike structure, the actual boiloff rate, and details of the spill surface geometry. A second plume phase involves the heat transfer from the ground surface beyond the spill area which lowers plume density.

It is tempting to try to simulate the entire transient spill phenomenon in the laboratory including spill of cryogenic fluid into the dike, heat transfer from the tank and dike materials to the cryogenic fluid, phase change of the liquid and subsequent dispersal of cold gas downwind. Unfortunately, the different scaling laws for the conduction and convection suggest that markedly different time scales occur for these various processes as the length scale changes. Since the volume of dike material storing sensible heat scales with the cube of the length scale whereas the pertinent surface area scales as the square of the length scale one perceives that heat is transferred to a model cold plume much too rapidly within the model containment structures. This effect is

apparently unavoidable since a material having a thermal diffusivity low enough to compensate for this effect does not appear to exist. Calculations for the full-scale situation suggest minimal heating of a cold gas plume by the tank-dike structure; thus it may suffice to cool the model tank-dike walls to reduce the heat transfer to a cold model vapor and study the resultant cold plume.

Boyle and Kneebone [1973] released room temperature propane and LNG onto a water surface under equivalent conditions. The density of propane at ambient temperatures and methane at -161°C relative to air are the same. Using the modified Froude number as a model law they concluded that the dispersion characteristics were equivalent within experimental error.

A mixture of 50 percent helium and 50 percent nitrogen pre-cooled to 115°K was released from model tank-dike systems by Meroney et al. [1977], to simulate equivalent LNG spill behavior. There was no guarantee that these experiments reproduced quantitatively similar situations in the field. Rather it was expected that the gross influence of different heat transfer conditions could be determined. Since the turbulence characteristics of the flow are dominated by roughness, upstream wind profile shape, and stratification one expects the Stanton number in the field will equal that in the model, and heat transfer rates in the two cases should be in proper relation to plume entrainment rates. On the other hand, if temperature differences are such that free convection heat transfer conditions dominate, scaling inequalities may exist; nevertheless, model dispersion rates would be conservative.

Visualization experiments performed with equivalent dense isothermal and dense cold plumes revealed no apparent change in plume geometry. Concentration data followed similar trends in both situations. No significant differentiation

appeared between insulated versus heat conducting ground surfaces or neutral versus stratified approach flows.

2.2.2 Implications of Small Simulation Errors during Repetitive Dilution

Since each set of post-field measurements was performed at several downwind distances including various heights and five repetitions at each location, the time required from initial calibration of the hot-wire system to completion of one full set of measurements ranged from 8 to 16 hours. Thus, it may be possible that small errors at the beginning of a laboratory run could accumulate during repetitive dilution of concentrations during the run. It would be valuable to specify the functional form of the distribution of error, however no serious theoretical discussion of the problem has been published. A reasonably useful heuristic argument (akin to Kolmogoroff's [1941] treatment of the size distribution of ground materials) is discussed by Csanady [1973]. This section considers errors present in laboratory concentration measurements and discusses the implications of errors on repetitive dilution of concentrations based on the ideas of Csanady.

Let's consider the following variables for this discussion.

C_o = initial concentration,

C_i = concentration after ith dilution,

ξ_i = diluting impulse which occurs at ith increment in a field test, and

e_i = error in ith laboratory run.

First, consider an ideal situation in a laboratory run which simulates the field test perfectly. If we follow the history of each small parcel of the original cloud, we may find it consists of a number of 'diluting impulses,' during each

of which the parcel is mixed with a certain portion of ambient fluid. Each such impulse produces a concentration decrease by a random factor $\xi_i < 1$, leading to a succession of concentration values which is described as

$$C_i = \xi_i \cdot \xi_{i-1} \cdot \xi_{i-2} \cdot \cdot \cdot \xi_2 \cdot \xi_1 \cdot C_o \qquad (5\text{-}12)$$

$$\ln C_i = \ln \xi_i + \ln \xi_{i-1} + \cdot \cdot \cdot + \ln \xi_2 + \ln \xi_1 + \ln C_o$$

Now, consider a laboratory simulation which produces concentration data including a small simulation error, and let the random error be e_i the 'error factor'. Then the 'diluting factor' will be

$$(\xi_i)_L = \xi_i \times e_i$$

where $(\xi_i)_L$ = the diluting impulse which occurs at ith increment in a laboratory.

Thus, the concentration observed at a sampling instrument will be

$$C_i = (\xi_i e_i)(\xi_{i-1} e_{i-1}) \cdot \cdot \cdot (\xi_2 e_2)(\xi_1 e_1) C_o, \qquad (5\text{-}13)$$

and the logarithmic concentration will be

$$\ln C_i = (\ln \xi_i + \ln \xi_{i-1} + \cdots + \ln \xi_1) + (\ln e_i + \ln e_{i-1} + \cdots + \ln e_1) + \ln C_o.$$

Now we have C_i as a result of adding two sets of random numbers. It would be useful to know the functional form of the distribution of these random numbers. Then one could correct the predictions from laboratory tests to agree with field observations.

To illustrate how the random errors in Eq.(5-13) influence C_i, consider two different cases as follows.

(a) Two sets of random numbers are generated from the same distribution such that the random error remains constant, or

(b) Two sets of random numbers are generated from different distributions such that e_i changes for each impulse.

Case (a) is considered first with selected random numbers for ξ and e, and Table 1 presents the results. Numbers used are:

(1) $\xi = 0.5$; e = 0.9, 0.95, 0.99

(2) $\xi = 0.6$; e = 0.9, 0.95, 0.99

(3) $\xi = 0.8$; e = 0.9, 0.95, 0.99

(4) $\xi = 0.9$; e = 0.9, 0.95, 0.99

for i = 1, 10, 20, 30, 40, 50, 60, 70, 80, 90, and 100.

Table 2 shows results for case (b) using a random number generator to provide $\xi_i = (0.01)i$ and $e_i = f(\xi_i) = \xi_i^2$.

Table 1 and Table 2 show that even a very small repeated error (e.g. e = 0.99; i.e. 1 percent error) during dispersion can produce large variance as the dilution process continues. For example, for $\xi = 0.9$ and e = 0.9 (10 percent error) the calculation produces 100 percent variance as the iteration increases to 60, while for $\xi = 0.9$ and e = 0.99 (1 percent error) it produces a variance of 46 percent after the same number of impulses. Note that $\xi = 0.5$, e = 0.9 produces a variance of 100 percent at the 50th iteration, but e = 0.99 produces a variance of 39 percent at the same impluse iteration. It is clear that even a small error associated with a dilution process during a laboratory test can produce a significant difference in concentration measurements. Hence even modest agreement between a numerical or physical dispersion model and measured data implies an essentially correct replication of mixing processes.

3 EXPERIMENTAL MEASUREMENTS

In Chapter 2 a review of the extent to which wind tunnels can model plume dispersion in the atmospheric boundary layer was provided. In this section these background arguments will be applied to the physical modeling of the specific cases of Liquefied Natural Gas (LNG) spills from the Falcon Test Series performed by Lawrence Livermore National Laboratory (LLNL) in 1987 at the Department of Energy (DOE) spill site in Nevada. The laboratory instruments and operational techniques employed during the measurements of the physically modeled plumes formed during the Falcon Test Series are described.

3.1 WIND-TUNNEL FACILITIES

The Environmental Wind Tunnel (EWT) shown in Figure 4 was used for all model post-field tests. This wind tunnel incorporates several features such as adjustable ceiling, rotating turntables, transparent boundary walls, and a long test section to permit reproduction of micrometeorological behavior at small length scales. In addition to flow straightener honeycombs introduced at the tunnel entrance, spires were placed after the tunnel's entrance contraction to generate deep model boundary layers. Mean wind speeds which can be obtained in the EWT range from 0.15 to 14 m/s. The mean wind speeds used during the present study ranged from 23 cm/s to 128 cm/s at a height of 2 cm. A boundary layer depth of 1 m thickness at 6 m downstream of the test entrance was obtained through the use of vortex generators at the test section entrance and surface roughness on the floor. The flexible test section roof on the EWT was adjusted in height to set the longitudinal pressure gradient to zero.

3.2 MODELING OF PLUME DISPERSION DURING THE PRESENT STUDY

Table 3 summarizes the comparison parameters for prototype and model release conditions. The following equations were used to convert field values to model values.

$$L_m = \frac{1}{L.S.} L_p,$$

$$U_m = \left[\frac{S.G._m - 1}{S.G._p - 1}\right]^{1/2} \left[\frac{L_m}{L_p}\right]^{1/2} U_p,$$

$$Q_m = \left[\frac{S.G._m - 1}{S.G._p - 1}\right]^{1/2} \left[\frac{L_m}{L_p}\right]^{5/2} Q_p,$$

$$t_m = \left[\frac{S.G._p - 1}{S.G._m - 1}\right]^{1/2} \left[\frac{L_m}{L_p}\right]^{1/2} t_p,$$

where L is length, U is wind speed, Q[7] is plume vapor flow rate at the source, t is time, L.S. is length scale factor, and S.G. is the plume specific gravity at the source. The subscript m and p indicate model and prototype (field) conditions, respectively.

All tests were performed in the Environmental Wind Tunnel described in section 3.1. The plumes were released from an area source mounted to the wind tunnel floor and/or a pipe spider. The floor in the vicinity of the plume was always flat and smooth with no obstacles other than the vapor barrier fence and vortex generating barrier to cause wake effects.

---

[7]LNG vapor at the boiloff temperature of -162°C requires 253 times the volume as LNG.

3.2.1 Physical Modeling of the Field Site Atmospheric Surface Layer

During wind-tunnel simulation of the field site surface layer winds the approach flow characteristics must be similar. To achieve these upstream flow conditions, the wind tunnel flow must be modified through the introduction of surface roughness elements and boundary layer trip devices in such a way that similarity is obtained in both the mean velocity variation with height and the characteristic length scales of turbulence. A convenient parameter which characterizes the mean velocity variation with height is z_0, the aerodynamic roughness height [Sclichting, 1968], as defined by the log-linear description of velocity variation in a boundary layer.

The wind-tunnel pre-field tests were conducted by Neff et al. [1986]. The conditions in the wind tunnel were adjusted until this length scale was in the same proportion to its atmospheric equivalent (obtained by Counihan [1975]) as the geometric length scale chosen for the model terrain construction. The optimal geometric length scale was chosen to be 1:100. In the present study, four different length scale ratios (LSR) were tested including 1:50, 1:100, 1:150 and 1:200 to examine the sensitivity of results to various scaling arguments.

3.2.2 Physical Modeling of the Field Site LNG Spill Plume

The buoyancy of a plume resulting from an LNG spill is a function of both the mole fraction of methane and temperature. If the plume entrains air adiabatically, then the plume would remain negatively buoyant for its entire lifetime. If the humidity of the atmosphere were high then the buoyancy of the plume will vary from negative to weakly positive as moisture condenses.

Since the adiabatic plume assumption will yield the most conservative downwind dispersion estimates this situation was simulated in the pre-field test

by Neff et al. [1986]. (Conservative is defined here to be highest peak concentrations furthest downwind.) Several investigators have confirmed that the Froude number is the parameter which governs plume spread rate, trajectory, plume size and entrainment during initial dense plume dilution [Hoot et al., 1974; Boyle et al., 1973; Bodurtha, 1961; van Ulden, 1974]. The strict equality of model and prototype specific gravity was relaxed so that pure Argon gas (specific gravity at 1.38) could be used for the model source gas. The Froude number was maintained at equal values by adjusting reference wind speed.

Argon provides almost eight times the detection sensitivity for instantaneous concentration measurements as the carbon dioxide used in some studies [Meroney et al., 1977]. The use of an isothermal dense model gas such as Argon instead of cold methane vapor also results in a slight distortion of the local dynamic forces acting on equivalent plume volumes as the gas mixes. The thermal capacitance properties of methane result in plumes which are slightly more dense than the model equivalent. This results in less rapid prototype mixing. Analytical approximations based on the integral entrainment box model of Fay [1980] suggest that buoyancy forces are greater at equivalent time and space positions during adiabatic mixing of methane. Let $Fr = [U(h)^2/g(\Delta\rho/\rho_a)h]$ be a local Froude number, where h is local plume depth, U(h) is wind speed at plume depth, h, and $\Delta\rho/\rho_a$ is a local density difference ratio. Then given a power law wind profile $U(h) \sim h^p$ one finds

$$\frac{Fr_{\text{isothermal gas}}}{Fr_{\text{LNG vapor}}} = \frac{(1+\chi S)(\beta+(1-\beta)\theta)}{((1+\chi S)+(1+S)(1-\beta)\theta)} \left[\frac{(1+\chi S+\chi(1+S)\theta}{(1-\chi\theta)(1+\chi S)}\right]^{2p} \left[\frac{R_{LNG}}{R_{iso}}\right]^{2-4p}$$

where

χ = mole fraction methane vapor

R = local plume spread

$\beta = 1 - M_a/M_s \approx -0.81$

$\theta = 1 - T_s/T_a \approx 0.6$

$S = (Cp_s^*/Cp_a^* - 1) \approx 0.2$

p = velocity power law exponent ≈ 0.5.

The variation of this Froude number ratio with equivalent mole fraction methane is plotted in Figure 5. Fortunately, over most of the concentration range where buoyancy forces are dominant the variation of Froude number is reasonably simulated by the isothermal model gas.

In addition to Argon gas, 100 percent Freon-12 gas (specific gravity at 4.18) was introduced to simulate the Falcon 4 field data for geometric length scales of 1:150 and 1:200. It was expected that a better simulation would occur resulting from larger plume Reynolds numbers. Because of the increased specific gravity for a given length scale the reference velocity in the model was increased for Freon-12 compared to that with Argon gas at an equivalent Froude number.

The actual source condition, i.e. boiloff rate per unit area over the time duration of the spill, for a spill of LNG on land is highly unpredictable. However, data were available at locations inside the fence for the different LNG spills of the Falcon Test Series. Thus, the source conditions were approximated by assuming a steady boiloff rate for the duration of the spill over a constant area and adjusting the proportions of gas release from the modeled evaporation pond and pipe spider to result in the best simulation of the concentration time histories at positions inside the fence.

Since the thermally variable prototype gas was simulated by an isothermal simulation gas, the gas concentration measurements observed in the model must be

adjusted to equivalent concentrations measured in the field [Neff, 1986; Meroney, 1986]. This relationship is:

$$\chi_p = \frac{\chi_m}{\chi_m + (1 - \chi_m)\frac{T_s}{T_a}}$$

where

χ_m = volume or mole fraction measured during the model tests,

T_s = source temperature of LNG during field conditions,

T_a = ambient air temperature during field conditions, and

χ_p = volume or mole fraction in the field.

3.3 MODEL

During the wind-tunnel pre-field tests [Neff et al., 1986], it was concluded that the best reproduction of surface wind characteristics would occur at a model scale of 1:100 based on atmospheric data over sites similar to that of the field site. However, four different model scales (1:50, 1:100, 1:150 and 1:200) were tested during the post-field wind tunnel series to examine the sensitivity of results to model scale. Figure 6 displays the layout of the source area, the vortex generating barrier and the vapor fence. The field dimensions are in meters. To insure a uniform release of source gas over the 58.4 cm × 39.6 cm area modeled evaporation pond the model pond plenum was sectioned into twelve squares, and the plenum was filled with beads and covered with a metal screen. The 1:100 scale plenum was reconfigured to the proper size for the model scales of 1:150 and 1:200 by blocking unused plenum surface with masking tape. For a model scale of 1:50, the modeled pond used for the pre-field tests which has a size of 38 cm × 38 cm was combined with the 58.4 cm x 39.6 cm

plenum. Figure 7 through Figure 9 show the locations at which gas concentrations were measured in the wind tunnel. All dimensions shown are at field scale. The simulant gas, pure Argon or pure Freon-12, was stored in a pressurized cylinder and directed through a solenoid valve, a flowmeter, and into the model's vapor containment area or pipe spider.

3.4 FLOW VISUALIZATION

Smoke was used to define plume behavior over the modeled LNG spill site during the Falcon Test Series. The smoke was produced by passing the simulation gas through a Rosco Model 8215 Fog/Smoke Machine located outside the wind tunnel. The plume was illuminated with arc-lamp beams. Video tape recordings of the simulation of the Falcon 4 test for the 1:100 scale model were obtained from various view points using a VHS video camera.

3.5 VELOCITY DATA ACQUISITION

Mean wind and turbulent intensity profiles were measured for each Falcon Test and compared to the profiles obtained during the field tests. Spires were introduced at the test section entrance, and the upstream floor surface was selected to produce appropriate surface roughness for each model scale. Sixteen different post-field-spill tests were performed at model scales of 1:50, 1:100, 1:150 and 1:200 for the Falcon 2, 3, 4 and 5 tests. Mean velocity and turbulent intensity profiles were measured for each test series. An exposed cardboard corrugation was placed on the upwind surface for tests with models scaled to 1:50 and 1:100. Approach flow characteristics for length scales of 1:150 and 1:200 were simulated with a smooth wind tunnel floor.

Velocity profile measurements, reference wind speed conditions and turbulence measurements were obtained with a Thermo-Systems Inc. (TSI) 1050 anemometer and a TSI model 1210 hot-film probe. Since the voltage response of these anemometers is nonlinear with respect to velocity, a multi-point calibration of system response versus velocity was utilized for data reduction.

Figure 10 displays the velocity standard used in the present study. This velocity calibrator consisted of a Matheson model 8116-0154 mass flowmeter, a Yellowsprings thermistor and a profile conditioning section designed and calibrated by the FDDL staff at Colorado State. The mass flowmeter measures mass flow rate independent of temperature and pressure, the thermistor measures the temperature at the exit and the profile conditioning section forms a flat velocity profile of very low turbulence at the position where the probe is to be located. Incorporating a measurement of the ambient atmospheric pressure and a profile correction factor allows the calibration of velocity at the measurement station from 0.2 to 2.2 m/s ± 10 percent or ± 5.0 cm/s, whichever is smaller. King's law expression [Sandborn, 1972] with a variable exponent was used during the calibration of the single film probe to fit anemometer voltage response values over the velocity range of interest. This technique allows velocities the accuracy of approximately ± 2 percent of the actual longitudinal velocity.

The velocity sensor probes were mounted on a vertical traverse and positioned over the measurement locations in the wind tunnel. The anemometer's responses were digitized by a Data Translations, model 2821A, analog-to-digital converter at a sample rate of 25 Hz for 10 sec. Data were directly sent to a IBM AT computer for immediate interpretation.

3.6 CONCENTRATION MEASUREMENT TECHNIQUE

An aspirated, fast-response concentration sensor based on a hot-film anemometer was found to have a signal output linear with the volume concentration of the tracer gas. Rapid concentration fluctuations found during small-scale laboratory simulations require concentration sensors with a rise-time of the order of a millisecond, and such a detector was designed and constructed by Neff [1986] at Colorado State University.

A rack of eight hot-wire aspirating probes were manufactured to obtain the concentration time histories at points downwind of the spill site. A layout of this design is presented in Figure 11. The miniature films on these probes were replaced with 0.005 in. platinum wire to improve signal-to-noise characteristics. The eight instantaneous concentration sensors were connected to an eight-channel TSI model 1054B hot-wire anemometer system, the output voltages from the TSI unit were conditioned for input to the analog-to-digital converter by a DC-suppression circuit, a passive low-pass filter circuit set to 100 Hz, and an operational amplifier of five times gain. Furthermore, Wavetek Model 852 filters set to a 40 Hz upper band pass cut-off were used in some cases to eliminate noise. A block diagram of this process is shown in Figure 12.

3.6.1 Aspirating Hot-Wire Probes

Hot-wire katharometer probes allow one to specify concentration spectra, concentration standard deviation, peak to mean ratios, etc. at any point. For aspirated sensors the detector element in a chamber is isolated to reduce sensitivity to drift and noise and to provide a controlled and protected environment. While aspirated detectors have better signal-to-noise characteristics than direct contact probes, they may have poorer frequency response and

signal distortion resulting from the physical distortion of turbulent eddies and from molecular diffusion smearing of sharp concentration gradients as the sample is sucked along the sample line [Wilson and Netterville, 1981].

A vacuum source sufficient to choke the flow through the small orifice just downwind of the hot-wire sensor was applied and the sampling velocity was held constant by a choked orifice. The wire was operated in a constant temperature mode at a temperature above the ambient air temperature, and a feedback amplifier maintained a constant overheat ratio (1.65) by adjusting the heating current. A change in output voltage from this sensor circuit corresponds to a heat transfer change between the hot wire and the sampling environment.

The rate of heat transfer between a hot wire and a gas flowing over it depends primarily upon the wire diameter, the temperature difference between the wire and the gas, the thermal conductivity and viscosity of the gas, and the gas velocity. The gas velocity in an aspirated probe can be presented as a function of the specific heat ratio, the sound speed in the gas, and the ratio of the probe cross-sectional area at the wire position to the area at the throat. The gas composition and temperature determine the specific heat ratio, the speed of sound in the gas, the thermal conductivity, and the viscosity of the gas. With a fixed probe geometry, constant wire temperature, and an isothermal flow condition used in this study, the wire's response was only a function of gas composition.

The probes were calibrated with known compositions of either Argon-Air or Freon 12-Air mixtures, which were passed through a pre-heat exchanger to condition the gas to the tunnel temperature environment. Premixed Argon-Air gases provided by Matheson Laboratories with known compositions were used for the calibration, and Freon 12-Air gases with known compositions were produced by

combining pure Freon 12 and pure Air metered through an Omega, model FMA-78P4, four channel mass flow controller.

3.6.2 Errors in Concentration Measurements with Aspirating Probes

The effective sampling area of the probe inlet which is a function of the probe's aspiration rate and the distribution of approach velocities of the gases to be sampled was approximately 0.5 cm^2.

The upper frequency of the probe is limited by the travel time from the sensor to the sonic choke. The Colorado State aspirated probe has a 60 Hz frequency response, and this is well above the expected frequencies for concentration fluctuations in this test program. A 60 Hz frequency response for a model scale of 1:100 corresponds to 7 Hz at field scale. This is far above the 1 Hz frequency used during field tests.

The accumulative error, due to the combined effect of calibration uncertainties and nonlinear voltage drifting during the testing time, is estimated to be approximately ± 20 percent of component value in the range of 5-15 percent equivalent methane concentrations.

3.7 CONCENTRATION MEASUREMENT TESTS

Wind-tunnel laboratory tests were conducted from 1988 through 1989 to simulate the Falcon Series performed at the Department of Energy (DOE) Liquefied Gaseous Fuels Spill Test Facility (LGFSTF) in the Frenchman Flat Area of the Nevada Test Site (NTS). In addition to post-field simulations, further wind-tunnel laboratory tests were performed to evaluate the effects of several variables including change of wind orientation to the model and change of source configuration.

3.7.1 Post-field Tests

Sixteen different sets of post-field-spill tests were simulated in the Environmental Wind Tunnel (EWT) at model scales of 1:50, 1:100, 1:150 and 1:200. Each test was repeated 5 times to record the inherent variability of instantaneous concentrations due to turbulence. Table 4 summarizes the post-field-spill tests conducted. The table specifies the array angle of the model and the percentages of source gas released from the modeled evaporating pond and spider, respectively. Simulation of Falcon 2 and Falcon 4 tests were performed using models with length scales of 1:50, 1:100, 1:150 and 1:200. Falcon 3 and Falcon 5 tests were simulated with models of length scales of 1:100, 1:150 and 1:200. Post-field tests for Falcon 3 or 5 at a model scale of 1:50 were not performed since the model gas spill rate was too large to be supplied through available flow meters. Falcon 1 test could not be simulated, because the wind velocity for that model would be too low to be accurately maintained in the EWT. Pure Argon gas was used as a simulant gas for all test sets, but 100 percent Freon-12 gas was also used for the post-field test of Falcon 4 at model scales of 1:150 and 1:200.

Concentration measurements at X = 250 m for many of the test sets were not performed, because the measurement locations were not specified by LLNL in the field data report which was provided before performing those tests. However, a later data report which was available after conducting those tests showed measurement positions at X = 250 m. Thus, this downwind distance was included in those tests subsequently performed. At the model scale of 1:50 concentration measurements at X = 250 m were not made because of inadequate wind tunnel width.

3.7.2 Additional Tests

Additional tests were performed for other array angles to evaluate the effects of wind direction variation during the period of measurements. Various combinations of source gas from the modeled evaporating pond and the spider were also simulated to select that combination which resulted in the best simulation of inside fence plume behavior for each field trial.

3.7.2.1 Array Angle

Additional measurements were performed to investigate the dispersion of heavy gas plume according to the change of wind direction with respect to the fenced pond and test array. Since the wind direction was not constant during the period of field measurement the most representative angle for the field condition had to be chosen before the simulations. According to the field data provided from LLNL an average wind array angle of 225°T was selected for the post-field tests for the Falcon 2, Falcon 3 and Falcon 5 trials. However 225°T was not appropriate for a simulation of the Falcon 4 test. Thus, both 225°T and 235°T were used during the post-field tests of Falcon 4. Field measurements indicate there was strong lateral drift of the plume due to wind angle variations. Since the wind direction from the field tests varied continuously and the resultant response of concentrations to wind direction was also large, this made it more difficult to select representative concentration time histories inside the fence from the field trials.

3.7.2.2 Alternative Source Gas Configurations

Field trials of Falcon Test Series had various meteorological conditions resulting in different concentration profiles over time at a fixed location for

each run. Thus, an optimum combination of the model source gas supply from the modeled evaporating pond and the spider were selected prior to performing each set of post-field tests by referring to field data inside the fence.

First the source gas was released entirely from the spider. Concentration measurements were taken at specified locations inside the fence. Then 90 percent of the source gas was released from the spider, and 10 percent was released from the modeled evaporating pond. Gradually the source gas from the spider was decreased by 10 percent each run, and the rest of source gas was released from the pond. Concentrations were measured for each run at the same locations and were compared to field data for similarity of the concentration time histories.

3.7.3 Test Procedure

The test procedure consisted of:

(1) Setting the proper tunnel wind speed,

(2) Releasing a metered mixture of source gas from the release area source (the modeled evaporating pond and the spider),

(3) Withdrawing gas samples over a fixed time period, from the designated sampling locations,

(4) Recording the time series of concentration response from each probe onto hard disk storage on an IBM AT computer, and

(5) Storing all the data from post-field-spill tests onto magnetic tapes for future analysis.

4 REPRODUCTION OF ATMOSPHERIC FLOW SIMILARITY AND DATA

During field experiments flow conditions are not controlled; hence the wind field is typically nonstationary. Flow characteristics in the wind tunnel are statistically stationary, and measurements of the behavior of simulated LNG clouds dispersing over small-scale models permit evaluation of the fluid physics of dispersion in a controlled environment. Differences may exist between the resultant concentration fields depending on the severity of the nonstationarities existent during the field tests.

This chapter reviews the atmospheric flow similarity produced for the laboratory tests. Section 4.1 compares visual plume behavior obtained from the field and the laboratory tests. Section 4.2 discusses the approach wind field for both field and laboratory tests.

4.1 VISUAL PLUME BEHAVIOR

The technique employed in the visual plume data is described in section 3.4. Table 11 shows the run conditions for which visual plumes were recorded. Argon gas was used as a source gas, and Falcon 4 test was simulated with the length scale ratio (LSR) of 100. The plume behavior was video recorded from three different viewing angles.

The visual plume had appeared to be more turbulent and dispersed more quickly in the wind tunnel than in the field. On the other hand the apparent time span during the model dispersion is accelerated due to the scaling laws imposed to assure similarity. Indeed, for a 1:100 scale model for undistorted simulant densities model times are ten times shortened than field times (e.g. 60

seconds of field dispersion occurs over 6 seconds in the model). Another factor which influences perceptions gained while watching the video sequences is the smoke density. The model smoke plume was far more transparent than the vapor cloud formed during the field tests. Thus, one initially interprets the model plumes as more dilute. Nonetheless, many important features of the LNG cloud were reproduced during the model program. Plume slushing within the fence region, back flows generated by the separation cavity formed downwind of the vortex stimulator, corner overflows initiated by fence generated vortex separation regions, and downwind plume spread were all evident in both field and model visualization sequences.

Figure 13 presents sketches of plume behavior as time progresses. There is only spider generated mixing at $t = 0$, and upwind movement in the fence region is shown at $t = t_1$ which is caused by the vortex barrier generated second flow. As more time progresses plume slushing behavior appears within the fence area, and the plume spreads in downwind direction.

4.2 VELOCITY DATA

Section 3.5 describes the technique employed during velocity data acquisition. Similarity of the distribution of upwind turbulent velocities is a critical requirement in reproducing the laboratory plume measurements at atmospheric scales. It is normally considered sufficient to reproduce the mean velocity, and root-mean-square (rms) velocity profiles. Empirical correlations for mean wind spread and the turbulence intensity profiles are proposed in section 2.1.1. Section 4.2.1 discusses comparisons of model and prototype mean wind velocity, and the turbulent intensity profiles are compared in section 4.2.2.

4.2.1 Mean Wind Velocity Profiles

Figure 14 shows the mean wind variation with height for prototype Falcon 4 and Falcon 5 tests and for different model scales. The fence height (9.1 m in prototype) was used as a reference height, and the mean wind velocity at that height was the reference velocity. The roughness length, z_0, characterizing the field condition was 0.008 m, thus cardboard corrugation was introduced for LSR of 50 and 100, and smooth floor was used for LSR of 150 and 200 in an attempt to match approach wind velocity profiles. The calculated roughness length characterizing the wind tunnel shear profile was, z_0 = 0.007 m. The variance of mean wind speed at the reference height of 9.1 m (in prototype) was - 5 percent to + 10 percent.

4.2.2 Turbulent Intensity Profiles

The turbulent intensity of a turbulent velocity is a ratio of the rms of the fluctuating component of the velocity, σ_u, to the local mean velocity, $\overline{U}$. Figure 15 show the turbulent intensity variation with height for Falcon 4 and Falcon 5 and for different model scales. The figure indicates that the wind tunnel generally has higher turbulent intensity, especially near the ground. Since the mean wind velocity profile for both prototype and model conditions were close, this implies that the higher turbulent intensity is entirely due to larger velocity fluctuations in the wind tunnel.

4.2.3 Temperature Profiles

Figure 16 shows the temperature profiles during the Falcon test series. Conditions during Falcon 2 and 3 tests have slightly unstable conditions, while Falcon 4 and 5 tests have stable conditions. All wind tunnel tests were

performed for neutral condition, which explains the reason that turbulent intensity profiles for simulations of Falcon 4 and 5 have greater values than in the prototype.

5 DATA ANALYSIS OF LABORATORY SIMULATIONS

This section presents various interpretive schemes used to analyze the laboratory data acquired in the Environmental Wind Tunnel (EWT) and the field data taken at the field site. Table 5 presents gas concentration measurement locations for the field site, and Table 6 through Table 10 specify measurement locations for the post-field-spill laboratory tests. Even though identical measurement points for both field and laboratory tests were sought, it was not possible due to physical limitations such as minimum distance between hot-wire probes and a spatial restrictions in the EWT to avoid some wall effects.

One objective of the wind-tunnel program was to determine how accurately physical modeling replicates field conditions. One desires to replicate both the spatial and temporal distribution of plume concentrations. For LNG hazard assessment, the spatial distribution of plume concentrations appears to be more critical than the temporal distribution. Thus a pattern comparability test is employed in section 5.2 to provide a quantitative measurement of how well the modeled spatial distribution of specified-level concentration agrees with real field observations. This method is applied to the laboratory data and the field data from the Falcon Test Series. These comparisons include overlays of peak concentration isopleths.

The remainder of this chapter presents various schemes to analyze plume concentrations acquired during the laboratory tests. Comparisons to be considered include contour plots of peak concentrations and plots of concentration time histories at measurement locations. Section 5.5 discusses laboratory data from the view point of different model scales to examine the sensitivity of

results to various scaling arguments. Section 5.6 discusses the similarity between plumes generated from Argon gas and Freon-12 gas, respectively, and section 5.7 analyzes laboratory data as influenced by model array angle.

5.1 ALTERNATIVE DESCRIPTIONS OF VARIOUS CONCENTRATIONS

Data analysis of concentration measurements examines either instantaneous concentrations or concentrations averaged over some specified time period. A number of parameters has been used to compare model predictions and observations depending on the varied interests of developers, users, and evaluators. In a health hazard assessment, one might be interested in the average concentration above some specified lower limit, while for flammable gases one might be interested in the instantaneous concentration. Table 12 summarizes definitions used for various concentration variables employed for this study and compares the symbols selected to nomenclature used in other literature.

5.2 SURFACE PATTERN COMPARISONS OF SPECIFIC LABORATORY/FIELD DATA

Among the five field tests performed by LLNL, runs which have the most trustworthy data are Falcon 1, Falcon 3 and Falcon 4. Liquid phase transition explosions occurred during the Falcon 3 test, and there was an explosion and fire which completely destroyed the field site during the Falcon 5 test. Falcon 1 could not be successfully simulated in the wind tunnel because the field site wind velocity was too low to simulate reliably. The Falcon 4 test provides the most complete data for comparisons with laboratory data followed by Falcon 3 test data. Thus, Falcon 4 test data are compared to post-spill-test data, and pattern comparison factors are discussed in this section. The pattern comparison method is described in Appendix A.

Contours of peak concentrations were plotted from Falcon 4 post-spill-measurement data. Plots were made with data from LSR of 100 with Argon gas and LSR of 150 and 200 with Freon-12 gas at Z = 1, 5, and 11 m. Figure 18 and Figure 19 show contours of peak concentrations from LSR of 100 with Argon and LSR of 150 with Freon-12 at Z = 5 m. Since laboratory data were taken only at three downwind distances (X), concentrations at other X distances were extrapolated assuming an exponential decrease in downwind direction, and linear variations were assumed for lateral interpolation.

Pattern factors were determined based on the method described in Appendix A, and results are presented in Figure 20 through Figure 24. First, a plot of f-N vs. spatial angle was made for several specified pattern factor levels for various run conditions. Figure 20 shows that 100 percent of the observations are covered by a shift of 15° for N = 1 and the shift decreases to 7° for N = 2 with Argon gas. For Freon-12 gas the angle shift needed to cover the observations increases to 20° and 8° for N = 1 and 2, respectively. However, this does not necessarily imply that Argon gas has better spatial simulations than Freon-12 gas, because Argon gas data from LSR = 100 and Freon-12 gas data from LSR = 150 were used in this study. Summary bar charts are provided in Figure 22 through Figure 24 to display the angles at which 100 percent agreement exists for two different factor ratios. Figure 22 through Figure 24 show that the pattern factor cumulative percent increases as the model size increases, suggesting that the model predicts the observations better spatially as the model size increases.

Pattern factors were calculated from wind-tunnel data produced by Davis and Inman [1986] from the Thorney Island HGDT progect [Shin and Meroney, 1989]. Most

data compared within a factor of 1 for angular displacements of 15 to 20 degrees, and this result is similar to values obtained from Falcon test.

Meroney [1986] conducted extensive surface pattern comparisons between field and wind-tunnel or numerical data. He used data from American Gas Association (AGA) Capistrano tests, China Lake spills (Avocet series and Burro series), and HSE Porton Downs Experiment. Pattern factors were determined from field and wind-tunnel data from tests mentioned above, and field data and FEM3 data [Chan and Ermak, 1983] from Burro series were also compared by surface pattern test. Comparisons of field and wind-tunnel data showed that most observations were covered for a factor of 1 by displacing 10 to 20 degrees, but comparisons of field and numerical data required angular displacements exceeding 45 degrees.

Considering the results described above, wind-tunnel data simulated field data spatially better than numerical model, and most wind-tunnel data covered 100 percent of field data for a factor of 1 by shifting 15 to 20 degrees.

5.3 STATISTICAL APPROACH

Statistical analysis methods are applied to the sets of field and laboratory data to determine whether there are significant differences between physical model predictions and field observations. Section 5.3.1 describes the performance measures, and more statistical tests are described in section 5.3.2.

5.3.1 Performance Measures

Performance measures relevant to the evaluation of hazardous gas models have been proposed by several researchers [Mercer, 1987; Ermak et al., 1988; Hanna et al., 1988]. Because of the potential hazard of LNG gases, the maximum

concentration over a specified averaging period must be correctly simulated by the model.

Once data for observed field concentrations (C_f) and predicted model concentrations (C_m) are available, they can be used to calculate the following performance measures: the fractional bias (FB) and the normalized mean square error (NMSE) defined by:

$$FB = (\overline{C_m} - \overline{C_f}) / [0.5(\overline{C_m} + \overline{C_f})]$$

$$NMSE = \overline{(C_m - C_f)^2} / \overline{C_m}\,\overline{C_f}$$

where an overbar indicates an average over all points in the data set.

There are several ways to select C_m and C_f. First, the magnitude of $\overline{C}_{MAX}$ is used to calculate NMSE and FB, and the result will show how well the model predicted $\overline{C}_{MAX}$ for a given field test. Alternatively, arrival time or departure time of a specified concentration is used as a variable. In this case a plot of NMSE vs. FB presents the degree of similarity of temporal distributions.

Data from post-spill-experiments from Falcon 2, Falcon 3 and Falcon 4 tests were examined. All downwind data points ($X > 0$ m) were included to calculate FB and NMSE, and concentration time series for both field and model tests were averaged over the same time period (11 sec at field scale). Data were analyzed for the magnitude of $\overline{C}_{MAX}$, the arrival time of concentration with a magnitude of 20 percent of $\overline{C}_{MAX}$, and the arrival time of $\overline{C}_{MAX}$.

It should be noted that all sets of tests were repeated five times; thus selecting data from only one run may not be a reasonable way to derive NMSE and FB. To check this point FB values for all five repetitions of a selected test were calculated and plotted against run number. The result showed that the range of repetition variability is within ± 20 percent.

Figure 25 is a plot of NMSE vs. FB for $\overline{C}_{MAX}$. This figure shows that all laboratory tests underpredicted $\overline{C}_{MAX}$. A perfect simulation would be represented on this figure at FB = 0 and NMSE = 0. Most of laboratory simulations have values between $-0.50 \leq FB \leq -0.25$ and $0.35 \leq NMSE \leq 0.70$. Hanna [1990] evaluated fourteen numerical hazardous gas models using data from the Desert Tortoise ammonia (NH_3) and Goldfish hydrogen fluoride (HF) field experiments. He calculated FB and NMSE for concentration predictions for each model and plotted NMSE vs. FB. His data suggest that there is a cluster of eight models with relatively good performance with values of $-0.4 \leq FB \leq 0.0$ and $0.25 \leq NMSE \leq 0.50$; hence, physical model data performs at least as well as numerical models predicting somewhat simpler release configurations.

Figure 26 presents a plot of NMSE vs. FB for arrival time of concentration with a magnitude of 20 percent of $\overline{C}_{MAX}$. Positive FB value means that the cloud arrives later in a wind tunnel than in the field. Most tests have FB values within a range of $\pm$ 0.38 and $0.0 \leq NMSE \leq 0.4$. Figure 27 shows NMSE and FB values for arrival time of $\overline{C}_{MAX}$. The figure shows FB values within a range of $\pm$ 0.30 and $0.0 \leq NMSE \leq 0.45$.

Figure 25 does not imply a specific relation between a length scale and performance, while values for both arrival times suggest that the performance improves as the length scale decreases. This may due to small $\overline{C}_{MAX}$ values in the edge of the plume.

5.3.2 Hazard Assessment on the Basis of Concentration Probability

A fairly well developed and reasonably satisfactory theory for the prediction of mean concentrations during turbulent diffusion of dense gases now exists [Blackmore et al., Ermak et al., and Woodward et al., 1982]. However, the

inadequacy of the mean-field theory to predict instantaneous concentrations is quite obvious in experimental work: 'instantaneous' concentration profiles may differ markedly from time or ensemble averages. Pollution models generally predict time-average concentrations at fixed points for periods of the order of 1/10 to 1 hour; hence, randomness does not play a role in these models. However, they are not suitable to predict the probability that a single accidental release will produce a hazard at a given time and location. Taking into account concentration fluctuations enables one to make a more satisfactory assessment of nuisance or hazard in pollution problems than is possible on the basis of mean-field theory alone.

Section 5.3.2.1 describes the theories for the prediction of fluctuations [Csanady, 1973; Chatwin, 1981, 1982] and the theory is applied to the data set of post-spill-tests of Falcon Series in section 5.3.2.2.

5.3.2.1 Statistical Measures of Dense Gas Dispersion

Potential spills or release of dense hazardous materials may occur in a steady (continuous) or unsteady (instantaneous or finite time) manner. The post-spill laboratory measurements of the Falcon Test Series provide data for the unsteady mean behavior of dense gas clouds released over a finite time into a simulated atmospheric boundary layer. These experiments are the foundation for the statistical interpretation provided here in terms of the characteristics employed in subsections of 5.3.2.2.

Probability Distribution of Concentration

Consider the concentration by volume of the dispersing gas at position x and time t to be $\chi(x,t)$. The statistical properties of $\chi(x,t)$ can then be meaningfully defined only for an ensemble of possible trials. The probability

density function (p.d.f.) of χ defines the prediction of the trials for which χ lies between C and C+Dc, or

$$p(C;x,t) = \text{prob}(C < \chi(x,t) < C+Dc) \tag{5-3}$$

The ensemble mean concentration may be defined as

$$\overline{C}_m(x,t) = \int_0^1 C\ p(C;x,t)Dc, \tag{5-4}$$

and the mean square fluctuation or standard deviation will be denoted by

$$\overline{c'^2}\ (x,t) = \int_0^1 [C - \overline{C}_m(x,t)]^2\ p(C;x,t)Dc. \tag{5-5}$$

At short times after the release of a dense gas cloud the cloud can be unmixed or there is a finite possibility that there are locations on the edge of the plume which have zero concentration. This state of affairs is described by an intermittency factor, G(C;x,t); i.e., the probability that the concentrations are zero is G(0;x,t). During hazard predictions a conservative assumption would be that G(C;x,t) equals unity where $0 < C < 1$.

Fackrell and Robins [1980] found that probability density functions follow an exponential distribution for elevated plumes, become log-normal as the plume approached the ground, and near the ground the distribution were very close to Gaussian. Li and Meroney [1983] also concluded that the log-normal distribution is a reasonable approximation in a building wake flow when it is assumed that the intermittency factor is one for every location in the wake.

The form of the log-normal distribution is

$$p(C,x) = \frac{1}{2}\left\{1 + \text{erf}\left[\frac{\ln C/C_{med}}{2^{0.5}\ \sigma_L}\right]\right\} \tag{5-6}$$

where

$$\text{erf}(a) = \frac{1}{\pi^{0.5}} \int_0^a \exp(-t^2)\ dt$$

C_{med} = the median concentration

$$= \overline{C_m} \; / \; (1 + \overline{c'^2} \; / \overline{C_m}^2)^{0.5} \qquad (5\text{-}7)$$

σ_L = the log-normal standard deviation

$$= \ln \; ((\overline{c'^2})^{0.5} / \overline{C_m} + 1). \qquad (5\text{-}8)$$

Then the probability density dp/dc is

$$\frac{dp}{dc} = \frac{1}{(2\pi)^{0.5} \; \sigma_L C} \exp\left\{ - \frac{(\ln C/C_{med})^2}{2 \; \sigma_L^{\,2}} \right\} \qquad (5\text{-}9)$$

The rms to mean concentration ratio depends only on the log-normal standard deviation:

$$i_c(x) = \frac{(\overline{c'^2})^{0.5}}{\overline{C_m}} = [\exp(\sigma_L^{\,2} - 1)]^{0.5} \qquad (5\text{-}10)$$

= relative intensity of concentration fluctuation.

Given the validity of the log-normal distribution for non-zero concentration readings, the three distributions $\overline{C_m}(x,y)$, $G(x,y)$ and $i_c(x,y)$ are sufficient to give a probabilistic description of the whole concentration field.

Now consider the 'peak to mean concentration ratio'. From Equations (5-6) and (5-7) we may deduce that

$$\frac{C_p}{\overline{C_m}} = \exp\left[- \frac{\sigma_L^{\,2}}{2} \right] \exp[2^{0.5} \; \sigma_L \; \mathrm{erf}^{-1}(1 - 2p)] \qquad (5\text{-}11)$$

where

$\sigma_L^{\,2} = \ln \; (i_c + 1)$

C_p = peak concentration

$p(C_p, x)$ = probability that concentration $\geq C_p$

erf^{-1} = the inverse of error function.

Thus the 'peak to mean ratio' is a function of σ_L alone once p is given provided that the intermittency factor G is unity.

Figure 28 is a plot of $C_p/\overline{C}_m$ versus i_c with several levels of $p(C_p)$ derived from Eq. (5-11). Thus, the peak to mean ratio, $C_p/\overline{C}_m$, can be determined from this figure once $p(C_p)$ and i_c are known. The figure also presents $C_p/\overline{C}_m$ values for p = 10 percent from laboratory data with Argon gas. It is shown that $C_p/\overline{C}_m$ values determined from laboratory data are higher than those derived from Eq. (5-11). Figure 29 and Figure 30 display probability density plots from Argon gas and Freon-12 gas with different length scales, and these distributions have a flatness factor between 3.3 and 6.8 implying broader skirts (more probable extremums) than Gaussian distribution. Thus, the result shown in Figure 28 is consistent with the behavior exhibited by Figure 29 and Figure 30, but it suggests that neutral and heavy density plumes exhibit different mixing physics.

5.3.2.2 Statistical Measures of Specific Laboratory/Field Data

Post-spill laboratory data of Falcon 4 test were analyzed for the statistical properties described in section 5.3.2.1. Data from LSR of 100 with Argon gas and LSR of 150 with Freon-12 gas were analyzed. Since plumes resulted from unsteady releases are considered in this study, two different approaches were employed to remove the unsteady mean behavior of the plume from all five repetitions of data for the analysis. The analysis was performed along the centerline.

The first approach used the following operations.

(1) Average the concentration time series for a specific time period (11 sec at field scale), and repeat this for all five repetitions at the same location.

(2) Subtract the averaged concentration time series from the original time series leaving only the fluctuating concentration part.

(3) Calculate the rms concentration for each repetition and weight it for the given time period.

(4) Calculate $C(t) - \overline{C}(t)$ for each repetition.

(5) Calculate the probability $P[(C(t) - \overline{C}(t))/(\overline{c'^2})^{0.5}]$ for each repetition.

(6) Average the probability P calculated in (5) from all repetitions.

The second approach used the following operations.

(1) Combine concentration time series of all repetitions and average it for a specific time period (11 sec in field scale) to get a time series of an ensemble average $\overline{C}_{ens}$.

(2) Subtract the time series of an ensemble average from each original time series of all repetitions.

(3) Repeat the same steps as in the first approach to calculate rms concentration and the probability.

Figure 29 and Figure 30 display probability density plots derived from the first approach and the second approach for data from Argon gas and Freon-12 gas with different length scales, respectively. Both figures show that the probability curve becomes flatter as the downwind distance increases for both Argon gas and Freon-12 gas. Skewness factor was between -0.38 and -0.75, and flatness factor was between 3.3 and 6.8 implying that probability density distribution of wind tunnel data have a higher center peak and broader skirts than a Gaussian distribution of the same standard deviation. That is, very small and very large values of concentrations are both more probable than for a normal distribution of the same standard deviation. Figure 31 compares probability

distribution curves of Argon gas data at X = 50 m derived from both approaches. The figure shows that both methods result in very similar curves.

5.4 ALTERNATIVE SOURCE GAS CONFIGURATIONS

Field trials of Falcon Test Series had various meteorological conditions resulting in different concentration profiles over time at a fixed location for each run. An optimum combination of the model source gas supply from the modeled evaporating pond and the spider had to be selected prior to performing each set of post-field tests by referring to field data inside the fence. As the gas supply from the spider increased, there was more turbulent mixing produced inside fences resulting in lower concentrations. Table 4 presents the combinations of source gas selected for wind tunnel simulations.

Figure 32 shows comparisons of concentration time histories at (- 62 m, 0 m, 2 m) for a model test of Falcon 2 with a LSR of 200 to the field data. Figure 33 is a plot at (- 62 m, 0 m, 2 m) from model data of Falcon 3 with a LSR of 150 and the Figure 34 is a plot at (- 62 m, - 20 m, 2 m) from model data of Falcon 4 with a LSR of 100.

5.5 EFFECT OF VARIOUS MODEL SCALES ON PLUME SIMILARITY

As noted in Table 4, four different model scales were used during post-field laboratory experiments. In this section post-field data from Falcon 4 test were analyzed at different model scales. Peak centerline concentrations, concentration time histories at specified locations, and concentration contours were compared.

5.5.1 Peak Centerline Concentration Comparisons

Figure 35 shows Falcon 4 peak centerline concentrations for all model scales with Argon gas. The maximum value of peak concentrations observed during all repetitions was used for the plot. Only two points for LSR of 150 and 200 are shown since concentration measurements were performed at only two different downwind distances. The physical model data with LSR of 100 predicts the field data well while the other model scales underpredict peak concentrations. Figure 36 is a plot of concentration reduction factor (C_m/C_f) versus downwind distance, where C_m is the model prediction and C_f is the field data. The figure shows the range of reduction factors for all model scales and it is clearly shown that the physical model underpredicts the field data up to 50 percent.

5.5.2 Concentration Time Histories Comparisons

A comparison of the actual concentration time histories at the similar downwind positions reveals many of the similarities and differences between model and field data. However, when comparing the time history curves one should be careful to choose the appropriate averaging strategy and time. Section 5.5.2.1 discusses the effect of their selection on the time history curves, and section 5.5.2.2 examines the variation among test repetitions. Section 5.5.2.3 compares the post-spill data of Falcon 4 test to the field data by use of concentration time histories.

5.5.2.1 Effect of Different Averaging Time and Strategies

There are several ways to prepare the concentration time histories depending on the magnitude of the averaging time or the averaging scheme chosen.

A reasonable averaging time or an appropriate averaging scheme is desired to be able to interpret the data correctly.

Figure 37 compares four different concentration time histories obtained using different averaging times. 30 second, 2 minute, and 4 minute averaging time were selected to smooth the original concentration time series, and a backward averaging scheme was used. As the figure shows, the time history curve becomes smoother, and the arrival time of the $\overline{C}_{MAX}$ increases as the averaging time increases.

Figure 38 and Figure 39 present comparisons of two different time history curves averaged with alternative weighing schemes. Both curves in Figure 38 were derived using 30 second averaging time, but a foreward or a backward averaging scheme was used for each curve, respectively. This figure shows that the selection of the averaging scheme produces somewhat different time histories from the same data. The difference increases when the averaging time employed is large, and Figure 39 shows an example. An averaging time of 11 second (at field scale) with a backward averaging scheme was used to produce most figures presented in the rest of this study. An 11 second averaging time was used by LLNL to smooth all field data.

5.5.2.2 Variance of Repetitions

All of wind-tunnel concentration measurements were repeated five times with the same initial conditions. Figure 40 compares concentration time histories from five such repetitions. The model data were averaged over a 30 second averaging time. The figure shows that the repetitions have fairly similar arrival and departure times, and the variance of the magnitude of $\overline{C}_{MAX}$ for each repetition is less than 15 percent. It was mentioned in section 5.3.1 that most

repetitions had Fractional Bias (FB) values within a range of ± 20 percent. Thus, consideration of such data suggests that we can select one data set out of the five repetitions, and consider that it is representative of the data set.

5.5.2.3 Comparisons of Specific Model/Field Data

Figure 41 compares concentration data from four different model scales with Argon gas to the field data at the same position. All data were averaged over an 11 second equivalent prototype time period. The figure shows that a model with LSR of 100 has the best prediction followed by LSRs of 50, 150, and 200. It was expected that as the model size increases the performance would improve, but the LSR 100 resulted in better performance than LSR 50. Compared to the field data, this model data underpredicts the magnitude of $\overline{C}_{MAX}$ and a delayed $\overline{C}_{TM}$ arrival time.

The range of concentration data at the same position is plotted in Figure 42. The magnitude of $\overline{C}_{MAX}$ varied as much as a factor of 2 depending on the LSR used. The arrival time and departure time were not influenced.

5.5.3 Concentration Contours Comparisons

Since concentrations were measured at only two downwind distances for cases with LSR of 50, 150 and 250 when Argon gas was used, concentration contours can not be generated for all four model scales. However, model tests with Freon-12 gas provide data at three downwind locations enabling us to produce contour plots to compare to the field values. Linear interpolation in lateral directions and exponential interpolation in downwind directions were used to produce these contours. A denser array of sensor locations was used during model measurements providing more data laterally. Table 5 through Table 9 present the sensor

locations for the field and model measurements. Since field measurements were taken over a sparse grid interpolated contour values are less accurate.

Figure 43 compares peak concentration distributions of model data with LSR of 150 and 200 to the field data. The maximum of peak concentrations for all the repetitions at the same position was used to plot the contours. The figure displays that the wind tunnel simulations underpredict the plume width. The greater meandering in wind direction during the field experiment may explain this phenomena. In the field the wind typically drifted in a range of 20°, but the average wind direction was used for the model test. The figure also shows that the prediction is better with LSR of 150 than with LSR of 200, and the lateral concentration distribution is wider with LSR of 150 than with LSR of 200.

Figure 44 through Figure 46 are comparisons of vertical concentration distributions of post-field data of Falcon 2 for LSRs of 100, 150, and 200. The model plumes have greater vertical mixing and narrower lateral dispersion as noted before. Table 3 shows that the $(Pe_*/Ri_*)_m$ ratio values for laboratory tests ranged from 0.0007 to 2.6, which are much smaller than the criterion of 0.2 proposed by Meroney [1982]. This suggests that the model tests might have underpredicted peak concentrations due to exaggerated dispersion resulting from molecularly enhanced dispersion, and this is checked using a numerical model in Chapter ?. Data for LSRs of 100 and 150 are similar; however a comparison of data from LSRs of 100 and 200 indicates that the vertical mixing decreases as the LSR increases.

5.5.4 Comparisons of NMSE and FB

As described in section 5.3.1, a plot of NMSE vs. FB provides a summary of comparisons for various length scales. Figure 25 through Figure 27 are plots of

NMSE vs. FB for $\overline{C}_{MAX}$ magnitude, arrival time of $0.2\overline{C}_{MAX}$, and arrival time of $\overline{C}_{MAX}$. Figure 25 does not show any specific trend associated with length scale, while Figure 26 and Figure 27 generally suggest that as the LSR decreases (i.e., model size increases) the performance improves.

5.6 EFFECT OF DENSITY RATIO RELAXATION ON PLUME SIMILARITY

When the density ratio equality between two plumes is relaxed several other parameters listed in section 2.2 also vary. Thus, one needs to select dominant parameters and maintain their equality. For the post-field data of Falcon Series the plume's vertical momentum may be neglected. According to previous studies [Neff and Meroney, 1981; Hall, 1977], the plume's mass ratio may also be relaxed. Then the Densimetric Froude Number ($Fr = U^2/g'L$) and the Volume Flux Ratio ($V = Q/UL^2$) remain. Since the Flux Froude Number ($\hat{F}r = U^3L/g'Q$) is the ratio of Fr/V its equality is guaranteed when equality in Fr and V are specified.

Simulation of Falcon 4 test was selected to evaluate this scheme. Two different simulant gases, pure Argon gas (specific gravity at 1.38) and pure Freon-12 gas (specific gravity at 4.18), were introduced to simulate Falcon 4 Test. Geometric length scales of 1:50, 1:100, 1:150, and 1:200 were used with Argon gas and 1:150 and 1:200 were used with Freon-12 gas. The reference velocities for tests with Freon-12 gas were increased to ensure Froude Number equality.

Data with both simulant gases are analyzed, and peak centerline concentration decay along downwind, concentration time histories, and concentration contours are compared in following subsections.

5.6.1 Peak Centerline Concentration Comparisons

Figure 47 and Figure 48 present comparisons of peak centerline concentrations decay in downwind distance for Argon and Freon-12 data. Data with LSR of 150 for both gases are compared at Z = 1 m and Z = 5 m, and the maximum and the minimum values of peak concentrations observed during all repetitions at each location are plotted. These figures suggest that physical models with both gases underpredict the peak concentration, but Freon-12 gas simulates the field data better. It is also noted that model prediction is better at Z = 5 m than at Z = 1 m. This might be explained by the fact that the wind tunnel produces greater vertical mixing than in the field, i.e., the microscopic diffusion is overly emphasized in wind tunnel causing larger vertical entrainment. Model data from Argon gas were plotted at x = 50 m and 150 m, since concentrations were measured at only these two downwind distances.

Figure 50 is a plot of centerline concentration reduction factor (C_m/C_f) versus downwind distance. The figure shows reduction factors in a range of 0.70 to 0.90 for Freon-12 gas data and a factor of 0.60 for Argon gas data. Peak concentration comparisons show that Freon-12 gas predicted field plume behavior better than Argon gas by about 20 percent implying that distorted density modeling of heavy gas spills will generally improve model accuracies. This improvement primarily results from improved simulation of wake behavior at increased model Reynolds numbers.

5.6.2 Concentration Time Histories Comparisons

Figure 51 shows concentration time series observed at (X=150 m, Y=-28 m, Z=5 m) for LSR of 150 with Argon gas and Freon-12 gas for the Falcon 4 test. The figure shows that Freon-12 gas data simulates $\overline{C}_{MAX}$ of field data better than

Argon gas data, while the arrival time of $\overline{C}_{MAX}$ from both gases are 17 to 30 percent later than field data.

5.6.3 Concentration Contours Comparisons

Figure 52 and Figure 53 display comparisons of lateral concentration contours from Argon gas data and Freon-12 gas data at Z = 1 m, and Z = 5 m. The maximum value of peak concentrations observed during all repetitions at each position was used to make contours. Model data for a LSR of 100 with Argon gas were compared to model data for a LSR of 150 with Freon-12 gas. These figures show that concentration contours are reproduced fairly well despite of different gases and different model scales.

Since the maximum of peak concentrations for all repetitions were used to plot contours compared above, the range of concentration contours were plotted from the maximum and the minimum values of peak concentrations for all repetitions to check the region which includes all peak concentration data. Figure 54 show the maximum and the minimum peak concentration contours at Z = 5 m with Freon-12 gas as a simulant gas. From this figure, one can see that it is possible to have concentration contours fall anywhere in the intermediate region due to repetition variability.

5.6.4 Comparisons of NMSE and FB

Figure 25 through Figure 27 again show that Freon-12 gas predicted overall field plume behavior better than Argon gas suggesting that improvement in plume Reynolds number magnitude is desirable.

5.7 EFFECT OF MEAN WIND DIRECTION ON PLUME DISPERSION

Tests of concentration measurements were performed to investigate the dispersion of heavy gas plumes as influenced by a change in wind direction. Since the wind direction was not constant during the period of field measurement, the most representative angle was chosen before model simulations. Based on field data provided from Lawrence Livermore National Laboratory (LLNL), an array angle of 225°T (T stands for the true north) was selected for simulations of Falcon 2, Falcon 3 and Falcon 5 trials, and 235°T was chosen for simulation of Falcon 4 trial. However, 225°T was also used for the post-field tests of Falcon 4 to examine the effect of wind direction on the dispersion of gas plume.

In this section post-field laboratory data with mean wind directions of 225°T and 235°T are analyzed and concentration time histories are compared. Since concentrations were measured only at two different downwind distance with array angle of 225°T, concentration contours were not plotted.

Figure 55 and Figure 56 show comparisons of concentration time histories at (X=50 m, Y=0 m, Z=1 m) and (X=50 m, Y=-50 m, Z=1 m) respectively with both array angles. Both figures clearly show that 10° shift of wind direction results in considerable changes in concentrations downwind. However, the plumes generated from both cases showed similar lateral width. Figure 57 displays the ratio of peak concentrations (C(235°)/C(225°)) in downwind distance. By shifting the approach wind direction by 10°, the peak concentration downwind shows a variance up to a factor of 3.5. The data do show measurement sensitivity to wind direction; however the maximum plume centerline values compare no worse than earlier comparisons (LLNL used the shifted plume comparison to validate their results).

6 CONCLUSIONS

This report includes the following topics concerning wind tunnel model simulation of heavy plume dispersion from a vapor detention system. Conclusions reached for each topic will be described in following subsections.

1. Similarity criteria required for the production of wind-tunnel model results at small scales.
2. Validation of wind-tunnel model for methods against field experiments by surface pattern comparison and statistical data analysis for different scales, density ratios, and wind orientations.

6.1 SIMILARITY CRITERIA FOR HEAVY PLUME SPILLS

The following similarity criteria should be satisfied to reproduce field scale heavy plume with physical model.

1. Densimetric Froude number equality produced satisfactory simulation.
2. Equal geometric length scale ratio must be used to reproduce physical model with similar geometric situations as the field.
3. The background wind profiles including the mean wind profile and turbulent intensity profile for the field and the model should be similar.
4. The volume flux ratio for both the field and the model should be the same.

This study does not permit any conclusions related to the effects of disoriented similarity modeling. For an expanded discussion, see Neff [1989].

6.2 SURFACE PATTERN COMPARISONS/STATISTICAL DATA ANALYSIS

Effects of Model Scale

Four different models were used to examine the effect of model scale on plume similarity. Comparison of centerline $\overline{C}_{MAX}$ from all model scales showed that the physical model data with length scale of 100 predicts the field data fairly well, while other model scales generally underpredict $\overline{C}_{MAX}$. When all downwind data points ($X > 0$ m) were considered to calculate performance measures, $\overline{C}_{MAX}$ of field data and post-field wind-tunnel simulations agreed within a range of $-0.50 \leq FB \leq -0.25$ and $0.35 \leq FB \leq 0.75$. There was no specific relation evident between length scale and performance. Arrival times for $0.2\overline{C}_{MAX}$ have FB values within $\pm$ 0.38 and $0.0 \leq NMSE \leq 0.4$. The arrival time for $\overline{C}_{MAX}$ have FB values in a range of $\pm$ 0.30 and $0.0 \leq NMSE \leq 0.45$. The performance of arrival time predictions improves as the model size increases. Thus, fluid modeling should predict dense gas dispersion in the vicinity of industrial complexes well within the accuracy required for hazard site evaluation.

Falcon 4 test data were compared to wind tunnel data, and pattern comparison factors were calculated to provide another measure of how well the modeled spatial distribution of peak concentrations agrees with field observations. It was shown that for Argon simulants 100 percent of the observations are included within a shift of 15° for N = 1, and the shift decreases to 7° for N = 2. For Freon-12 gas the shift needed to cover the observations increases to 20° and 8° for N = 1 and 2, respectively. However, this does not necessarily imply that Argon gas produced better spatial predictions than Freon-12 gas at all model scales, since both gases were not compared for the same model scale. The results did suggest that the pattern factor accuracy increases as the model length scale

ratio (LSR) decreases, suggesting that the model predicts the observations better spatially as the model size increases.

Effects of Density Ratio Relaxation

Argon gas and Freon-12 gas were used in this study to examine the effects of density ratio relaxation on plume similarity. The use of Freon-12 gas as the simulant gas improved model predictions of field plume centerline concentrations by about 20 percent. Thus, distorted density modeling of heavy gas spills will generally improve model accuracies. This improvement is primarily due to improved simulation of wake behavior resulting from increased model Reynolds numbers.

Effects of Change of Wind Orientation Angle

Falcon 4 was simulated using wind orientations of 225°T and 235°T to examine the effects of model array angle on plume dispersion. The ratio of peak concentrations (C(235°)/C(225°)) were compared at different positions, and the data showed a peak concentration variance as large as 3.5 results from shifting the approach wind direction by 10°. However, the plume produced from both cases had similar lateral width. Even though the data do show measurement sensitivity to wind directions, the maximum plume concentrations along the respective plume centerlines did not deviate significantly.

Visual Plume Data

Comparison of visual plume data suggested that the plume had more turbulence and dispersed more quickly in the wind tunnel than in the field. The model smoke plume was far more transparent than the vapor cloud formed during the field tests. Nevertheless, many important features of the LNG cloud were reproduced during the model program.

6.3 RECOMMENDATIONS

This report includes post-field wind-tunnel experiments of Falcon tests 2, 3, 4, and 5 which were performed over limited ranges of wind speed, spill rate, and spill volume. It would be useful to have additional data to validate extended numerical or analytical models.

1. If more experiments are to be performed, try alternative schemes of vapor detention to determine the most effective passive scheme to enhance heavy plume dispersion.
2. Perform dense gas dispersion experiments for cases with more complex obstacle and terrain geometry (e.g. undulating terrain, gorges, escarpments, groups of buildings, typical industrial arrangements of tanks and buildings).
3. Examine the joint effectiveness of vapor fences, barriers and water or steam sprays. Further study to develop a numerical model which uses both vapor fences and water or steam sprays is recommended.
4. Examine the dispersion of heavy gas plume released inside of industrial buildings. It is very likely that critically flammable or toxic situations may arise in confined environments.
5. During future physical modeling of heavy gas spills, it would be proper to use model gas with distorted density simulant gases, since they would permit large model velocities resulting in increased model Reynolds number.
6. Data from wind tunnel experiments were analyzed statistically using surface pattern comparisons, performance measures, and direct comparison method. It should be recognized that various definitions of concentrations were used to provide appropriate data basis for

each method (refer to Table 12). All the wind tunnel data from this study are available for further statistical analysis, and special attention is advised in selecting the appropriate concentration definition for each method.

7. Each wind tunnel test was repeated five times to examine the variability of instantaneous concentrations due to turbulence. However, data from a sufficiently large number of tests should be analyzed to estimate a confidence level for these tests. Criteria such as the student t test may be used to specify the number of tests required to designate a given level of confidence.

TABLES

Table 1 Implications of errors in Repetitive Dilution: Case (a)

$\epsilon = 0.5$

CONC.	FIELD CONC.	e = 0.90 LAB. CONC.	e = 0.90 VARIANCE	e = 0.95 LAB. CONC.	e = 0.95 VARIANCE	e = 0.99 LAB. CONC.	e = 0.99 VARIANCE
C_0	1.00	1.00	0 %	1.00	0 %	1.00	0 %
C_1	0.50	0.45	10 %	0.48	5 %	0.50	1 %
C_{10}	9.8×10^{-4}	3.4×10^{-4}	65 %	5.8×10^{-4}	41 %	8.8×10^{-4}	10 %
C_{20}	9.5×10^{-7}	1.2×10^{-7}	87 %	3.4×10^{-7}	64 %	7.8×10^{-7}	18 %
C_{30}	9.3×10^{-10}	3.9×10^{-11}	96 %	2.0×10^{-10}	78 %	6.9×10^{-10}	26 %
C_{40}	9.1×10^{-13}	1.3×10^{-13}	99 %	1.2×10^{-13}	87 %	6.1×10^{-13}	33 %
C_{50}	8.9×10^{-16}	4.6×10^{-18}	100 %	6.8×10^{-17}	92 %	5.4×10^{-16}	39 %
C_{60}	8.7×10^{-19}	1.6×10^{-21}	100 %	4.0×10^{-20}	95 %	4.7×10^{-19}	46 %
C_{70}	8.5×10^{-22}	5.3×10^{-25}	100 %	2.3×10^{-23}	97 %	4.2×10^{-22}	51 %
C_{80}	8.3×10^{-25}	1.8×10^{-28}	100 %	1.4×10^{-26}	98 %	3.7×10^{-25}	55 %
C_{90}	8.1×10^{-28}	6.2×10^{-32}	100 %	8.0×10^{-30}	99 %	3.3×10^{-28}	59 %
C_{100}	7.9×10^{-31}	2.1×10^{-35}	100 %	4.7×10^{-33}	99 %	2.9×10^{-31}	63 %

$\epsilon = 0.6$

CONC.	FIELD CONC.	e = 0.90 LAB. CONC.	e = 0.90 VARIANCE	e = 0.95 LAB. CONC.	e = 0.95 VARIANCE	e = 0.99 LAB. CONC.	e = 0.99 VARIANCE
C_0	1.00	1.00	0 %	1.00	0 %	1.00	0 %
C_1	0.60	0.54	10 %	0.57	5 %	0.59	1 %
C_{10}	6.0×10^{-3}	2.1×10^{-3}	65 %	3.6×10^{-3}	40 %	5.5×10^{-3}	8 %
C_{20}	3.7×10^{-5}	4.4×10^{-6}	88 %	1.3×10^{-5}	65 %	3.0×10^{-5}	19 %
C_{30}	2.2×10^{-7}	9.4×10^{-9}	96 %	4.7×10^{-8}	79 %	1.6×10^{-7}	27 %
C_{40}	1.3×10^{-9}	2.0×10^{-11}	98 %	1.7×10^{-10}	87 %	8.9×10^{-10}	32 %
C_{50}	8.1×10^{-12}	4.2×10^{-14}	99 %	6.2×10^{-13}	92 %	4.9×10^{-12}	40 %
C_{60}	4.9×10^{-14}	8.8×10^{-17}	100 %	2.3×10^{-15}	95 %	2.7×10^{-14}	45 %
C_{70}	3.0×10^{-16}	1.9×10^{-19}	100 %	8.2×10^{-18}	97 %	1.5×10^{-16}	50 %
C_{80}	1.8×10^{-18}	3.9×10^{-22}	100 %	3.0×10^{-20}	98 %	8.0×10^{-19}	56 %
C_{90}	1.1×10^{-20}	8.2×10^{-25}	100 %	1.1×10^{-22}	99 %	4.4×10^{-21}	60 %
C_{100}	6.5×10^{-23}	1.7×10^{-27}	100 %	3.9×10^{-25}	99 %	2.4×10^{-23}	63 %

$\epsilon = 0.8$

CONC.	FIELD CONC.	e = 0.90 LAB. CONC.	e = 0.90 VARIANCE	e = 0.95 LAB. CONC.	e = 0.95 VARIANCE	e = 0.99 LAB. CONC.	e = 0.99 VARIANCE
C_0	1.00	1.00	0 %	1.00	0 %	1.00	0 %
C_1	0.80	0.72	10 %	0.76	1 %	0.79	1 %
C_{10}	1.1×10^{-1}	3.7×10^{-2}	66 %	6.4×10^{-2}	12 %	9.7×10^{-2}	12 %
C_{20}	1.2×10^{-2}	1.4×10^{-3}	88 %	4.1×10^{-3}	22 %	9.4×10^{-3}	22 %
C_{30}	1.2×10^{-3}	5.2×10^{-5}	96 %	2.7×10^{-4}	23 %	9.2×10^{-4}	23 %
C_{40}	1.3×10^{-4}	2.0×10^{-6}	98 %	1.7×10^{-5}	32 %	8.9×10^{-5}	32 %
C_{50}	1.4×10^{-5}	7.4×10^{-8}	99 %	1.1×10^{-6}	39 %	8.6×10^{-6}	39 %
C_{60}	1.5×10^{-6}	2.8×10^{-9}	100 %	7.1×10^{-8}	44 %	8.4×10^{-7}	44 %
C_{70}	1.6×10^{-7}	1.0×10^{-10}	100 %	4.5×10^{-9}	49 %	8.1×10^{-8}	49 %
C_{80}	1.8×10^{-8}	3.9×10^{-12}	100 %	2.9×10^{-10}	56 %	7.9×10^{-9}	56 %
C_{90}	1.9×10^{-9}	1.4×10^{-13}	100 %	1.9×10^{-11}	59 %	7.7×10^{-10}	59 %
C_{100}	2.0×10^{-10}	5.4×10^{-15}	100 %	1.2×10^{-12}	63 %	7.5×10^{-11}	63 %

$\epsilon = 0.9$

CONC.	FIELD CONC.	e = 0.90 LAB. CONC.	e = 0.90 VARIANCE	e = 0.95 LAB. CONC.	e = 0.95 VARIANCE	e = 0.99 LAB. CONC.	e = 0.99 VARIANCE
C_0	1.00	1.00	0 %	1.00	0 %	1.00	0 %
C_1	0.90	0.81	10 %	0.86	5 %	0.89	1 %
C_{10}	0.35	0.12	66 %	0.21	40 %	3.2×10^{-1}	9 %
C_{20}	1.2×10^{-1}	1.5×10^{-2}	88 %	4.4×10^{-2}	63 %	9.9×10^{-2}	18 %
C_{30}	4.2×10^{-2}	1.8×10^{-3}	96 %	9.1×10^{-3}	78 %	3.1×10^{-2}	26 %
C_{40}	1.5×10^{-2}	2.2×10^{-4}	99 %	1.9×10^{-3}	87 %	9.9×10^{-3}	34 %
C_{50}	5.2×10^{-3}	2.7×10^{-5}	99 %	4.0×10^{-4}	92 %	3.1×10^{-3}	40 %
C_{60}	1.8×10^{-3}	3.2×10^{-6}	100 %	8.3×10^{-5}	95 %	9.8×10^{-4}	46 %
C_{70}	6.3×10^{-4}	3.9×10^{-7}	100 %	1.7×10^{-5}	97 %	3.1×10^{-4}	51 %
C_{80}	2.2×10^{-4}	4.8×10^{-8}	100 %	3.6×10^{-6}	98 %	9.8×10^{-5}	55 %
C_{90}	7.6×10^{-5}	5.8×10^{-9}	100 %	7.5×10^{-7}	99 %	3.1×10^{-5}	59 %
C_{100}	2.7×10^{-5}	7.1×10^{-10}	100 %	1.6×10^{-7}	99 %	9.7×10^{-6}	64 %

Table 2 Implications of Errors in Repetitive Dilution: Case (b)

Conc.	ξ_i	e_i	FIELD CONC.	LAB. CONC.	VARIANCE
C_0	0.0	0.00	1.00	1.0	0 %
C_{10}	0.1	0.01	0.10	1.0×10^{-3}	99 %
C_{20}	0.2	0.04	0.02	8.0×10^{-6}	100 %
C_{30}	0.3	0.09	6.0×10^{-3}	2.1×10^{-7}	100 %
C_{40}	0.4	0.16	2.4×10^{-3}	1.4×10^{-8}	100 %
C_{50}	0.5	0.25	1.2×10^{-3}	1.7×10^{-9}	100 %
C_{60}	0.6	0.36	7.2×10^{-4}	3.7×10^{-10}	100 %
C_{70}	0.7	0.49	5.0×10^{-4}	1.3×10^{-10}	100 %
C_{80}	0.8	0.64	4.0×10^{-4}	6.5×10^{-11}	100 %
C_{90}	0.9	0.81	3.6×10^{-4}	4.8×10^{-11}	100 %

$\xi_i = 0.01 \times i$
$e_i = f(\xi_i) = \xi_i^2$
i = 0, 10, 20, 30, 40, 50, 60, 70, 80, and 90

Variance = $(C_F - C_L) / C_F \times 100$
C_F = Field concentration
C_L = Laboratory concentration

Table 3 Comparison of Parameters of Prototype and Model

Trial Name	Scale Ratio	$(S.G.)_p$	$(S.G.)_m$	$(Vol)_B$ m^3	$(Vol)_m$ cm^3	$(Rate)_p$ m^3/min	$(Rate)_m$ cm^3/sec	$(U_2)_p$ m/s	$(U_2)_m$ cm/sec	$(Re)_p$	$(Re)_m$
Falcon 1	50	1.50	1.38	66.4	134393	28.7	5968	1.6	19.73	773059	1906
Falcon 2	50	1.50	1.38	20.6	41694	15.9	3306	4.7	57.95	986187	2431
Falcon 3	50	1.50	1.38	50.7	102616	18.9	3930	4.0	49.32	991911	2445
Falcon 4	50	1.50	1.38	44.9	90877	8.7	1809	5.1	62.88	759900	1873
Falcon 5	50	1.50	1.38	43.9	88853	30.3	6300	2.7	33.29	1031847	2544
Falcon 1	100	1.50	1.38	66.4	16799	28.7	1055	1.6	13.95	773057	673
Falcon 2	100	1.50	1.38	20.6	5211	15.9	584	4.7	40.97	986187	859
Falcon 3	100	1.50	1.38	50.7	12827	18.9	694	4.0	34.87	991911	864
Falcon 4	100	1.50	1.38	44.9	11359	8.7	319	5.1	44.46	759900	662
Falcon 5	100	1.50	1.38	43.9	11106	30.3	1113	2.7	23.54	1031847	899
Falcon 1	150	1.50	1.38	66.4	4977	28.7	382	1.6	11.39	773057	366
Falcon 2	150	1.50	1.38	20.6	1544	15.9	212	4.7	33.45	986187	467
Falcon 3	150	1.50	1.38	50.7	3800	18.9	252	4.0	28.47	991911	470
Falcon 4	150	1.50	1.38	44.9	3365	8.7	116	5.1	36.30	759900	360
Falcon 5	150	1.50	1.38	43.9	3290	30.3	404	2.7	19.22	1031847	489
Falcon 1	200	1.50	1.38	66.4	2099	28.7	186	1.6	9.86	773057	238
Falcon 2	200	1.50	1.38	20.6	651	15.9	103	4.7	28.97	986187	303
Falcon 3	200	1.50	1.38	50.7	1603	18.9	122	4.0	24.66	991911	305
Falcon 4	200	1.50	1.38	44.9	1419	8.7	56	5.1	31.44	759900	234
Falcon 5	200	1.50	1.38	43.9	1388	30.3	196	2.7	16.64	1031847	318
Falcon 4	150	1.50	4.18	44.9	3365	8.7	336	5.1	105.35	759900	1046
Falcon 4	150	1.50	4.18	43.9	1419	8.7	164	5.1	91.23	759900	679

Trial Name	Scale Ratio	$(S.G.)_p$	$(S.G.)_m$	$(U.)_p$ m/sec	$(U.)_m$ cm/sec	$(Ri)_B$	$(Pe/Ri)_m$	$(Pe./Ri.)_m$
Falcon 1	50	1.50	1.38	0.061	0.75	0.145	6.89	0.0058
Falcon 2	50	1.50	1.38	0.357	4.40	-0.023	174.73	1.1671
Falcon 3	50	1.50	1.38	0.305	3.76	-0.006	107.71	0.7283
Falcon 4	50	1.50	1.38	0.369	4.55	0.029	223.25	1.2905
Falcon 5	50	1.50	1.38	0.156	1.93	0.094	33.12	0.0985
Falcon 1	100	1.50	1.38	0.061	0.53	0.145	2.44	0.0020
Falcon 2	100	1.50	1.38	0.357	3.11	-0.023	61.78	0.4121
Falcon 3	100	1.50	1.38	0.305	2.67	-0.006	38.08	0.2608
Falcon 4	100	1.50	1.38	0.369	3.22	0.029	78.93	0.4574
Falcon 5	100	1.50	1.38	0.156	1.37	0.094	11.7	0.0352
Falcon 1	150	1.50	1.38	0.061	0.43	0.145	1.33	0.0011
Falcon 2	150	1.50	1.38	0.357	2.54	-0.023	33.63	0.2245
Falcon 3	150	1.50	1.38	0.305	2.17	-0.006	20.73	0.1340
Falcon 4	150	1.50	1.38	0.369	2.63	0.029	42.96	0.2492
Falcon 5	150	1.50	1.38	0.156	1.11	0.094	6.38	0.0187
Falcon 1	200	1.50	1.38	0.061	0.37	0.145	0.86	0.0007
Falcon 2	200	1.50	1.38	0.357	2.20	-0.023	21.84	0.1459
Falcon 3	200	1.50	1.38	0.305	1.88	-0.006	13.46	0.0910
Falcon 4	200	1.50	1.38	0.369	2.28	0.029	27.90	0.1624
Falcon 5	200	1.50	1.38	0.156	0.96	0.094	4.14	0.0121
Falcon 4	150	1.50	4.18	0.369	9.32	0.029	124.67	2.6240
Falcon 4	150	1.50	4.18	0.369	6.59	-0.029	80.98	0.9276

Table 4 Wind-Tunnel Test Conducted

Test	Length Scale	Source Combination	Array Angle	Locations Tests Argon	Freon-12	Angle Change	Source Change
Falcon 1	50			X(a)			
	100			X(b)			
	150			X(c)			
	200			X(d)			
Falcon 2	50	10% S + 90% P	225°T	114			
	100	50% S + 50% P	225°T	161			
	150	100% S	225°T	161			
	200	100% S	225°T	90			
Falcon 3	50			X(e)			
	100	70% S + 30% P	225°T	161			
	150	50% S + 50% P	225°T	105			
	200	70% S + 30% P	225°T	77			
Falcon 4	50	90% S + 10% P	235°T	114		225°T	
	100	70% S + 30% P	235°T	161		225°T	
	150	70% S + 30% P	235°T	116	132	225°T	
	200	70% S + 30% P	235°T	88	90	225°T	
	100	100% S				225,232°T	
	100		225°T				YES
Falcon 5	50			X(e)			
	100	70% S + 30% P	225°T	161			
	150	50% S + 50% P	225°T	90			
	200	50% S + 50% P	225°T	77			

Locations Tested: Measurement locations (Repetitions - 5 times each)
S: Spider
P: Plenum
X: No experiment
X(a) - X(d): Wind velocity was too low to simulate in EWT.
X(e) :Gas flow rate was too large to supply through model source tube

Table 5 Measurement Locations of Field Tests

FALCON 1			FALCON 2			FALCON 3			FALCON 4			FALCON 5		
X(m)	Y(m)	Z(m)	X(m)	Y(m)	Z(m)	X(m)	Y(m)	Z(m)	X(m)	Y(m)	Z(m)	X(m)	Y(m)	Z(m)
50	-66	17	-62	20	2	-62	20	2	-62	20	2	-32	0	1
50	-22	17	-62	0	2	-62	0	2	-62	0	2	50	-66	1,5,11,17
50	0	17	-32	0	1	-32	0	1	-32	0	1	50	-50	1,5,11,17
50	22	17	50	-66	17	50	-66	1,5,11,17	-2	0	1	50	-33	1,5,11
50	44	17	50	-44	17	50	-44	1,5,11,17	50	-66	1,5,11,17	50	33	1,5,11,17
50	66	17	50	-22	17	50	-22	1,5,11	50	-50	1,5,11,17	50	50	1,11,17
150	-75	11	50	0	17	50	22	1,5,11,17	50	-33	1,5,11,17	50	66	1,5,11,17
150	-50	11	50	22	17	50	44	1, 11,17	50	0	1,5,11,17	150	-100	1,5,11
150	-25	11,17	50	44	17	50	66	17	50	33	1,5,11,17	150	-75	1,5,11
150	0	11,17	50	66	17	150	-75	1,5	50	50	1,5,11,17	150	-25	1,5,11,17
150	25	11,17	150	-75	11	150	-50	1,5,11	50	66	1,5,11,17	150	0	1,5,11,17
150	50	11	150	-50	11	150	-25	1,5,11,17	150	-100	1,5,11	150	25	1,5,11,17
150	75	11	150	-25	11,17	150	0	1,5,11,17	150	-75	1,5,11	150	75	1,5,11
250	-84	1,5,11	150	0	11,17	150	25	1,5,11,17	150	-25	1,5,11,17	150	100	1,5,11
250	-56	5,11	150	25	11,17	150	50	1,5,11	150	0	1,5,11,17			
250	-28	5,11	150	50	11	150	75	1,5,11	150	25	1,5,11,17			
250	0	1, 11	150	75	11	250	-84	1,5	150	75	1,5,11			
250	28	5,11	250	-84	1,5,11	250	-56	1,5,11,17	150	100	1,5,11			
250	56	5,11	250	-56	5,11	250	-28	1,5	250	-84	1,5			
250	84	1,5,11	250	-28	5,11	250	0	1,5,11	250	-56	1,5,11			
			250	0	1, 11	250	28	1,5	250	-28	1,5			
			250	28	5,11	250	56	1,5,11	250	0	1,5,11			
			250	56	5,11	250	84	1,5	250	28	1,5			
			250	84	1,5,11				250	56	1,5,11			

Table 6 Measurement Locations of Laboratory Tests: Falcon 2, Array Angle = 225°T

LSR* = 50			LSR = 100			LSR = 150			LSR = 200		
X(m)	Y(m)	Z(m)	X(m)	Y(m)	Z(m)	X(m)	Y(m)	Z(m)	X(m)	Y(m)	Z(m)
-62	0	2	-62	-20	2	-62	-20	2	-62	-30	2
-62	5	2	-62	-10	2	-62	-10	2	-62	-20	2
-62	10	2	-62	0	2	-62	0	2	-62	0	2
-62	15	2	-62	10	2	-62	10	2	-62	10	2
-62	20	2	-62	20	2	-62	20	2	-62	20	2
-62	25	2	-62	30	2	-62	30	2	-62	30	2
-32,-2	0	1	-62	40	2	-62	40	2	-32	-30	1
-32,-2	5	1	-32,-2	-20	1	-32,-2	-20	1	-32	-20	1
-32,-2	10	1	-32,-2	-10	1	-32,-2	-10	1	-32	0	1
-32,-2	15	1	-32,-2	0	1	-32,-2	0	1	-32	10	1
-32,-2	20	1	-32,-2	10	1	-32,-2	10	1	-32	20	1
-32,-2	25	1	-32,-2	20	1	-32,-2	20	1	-32	30	1
50,150	-44	1,5,11,17	-32,-2	30	1	-32,-2	30	1	50	-44	1,5,11,17
50,150	-28	1,5,11,17	-32,-2	40	1	-32,-2	40	1	50	-22	1,5,11,17
50,150	-25	1,5,11,17	50	-75	1,5,11,17	50,150	-75	1,5,11,17	50	0	1,5,11,17
50,150	-22	1,5,11,17	50	-66	1,5,11,17	50,150	-66	1,5,11,17	50	22	1,5,11,17
50,150	-11	1,5,11,17	50	-56	1,5,11,17	50,150	-56	1,5,11,17	50	44	1,5,11,17
50,150	0	1,5,11,17	50	-44	1,5,11,17	50,150	-44	1,5,11,17	50	66	1,5,11,17
50,150	22	1,5,11,17	50	-28	1,5,11,17	50,150	-28	1,5,11,17	150,250	-56	1,5,11,17
50,150	25	1,5,11,17	50	-22	1,5,11,17	50,150	-22	1,5,11,17	150,250	-28	1,5,11,17
50,150	28	1,5,11,17	50	0	1,5,11,17	50,150	0	1,5,11,17	150,250	0	1,5,11,17
50,150	44	1,5,11,17	50	22	1,5,11,17	50,150	22	1,5,11,17	150,250	28	1,5,11,17
50,150	50	1,5,11,17	50	28	1,5,11,17	50,150	28	1,5,11,17	150,250	56	1,5,11,17
50,150	56	1,5,11,17	50	44	1,5,11,17	50,150	44	1,5,11,17	150,250	75	1,5,11,17
			50	56	1,5,11,17	50,150	56	1,5,11,17			
			50	66	1,5,11,17	50,150	66	1,5,11,17			
			50	75	1,5,11,17	50,150	75	1,5,11,17			
			150	-75	1,5,11,17	250	0	1,5,11,17			
			150	-56	1,5,11,17	250	22	1,5,11,17			
			150	-50	1,5,11,17	250	28	1,5,11,17			
			150	-44	1,5,11,17	250	44	1,5,11,17			
			150	-28	1,5,11,17	250	56	1,5,11,17			
			150	-22	1,5,11,17	250	66	1,5,11,17			
			150	0	1,5,11,17	250	75	1,5,11,17			
			150	22	1,5,11,17						
			150	28	1,5,11,17						
			150	44	1,5,11,17						
			150	50	1,5,11,17						
			150	56	1,5,11,17						
			150	75	1,5,11,17						
			250	0	1,5,11,17						
			250	22	1,5,11,17						
			250	28	1,5,11,17						
			250	44	1,5,11,17						
			250	56	1,5,11,17						
			250	66	1,5,11,17						
			250	75	1,5,11,17						

LSR* = Length Scale Ratio

Table 7 Measurement Locations of Laboratory Tests: Falcon 3, Array Angle = 225°T

LSR* = 100			LSR = 150			LSR = 200		
X(m)	Y(m)	Z(m)	X(m)	Y(m)	Z(m)	X(m)	Y(m)	Z(m)
-62	-20	2	-62	-20	2	-62	-30	2
-62	-10	2	-62	-10	2	-62	-20	2
-62	0	2	-62	0	2	-62	0	2
-62	10	2	-62	10	2	-62	10	2
-62	20	2	-62	20	2	-62	20	2
-62	30	2	-62	30	2	-62	30	2
-62	40	2	-62	40	2	-32	-30	1
-32,-2	-20	1	-32,-2	-20	1	-32	-20	1
-32,-2	-10	1	-32,-2	-10	1	-32	0	1
-32,-2	0	1	-32,-2	0	1	-32	10	1
-32,-2	10	1	-32,-2	10	1	-32	20	1
-32,-2	20	1	-32,-2	20	1	-32	30	1
-32,-2	30	1	-32,-2	30	1	50	-44	1,5,11,17
-32,-2	40	1	-32,-2	40	1	50	-22	1,5,11,17
50	-75	1,5,11,17	50,150	-75	1,5,11,17	50	0	1,5,11,17
50	-66	1,5,11,17	50,150	-66	1,5,11,17	50	22	1,5,11,17
50	-56	1,5,11,17	50,150	-56	1,5,11,17	50	44	1,5,11,17
50	-44	1,5,11,17	50,150	-44	1,5,11,17	50	66	1,5,11,17
50	-28	1,5,11,17	50,150	-28	1,5,11,17	150,250	-56	1,5,11,17
50	-22	1,5,11,17	50,150	-22	1,5,11,17	150,250	-28	1,5,11,17
50	0	1,5,11,17	50,150	0	1,5,11,17	150,250	0	1,5,11,17
50	22	1,5,11,17	50,150	22	1,5,11,17	150,250	28	1,5,11,17
50	28	1,5,11,17	50,150	28	1,5,11,17	150,250	56	1,5,11,17
50	44	1,5,11,17	50,150	44	1,5,11,17	150,250	75	1,5,11,17
50	56	1,5,11,17	50,150	56	1,5,11,17			
50	66	1,5,11,17	50,150	66	1,5,11,17			
50	75	1,5,11,17	50,150	75	1,5,11,17			
150	-75	1,5,11,17	250	0	1,5,11,17			
150	-56	1,5,11,17	250	22	1,5,11,17			
150	-50	1,5,11,17	250	28	1,5,11,17			
150	-44	1,5,11,17	250	44	1,5,11,17			
150	-28	1,5,11,17	250	56	1,5,11,17			
150	-22	1,5,11,17	250	66	1,5,11,17			
150	0	1,5,11,17	250	75	1,5,11,17			
150	22	1,5,11,17						
150	28	1,5,11,17						
150	44	1,5,11,17						
150	50	1,5,11,17						
150	56	1,5,11,17						
150	75	1,5,11,17						
250	0	1,5,11,17						
250	22	1,5,11,17						
250	28	1,5,11,17						
250	44	1,5,11,17						
250	56	1,5,11,17						
250	66	1,5,11,17						
250	75	1,5,11,17						

LSR* = Length Scale Ratio

Table 8 Measurement Locations of Laboratory Tests: Falcon 4, Array Angle = 235°T

LSR* = 50			LSR = 100			LSR = 150			LSR = 200		
X(m)	Y(m)	Z(m)	X(m)	Y(m)	Z(m)	X(m)	Y(m)	Z(m)	X(m)	Y(m)	Z(m)
-62	0	2	-62	-20	2	-62	-20	2	-62	-30	2
-62	5	2	-62	-10	2	-62	-10	2	-62	-20	2
-62	10	2	-62	0	2	-62	0	2	-62	0	2
-62	15	2	-62	10	2	-62	10	2	-62	10	2
-62	20	2	-62	20	2	-62	20	2	-62	20	2
-62	25	2	-62	30	2	-62	30	2	-62	30	2
-32,-2	0	1	-62	40	2	-32,-2	-20	1	-32	-30	1
-32,-2	5	1	-32,-2	-20	1	-32,-2	-10	1	-32	-20	1
-32,-2	10	1	-32,-2	-10	1	-32,-2	0	1	-32	0	1
-32,-2	15	1	-32,-2	0	1	-32,-2	10	1	-32	10	1
-32,-2	20	1	-32,-2	10	1	-32,-2	20	1	-32	20	1
-32,-2	25	1	-32,-2	20	1	-32,-2	30	1	-32	30	1
50,150	-66	1,5,11,17	-32,-2	30	1	50	-66	1,5,11,17	50	-66	1,5,11,17
50,150	-56	1,5,11,17	-32,-2	40	1	50	-50	1,5,11,17	50	-50	1,5,11,17
50,150	-50	1,5,11,17	50	-66	1,5,11,17	50	-33	1,5,11,17	50	-33	1,5,11,17
50,150	-33	1,5,11,17	50	-58	1,5,11,17	50	0	1,5,11,17	50	0	1,5,11,17
50,150	-28	1,5,11,17	50	-50	1,5,11,17	50	33	1,5,11,17	50	33	1,5,11,17
50,150	-25	1,5,11,17	50	-42	1,5,11,17	50	50	1,5,11,17	50	50	1,5,11,17
50,150	0	1,5,11,17	50	-33	1,5,11,17	50	66	1,5,11,17	50	66	1,5,11,17
50,150	11	1,5,11,17	50	-17	1,5,11,17	150	100	1,5,11,17	150	100	1,5,11,17
50,150	22	1,5,11,17	50	0	1,5,11,17	150	-84	1,5,11,17	150	-75	1,5,11,17
50,150	25	1,5,11,17	50	17	1,5,11,17	150	-75	1,5,11,17	150	-56	1,5,11,17
50,150	28	1,5,11,17	50	33	1,5,11,17	150	-56	1,5,11,17	150	-25	1,5,11,17
50,150	33	1,5,11,17	50	42	1,5,11,17	150	-28	1,5,11,17	150	0	1,5,11,17
			50	50	1,5,11,17	150	-25	1,5,11,17	150	25	1,5,11,17
			50	58	1,5,11,17	150	0	1,5,11,17	150	56	1,5,11,17
			50	66	1,5,11,17	150	25	1,5,11,17	150	75	1,5,11,17
			150	-80	1,5,11,17	150	28	1,5,11,17			
			150	-75	1,5,11,17	150	56	1,5,11,17			
			150	-56	1,5,11,17	150	75	1,5,11,17			
			150	-28	1,5,11,17	150	84	1,5,11,17			
			150	-25	1,5,11,17	150	100	1,5,11,17			
			150	-17	1,5,11,17						
			150	0	1,5,11,17						
			150	17	1,5,11,17						
			150	25	1,5,11,17						
			150	28	1,5,11,17						
			150	56	1,5,11,17						
			150	75	1,5,11,17						
			150	80	1,5,11,17						
			250	-58	1,5,11,17						
			250	-50	1,5,11,17						
			250	-33	1,5,11,17						
			250	-25	1,5,11,17						
			250	0	1,5,11,17						
			250	17	1,5,11,17						
			250	28	1,5,11,17						

LSR* = Length Scale Ratio

Table 9 Measurement Locations of Laboratory Tests: Falcon 4 with Freon-12, Array Angle = 235°T

LSR* = 150			LSR = 200		
X(m)	Y(m)	Z(m)	X(m)	Y(m)	Z(m)
-62	-20	2	-62	-30	2
-62	-10	2	-62	-20	2
-62	0	2	-62	0	2
-62	10	2	-62	10	2
-62	20	2	-62	20	2
-62	30	2	-62	30	2
-32,-2	-20	1	-32,-2	-30	1
-32,-2	-10	1	-32,-2	-20	1
-32,-2	0	1	-32,-2	0	1
-32,-2	10	1	-32,-2	10	1
-32,-2	20	1	-32,-2	20	1
-32,-2	30	1	-32,-2	30	1
50	-75	1,5,11,17	50	-75	1,5,11,17
50	-66	1,5,11,17	50	-50	1,5,11,17
50	-50	1,5,11,17	50	-25	1,5,11,17
50	-33	1,5,11,17	50	0	1,5,11,17
50	-25	1,5,11,17	50	25	1,5,11,17
50	0	1,5,11,17	50	50	1,5,11,17
50	25	1,5,11,17	150	-75	1,5,11,17
50	33	1,5,11,17	150	-56	1,5,11,17
50	50	1,5,11,17	150	-25	1,5,11,17
50	66	1,5,11,17	150	0	1,5,11,17
50	75	1,5,11,17	150	25	1,5,11,17
150	-75	1,5,11,17	150	56	1,5,11,17
150	-56	1,5,11,17	250	-75	1,5,11,17
150	-50	1,5,11,17	250	-56	1,5,11,17
150	-28	1,5,11,17	250	-25	1,5,11,17
150	-25	1,5,11,17	250	0	1,5,11,17
150	0	1,5,11,17	250	25	1,5,11,17
150	25	1,5,11,17	250	56	1,5,11,17
150	28	1,5,11,17			
150	50	1,5,11,17			
150	56	1,5,11,17			
150	75	1,5,11,17			
250	-75	1,5,11,17			
250	-50	1,5,11,17			
250	-33	1,5,11,17			
250	-25	1,5,11,17			
250	0	1,5,11,17			
250	25	1,5,11,17			

LSR* = Length Scale Ratio

Table 10 Measurement Locations of Laboratory Tests: Falcon 5, Array Angle = 225°T

LSR* = 100			LSR = 150			LSR = 200		
X(m)	Y(m)	Z(m)	X(m)	Y(m)	Z(m)	X(m)	Y(m)	Z(m)
-62	-20	2	-62	-20	2	-62	-30	2
-62	-10	2	-62	-10	2	-62	-20	2
-62	0	2	-62	0	2	-62	0	2
-62	10	2	-62	10	2	-62	10	2
-62	20	2	-62	20	2	-62	20	2
-62	30	2	-62	30	2	-62	30	2
-62	40	2	-32,-2	-20	1	-32	-30	1
-32,-2	-20	1	-32,-2	-10	1	-32	-20	1
-32,-2	-10	1	-32,-2	0	1	-32	0	1
-32,-2	0	1	-32,-2	10	1	-32	10	1
-32,-2	10	1	-32,-2	20	1	-32	20	1
-32,-2	20	1	-32,-2	30	1	-32	30	1
-32,-2	30	1	50	-66	1,5,11,17	50	-66	1,5,11,17
-32,-2	40	1	50	-50	1,5,11,17	50	-50	1,5,11,17
50	-75	1,5,11,17	50	-33	1,5,11,17	50	-33	1,5,11,17
50	-66	1,5,11,17	50	0	1,5,11,17	50	0	1,5,11,17
50	-56	1,5,11,17	50	33	1,5,11,17	50	33	1,5,11,17
50	-44	1,5,11,17	50	50	1,5,11,17	50	50	1,5,11,17
50	-33	1,5,11,17	50	66	1,5,11,17	50	66	1,5,11,17
50	-22	1,5,11,17	150	-84	1,5,11,17	150	-84	1,5,11,17
50	0	1,5,11,17	150	-75	1,5,11,17	150	-56	1,5,11,17
50	22	1,5,11,17	150	-56	1,5,11,17	150	-28	1,5,11,17
50	33	1,5,11,17	150	-50	1,5,11,17	150	0	1,5,11,17
50	44	1,5,11,17	150	-25	1,5,11,17	150	28	1,5,11,17
50	56	1,5,11,17	150	0	1,5,11,17	150	56	1,5,11,17
50	66	1,5,11,17	150	25	1,5,11,17	150	84	1,5,11,17
50	75	1,5,11,17	150	50	1,5,11,17			
150	-84	1,5,11,17	150	56	1,5,11,17			
150	-75	1,5,11,17	150	75	1,5,11,17			
150	-56	1,5,11,17	150	84	1,5,11,17			
150	-50	1,5,11,17						
150	-33	1,5,11,17						
150	-28	1,5,11,17						
150	0	1,5,11,17						
150	28	1,5,11,17						
150	33	1,5,11,17						
150	50	1,5,11,17						
150	56	1,5,11,17						
150	75	1,5,11,17						
150	84	1,5,11,17						
250	0	1,5,11,17						
250	22	1,5,11,17						
250	33	1,5,11,17						
250	44	1,5,11,17						
250	56	1,5,11,17						
250	66	1,5,11,17						
250	75	1,5,11,17						

LSR* = Length Scale Ratio

Table 11 Run Conditions of Plume Visualization

Test	Length Scale	Source Combination	Array Angle
Falcon 4	100	100% P	225°
	100	100% S	225°
	100	50% P + 50% S	225°
	100	100% P	235°
	100	100% S	235°
	100	50% P + 50% S	235°

S: Spider
P: Plenum

Table 12 Description of Concentration Variables

Variables used in the text	Variables used by Ermak and Merry* (1988)	Definition
$C(x,y,z)_i$	$C(x,y,z)$	measured concentration at (x,y,z) for a realization i for all times
$C_p(x,y,z)_i$		measured peak concentrations at (x,y,z) for all realizations and all times
MAX $C_p(x,y,z)$		the maximum of peak concentrations at (x,y,z) for all realizations and all times
$C_p(x)$	$C^m(x)$	the measured peak concentration at downwind distance x
$\overline{C}_p$	$\overline{C}$	mean of peak concentrations for all realizations and all times
$(\overline{C}_{MAX})_{i,T}$	C_{MAX}	the maximum of a time averaged concentrations for a realization i for all times with an averaging time T
MAX $[\overline{C}_{MAX}(x,y,z)]_T$		the maximum of $\overline{C}_{MAX}$ at (x,y,z) for all realizations and all times with an averaging time T
$[\overline{C}_{MAX}(x,y,z)]_{T,E}$		mean of $\overline{C}_{MAX}(x,y,z)$ for all realizations and all times with an averaging time T

*: Ermak, D.L., and Merry, M.H., "A Methodology for evaluating Heavy Gas Dispersion Models," February, 1988.

FIGURES

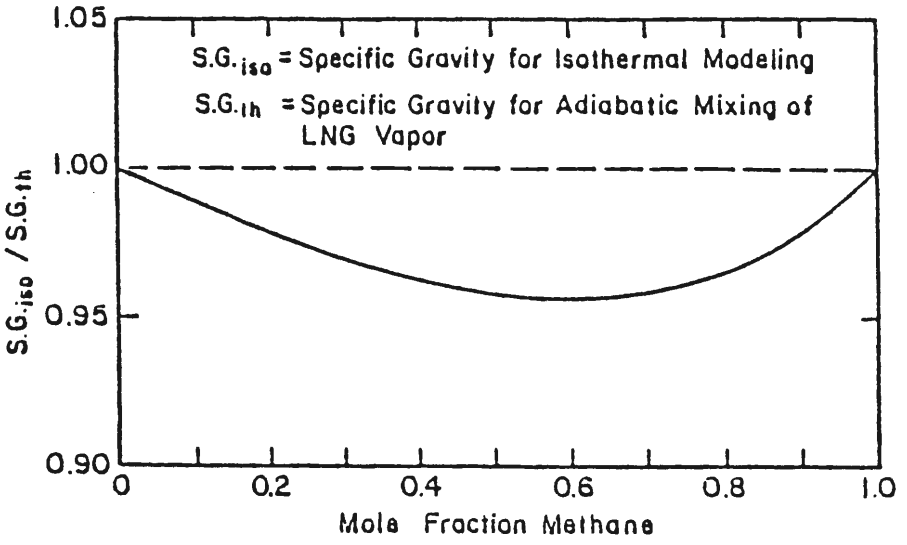

Figure 1 Specific gravity deviation in an isothermal model of LNG vapor dispersion

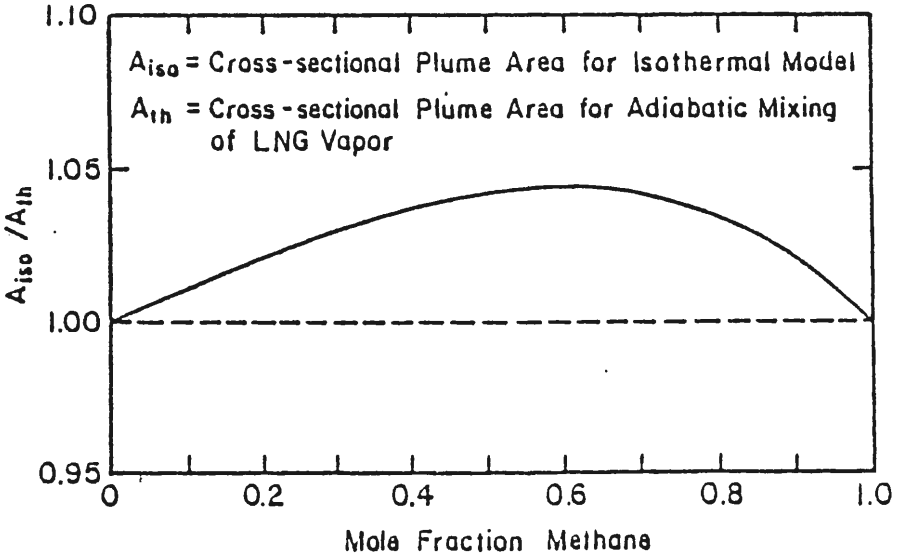

Figure 2 Plume cross-sectional area deviation in an isothermal model of LNG vapor dispersion

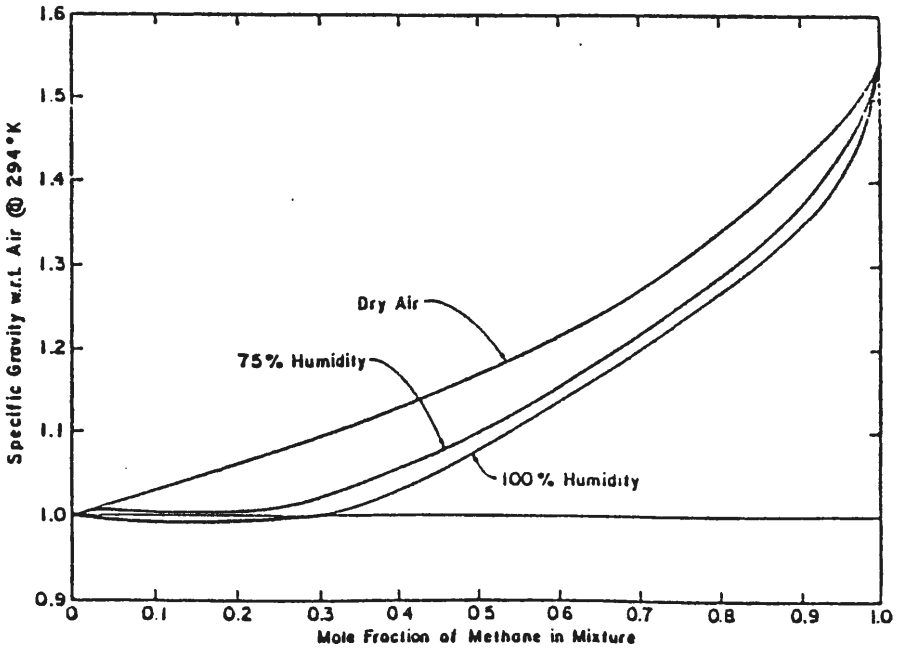

Figure 3 Specific gravity of LNG vapor-humid atmosphere mixtures

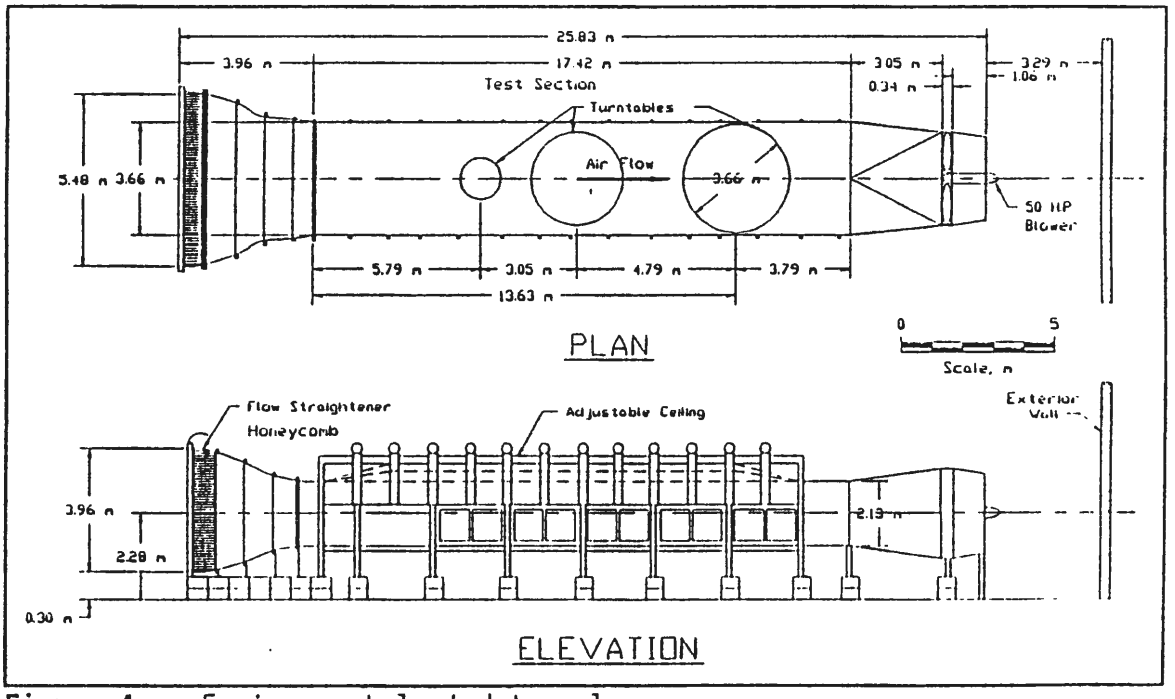

Figure 4 Environmental wind tunnel

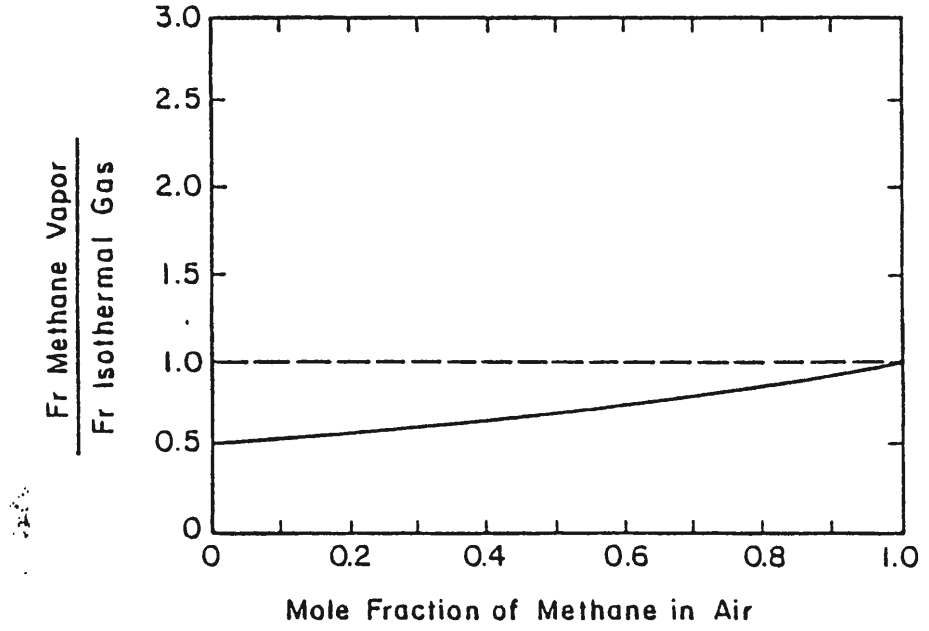

Figure 5 Variation of isothermal plume behavior from equivalent cold methane plume behavior

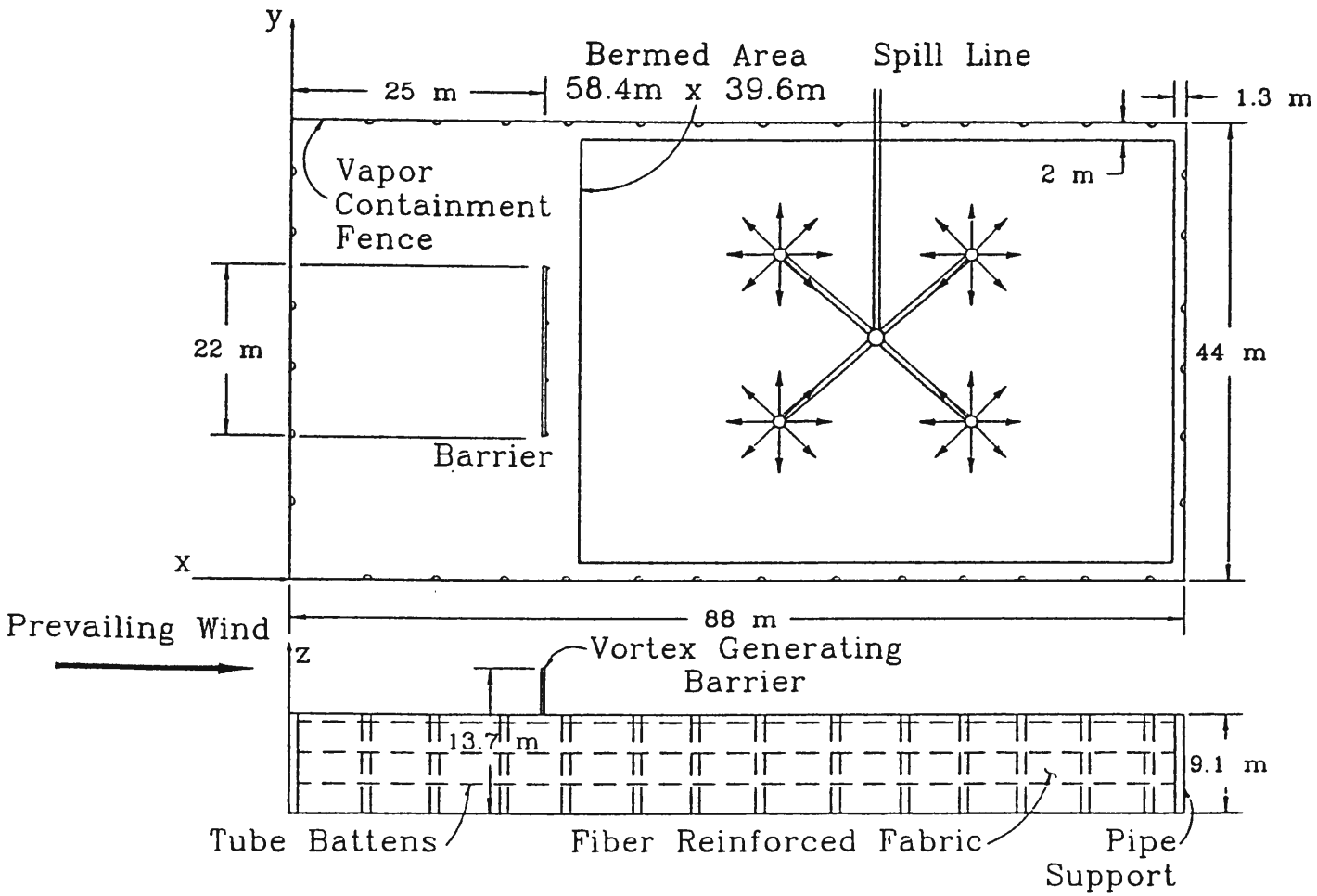

Figure 6 Field test facility

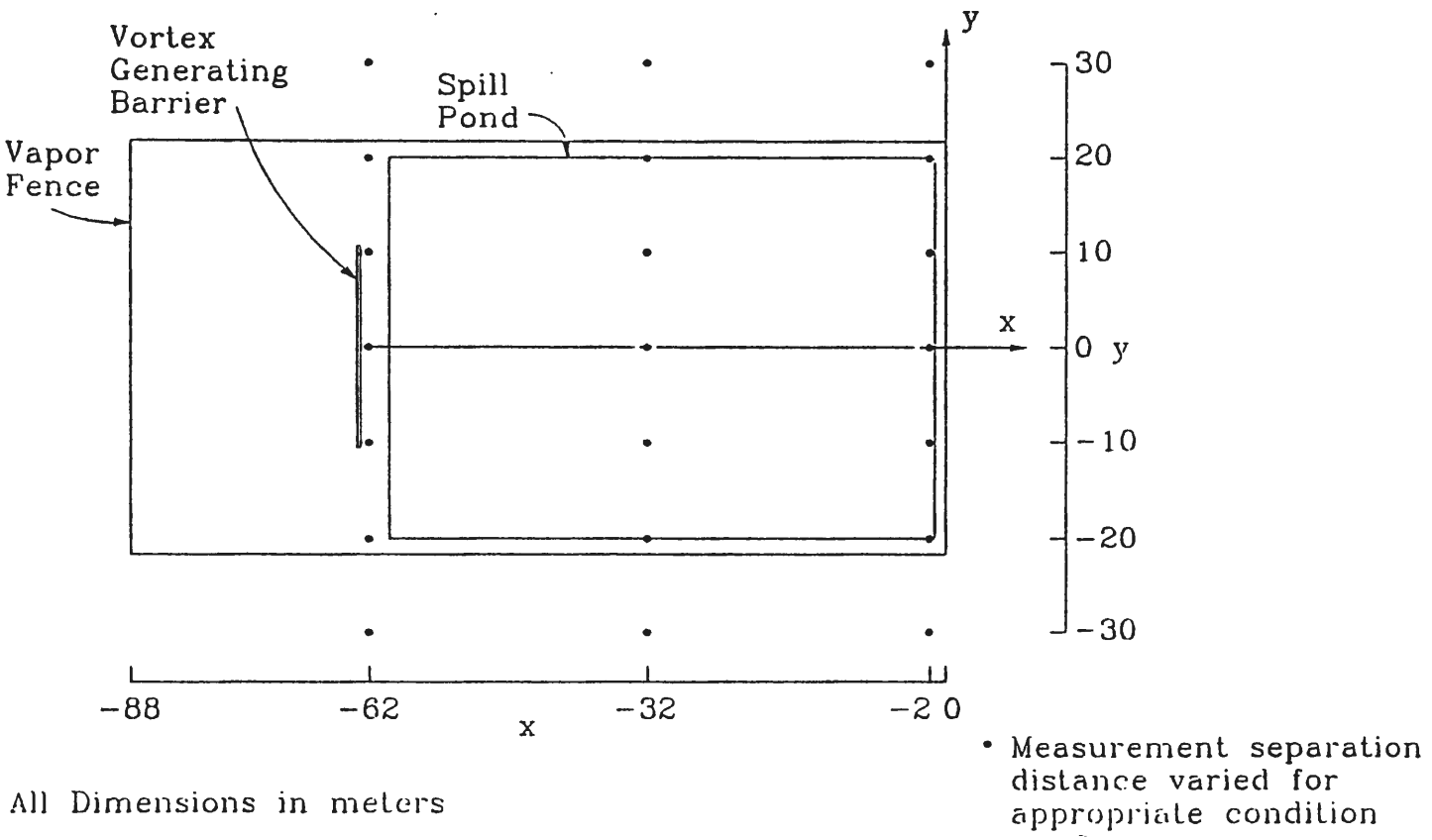

Figure 7 Concentration measurement locations: inside fence

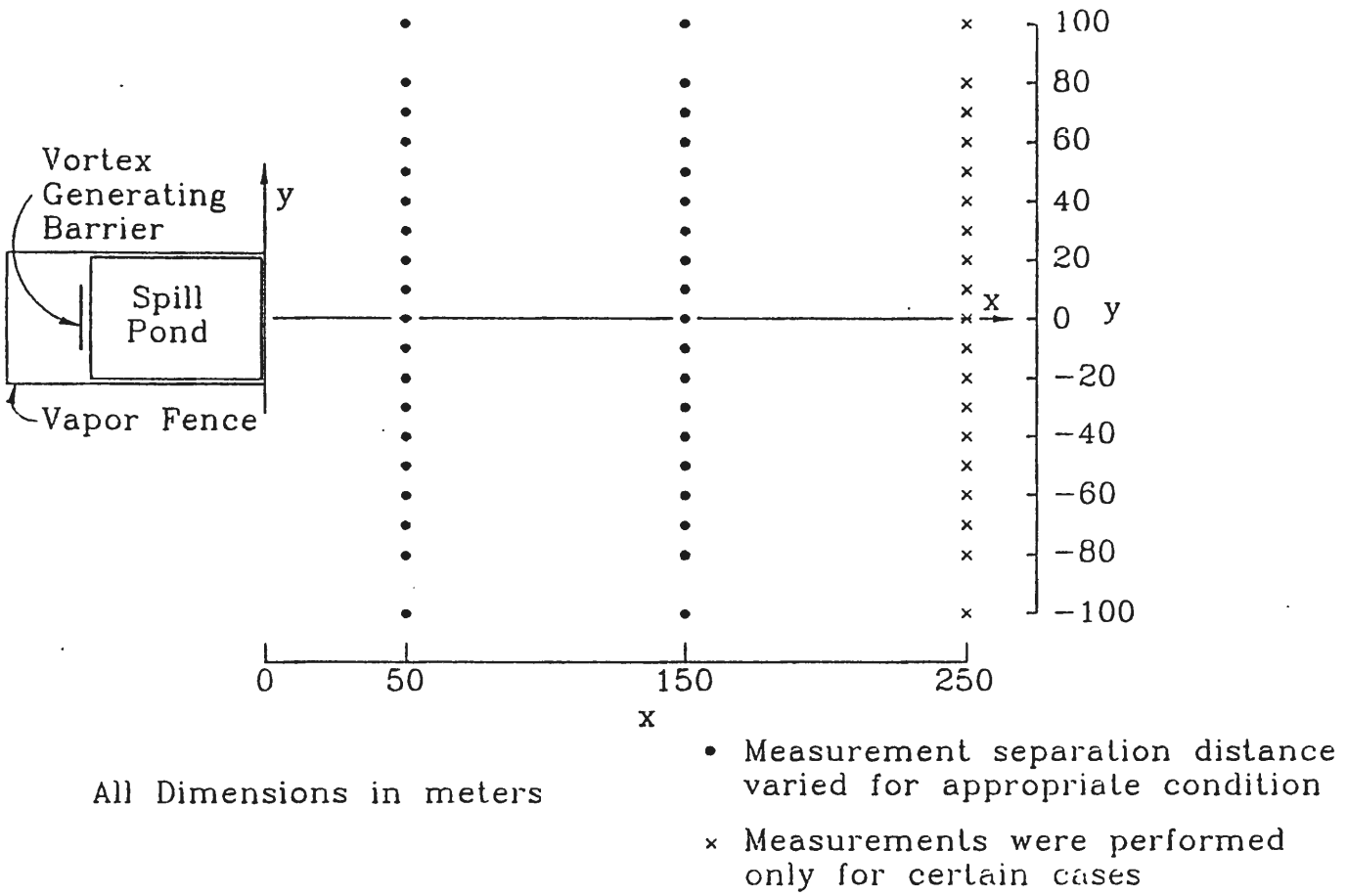

Figure 8 Concentration measurement locations: outside fence

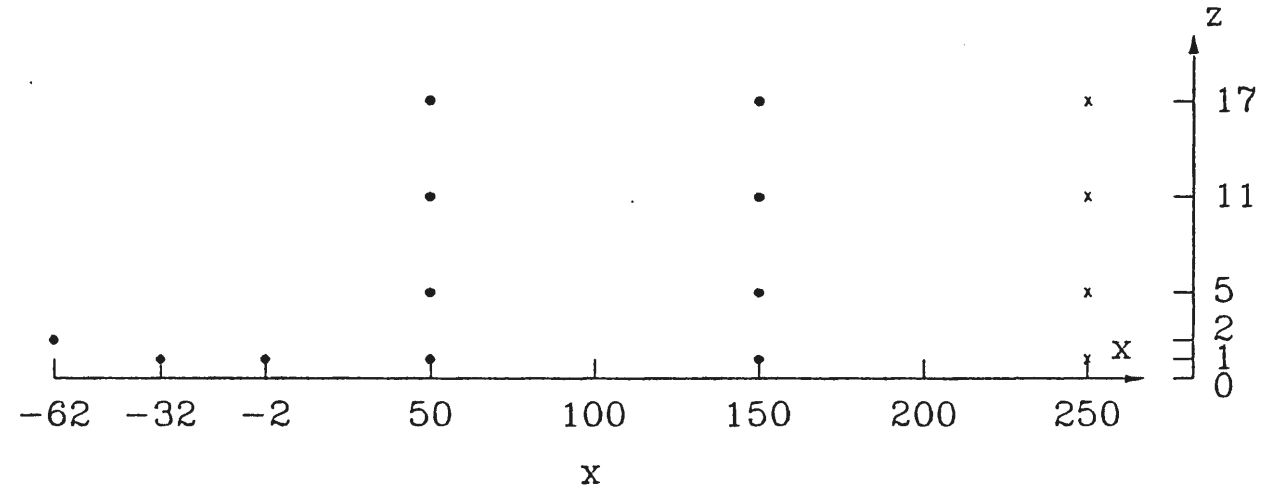

All Dimensions in meters

• Measurement points for all cases

x Measurements were performed only for certain cases

Figure 9 Concentration measurement locations: vertical locations

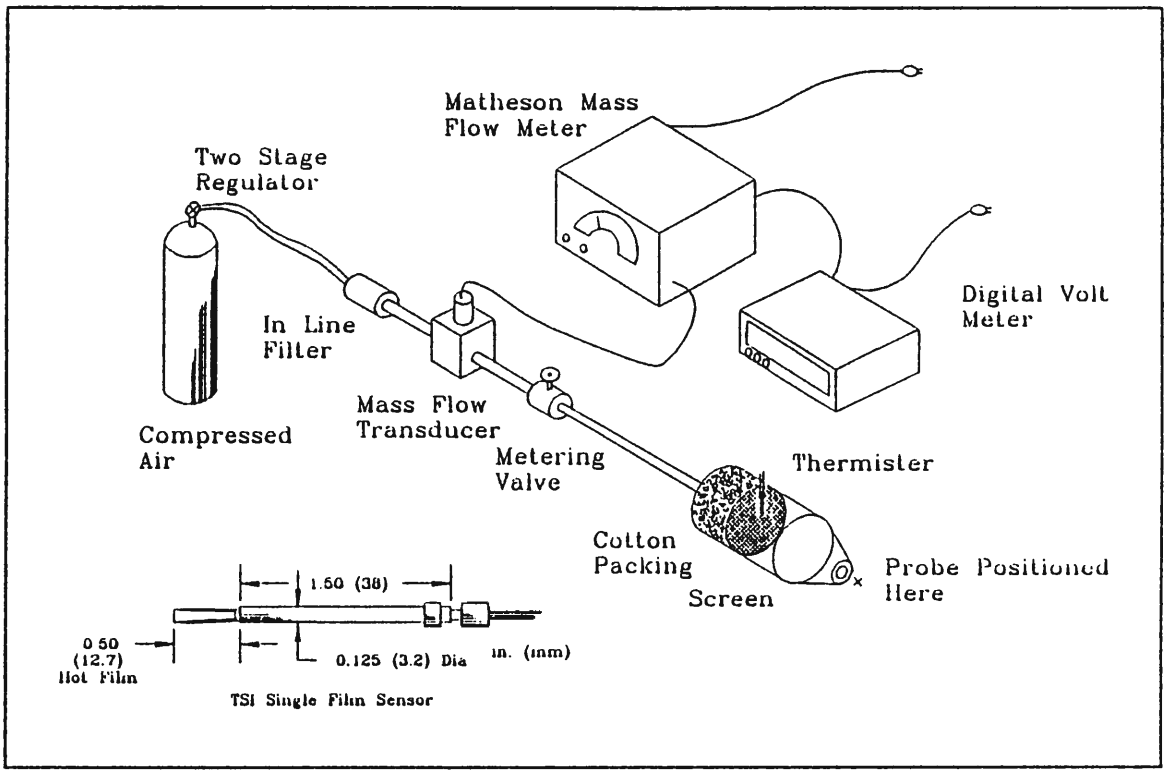

Figure 10 Velocity probes and velocity standard

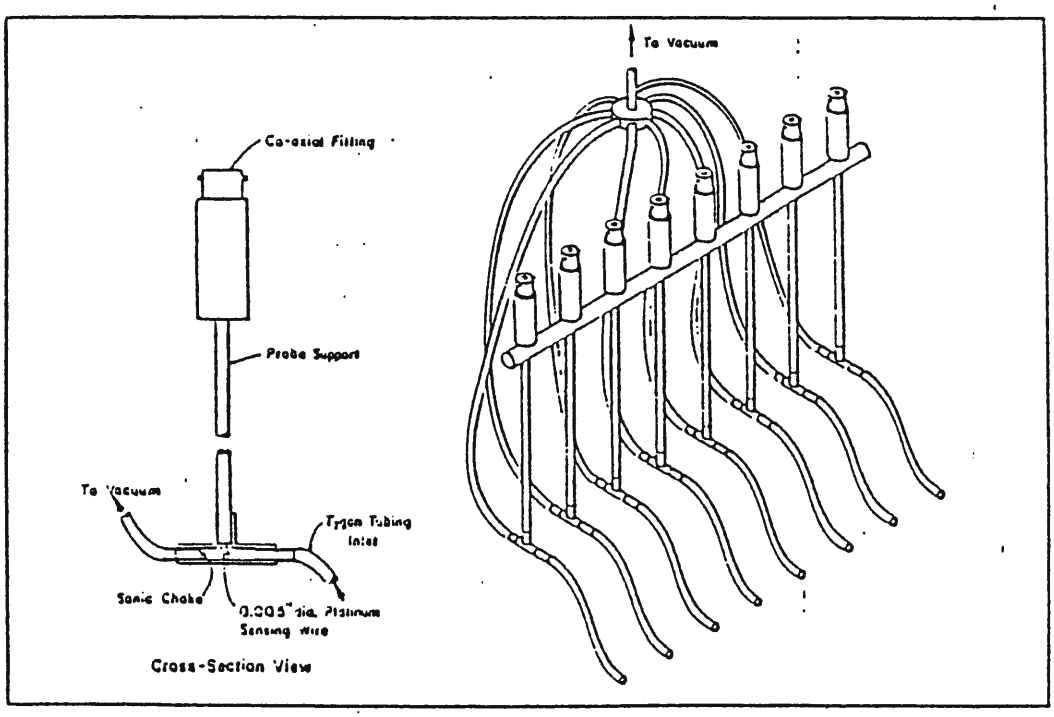

Figure 11 Hot-Wire katharometer probes

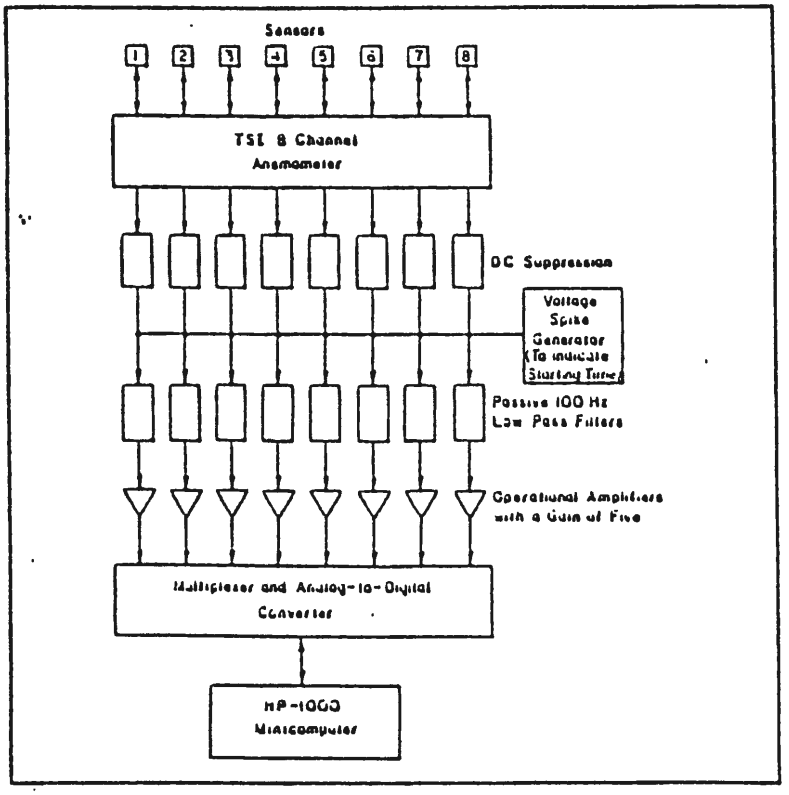

Figure 12 Block diagram for katharometer data reduction

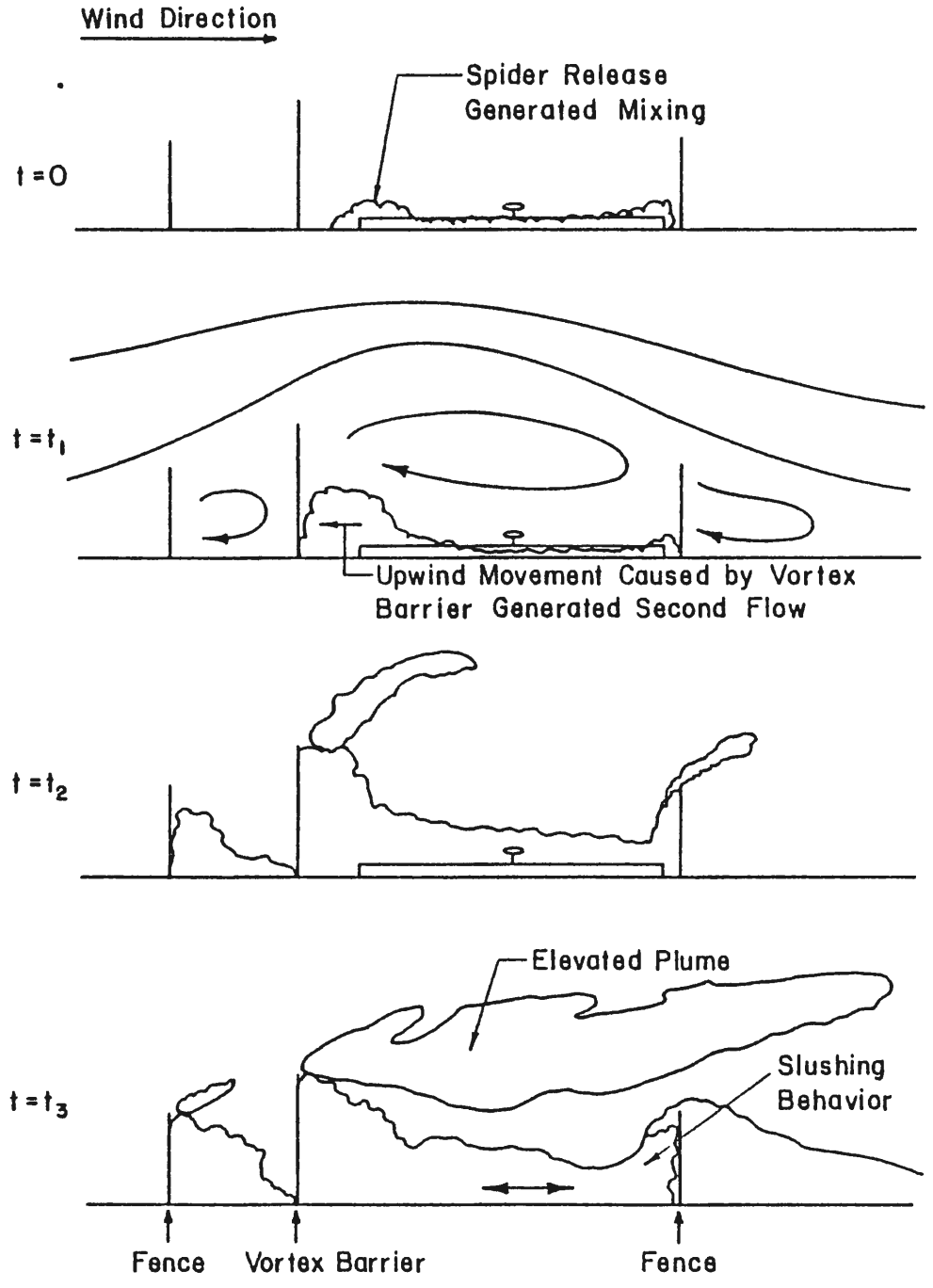

Figure 13 Sketch of plume behavior as time progresses ($0<t_1<t_2<t_3$)

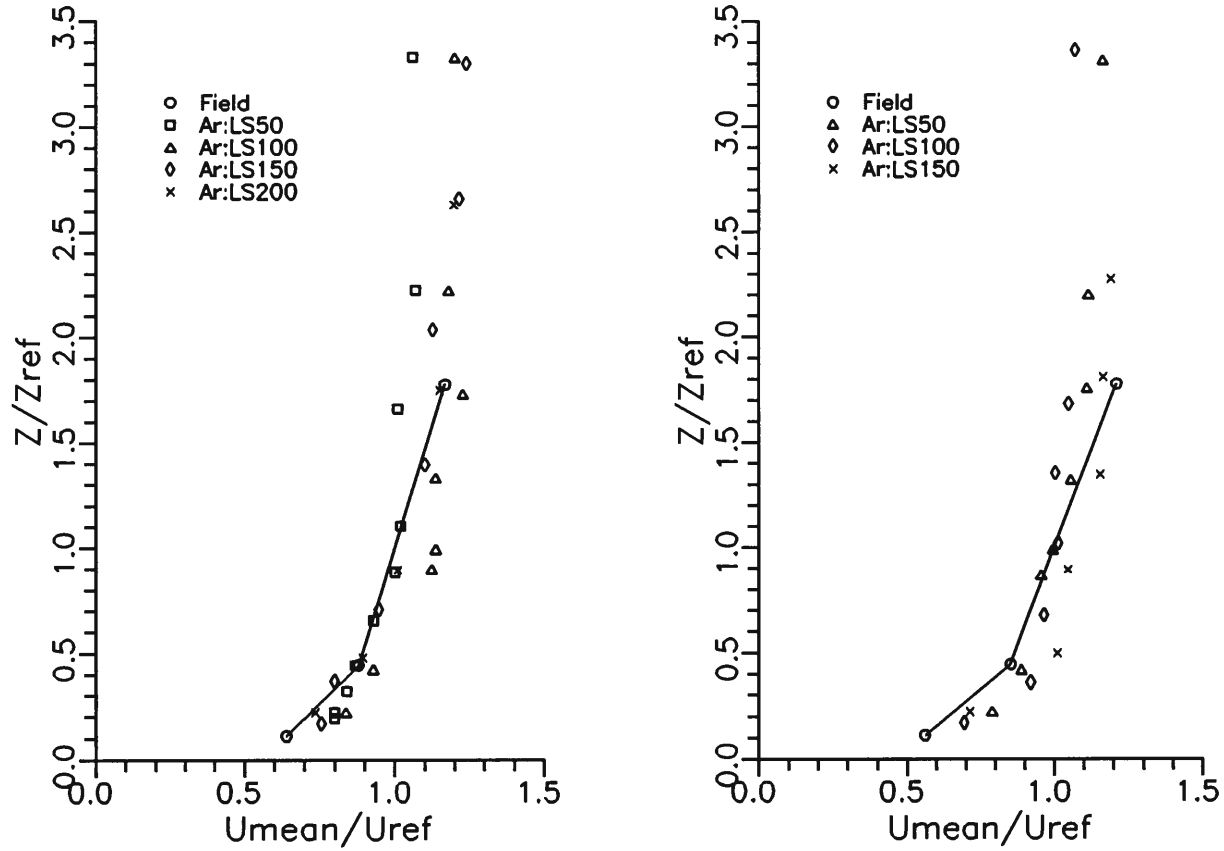

Figure 14 Mean velocity profile comparison between the model and field data: Falcon 4 and Falcon 5 tests

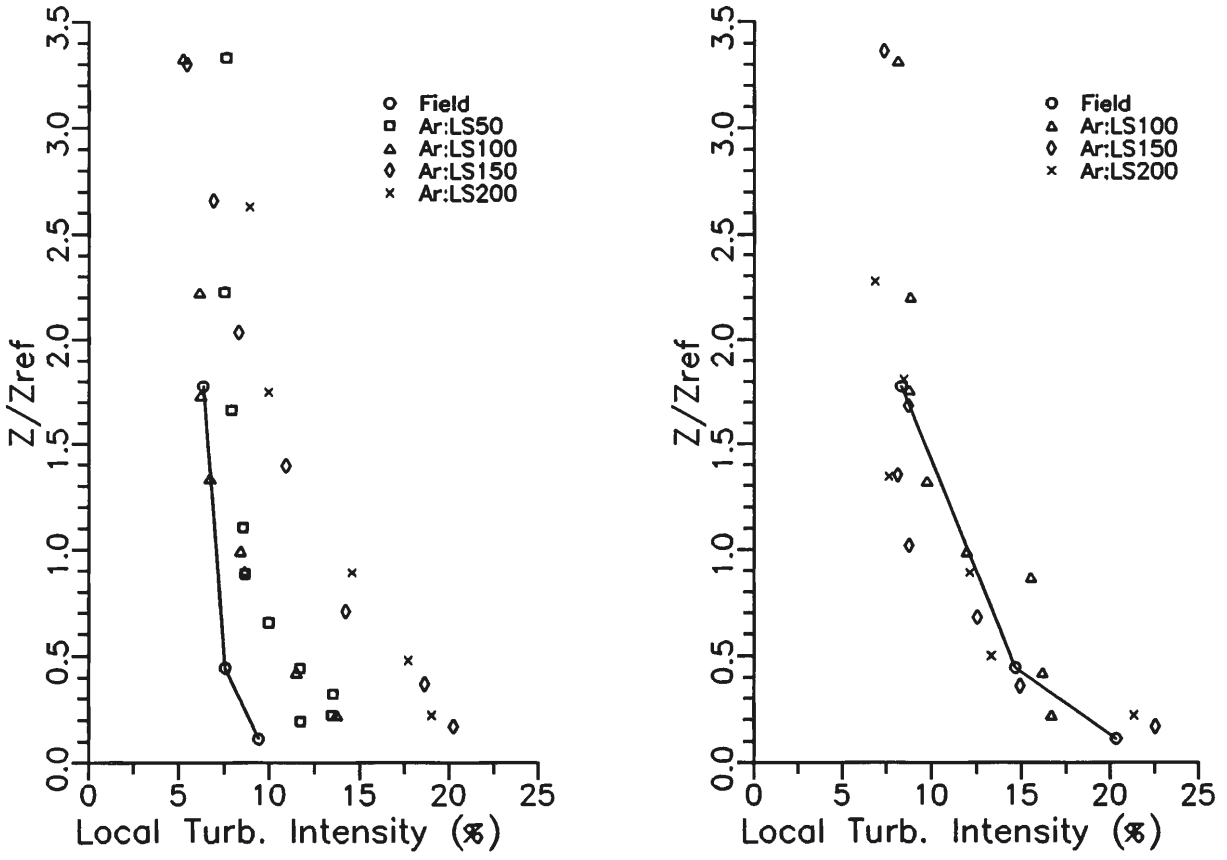

Figure 15 Turbulent intensity profile comparison between the model and field data: Falcon 4 and Falcon 5 tests

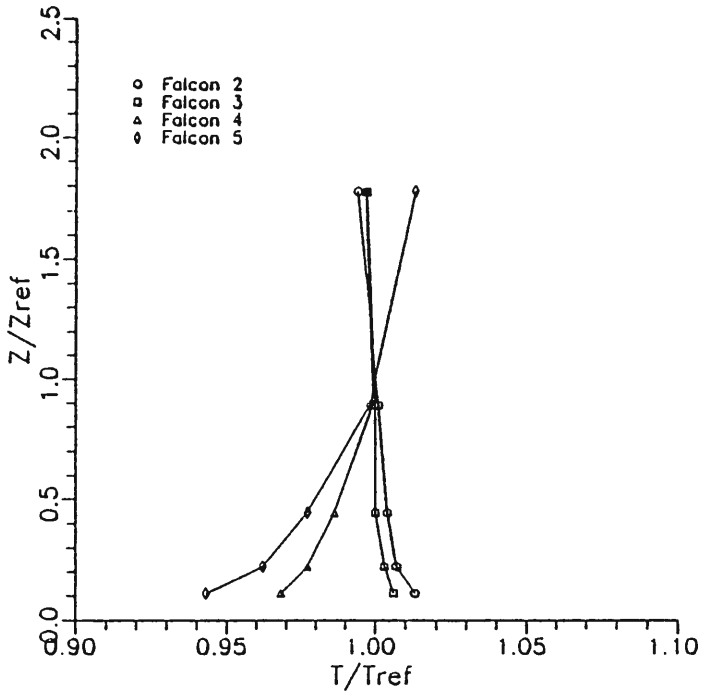

Figure 16 Temperature profiles during Falcon experiments 2 to 5: $T_{ref,2}$ = 31.4°C, $T_{ref,3}$ = 34.8°C, $T_{ref,4}$ = 31.8°C, $T_{ref,5}$ = 32.9°C, and Z_{ref} = 9 m

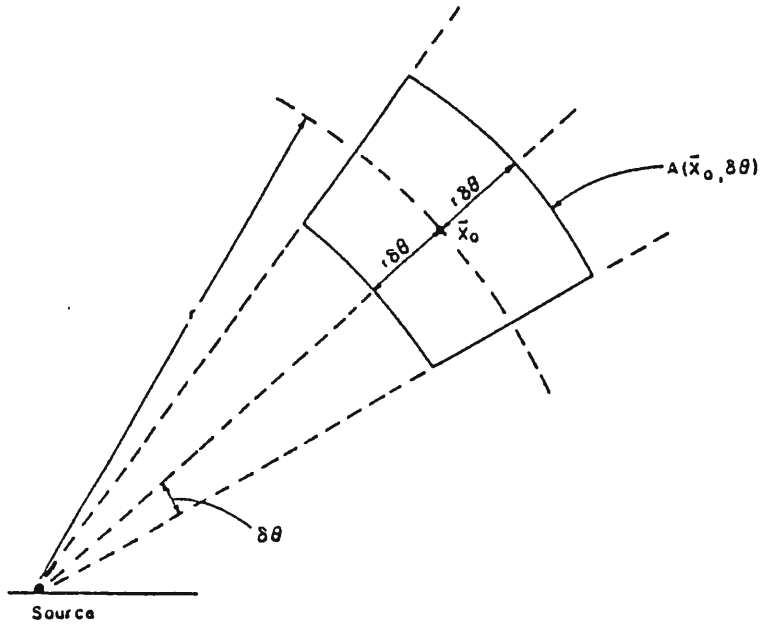

Figure 17 Schematic of the area segment $A(x_i, \alpha\theta)$

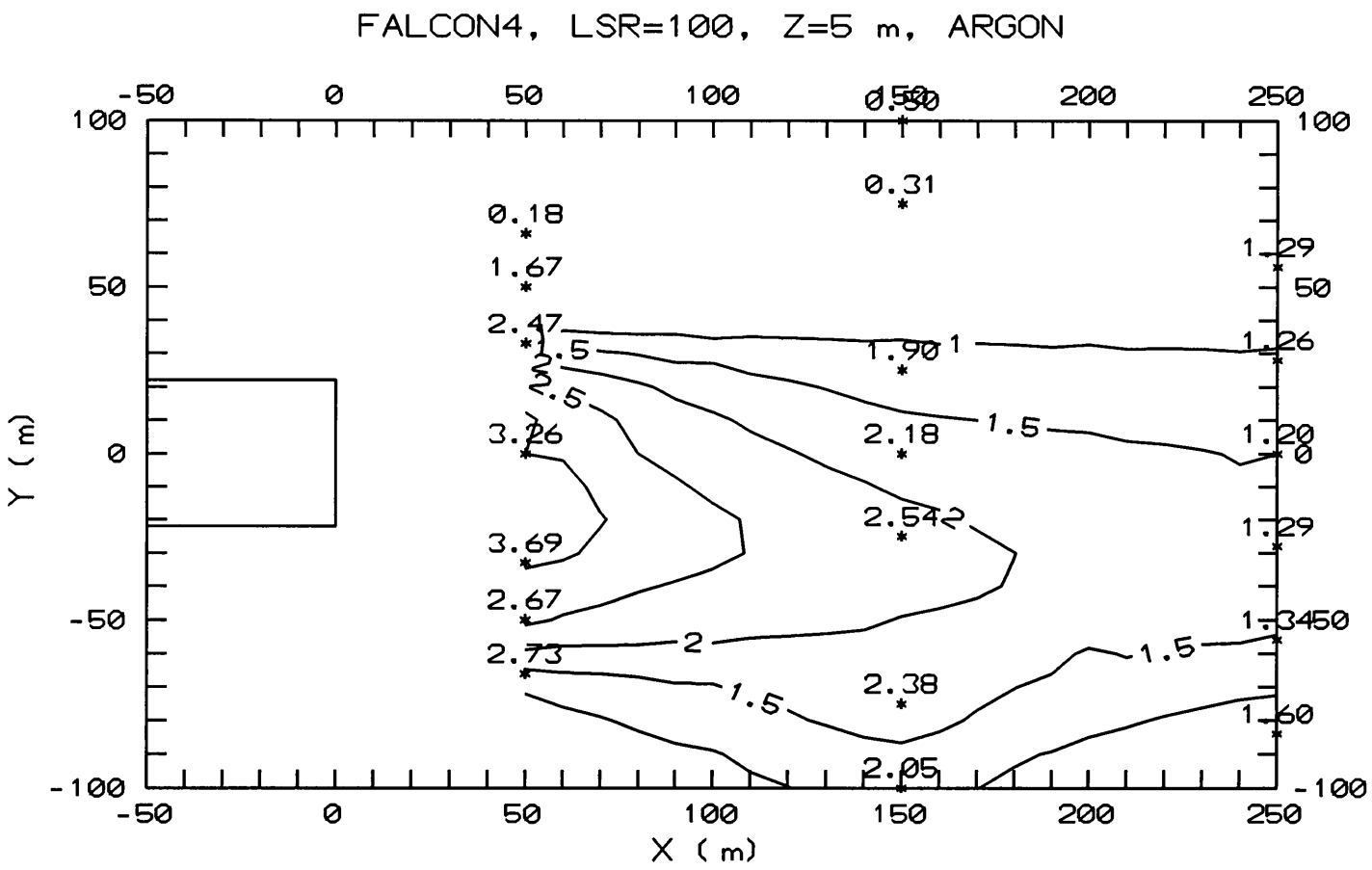

Figure 18 Lateral concentration distribution comparison between the model (contour) and the field data (numbers) at Z=5 m: Falcon 4, Argon gas, LSR=100

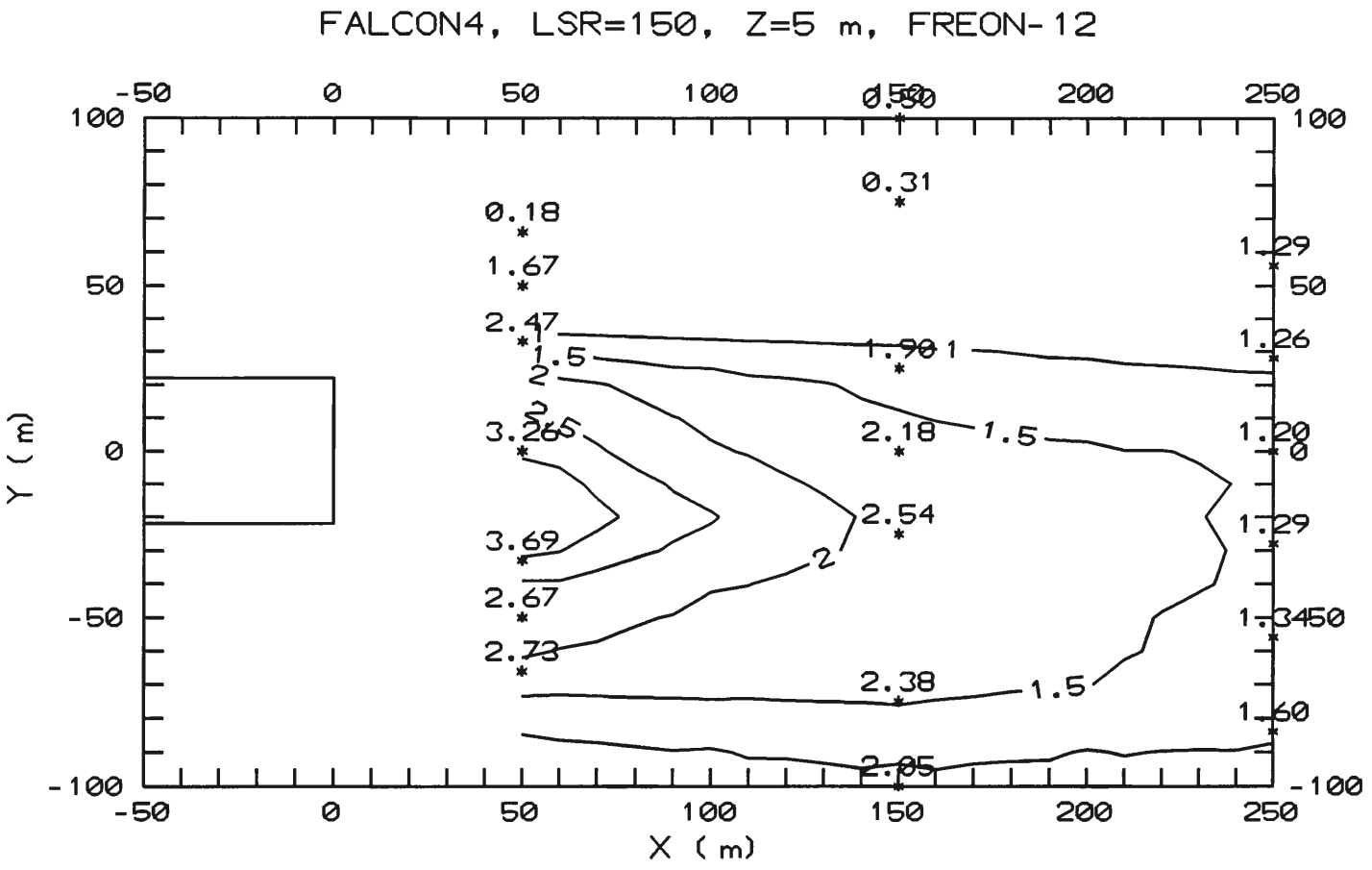

Figure 19 Lateral concentration distribution comparison between the model (contour) and the field data (numbers) at Z=5 m: Falcon 4, Freon-12 Gas, LSR=150

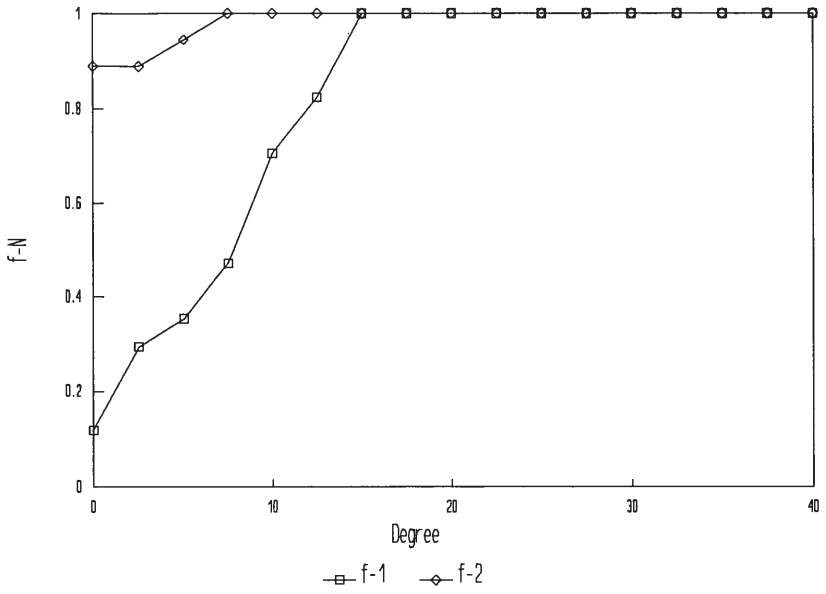

Figure 20 Pattern comparison plot: Falcon 4, Argon gas, LSR=100, Z=5 m

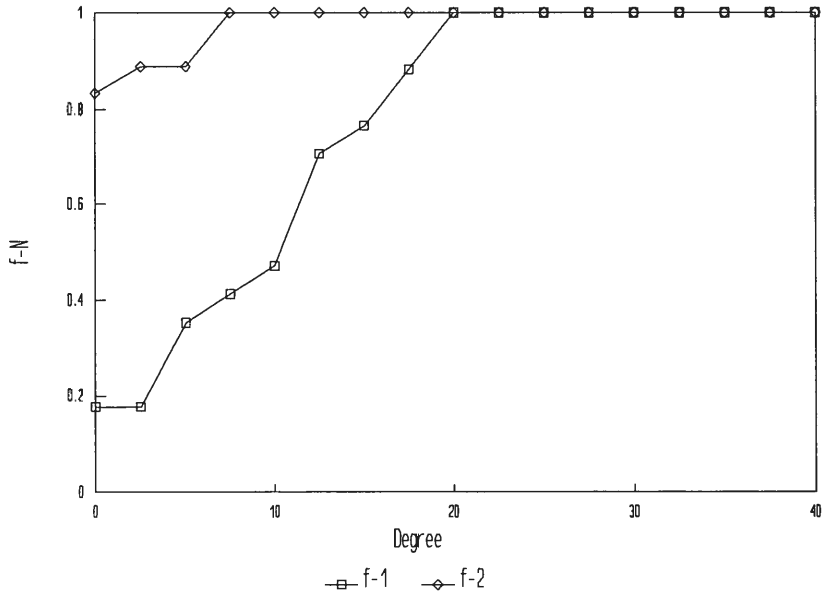

Figure 21 Pattern comparison plot: Falcon 4 (Freon-12), LSR=150, Z=5 m

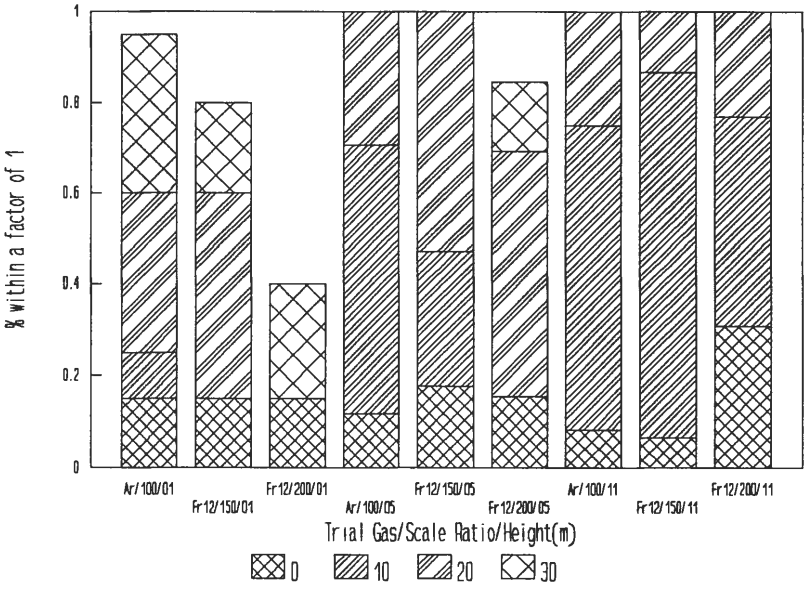

Figure 22 Pattern comparison test summary bar chart for % compatibility of factor 1 at θ angles between 0° and 30°

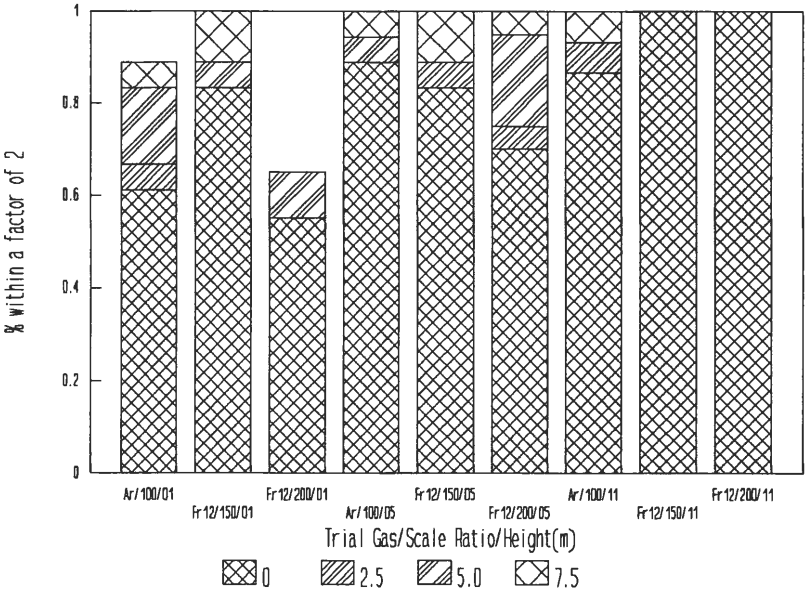

Figure 23 Pattern comparison test summary bar chart for % compatibility of factor 2 at θ angles between 0° and 7.5°

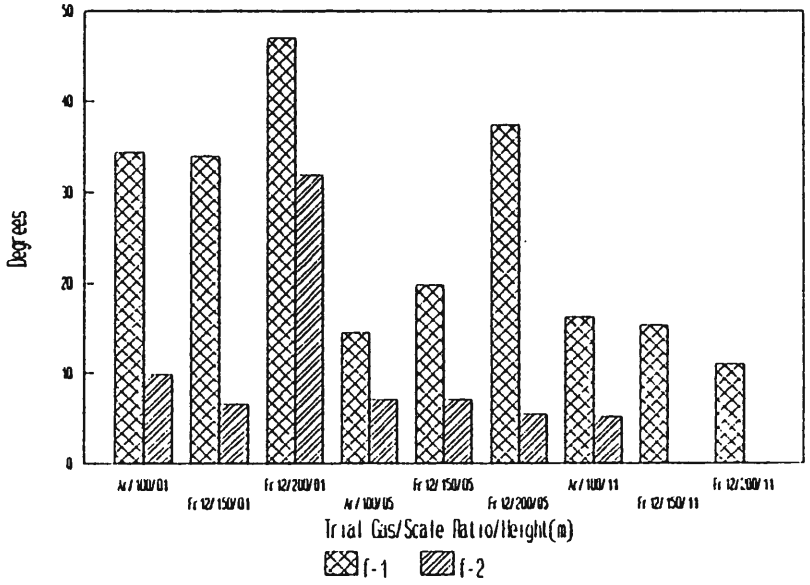

Figure 24 Pattern comparison test summary bar chart for θ intercept (degrees)

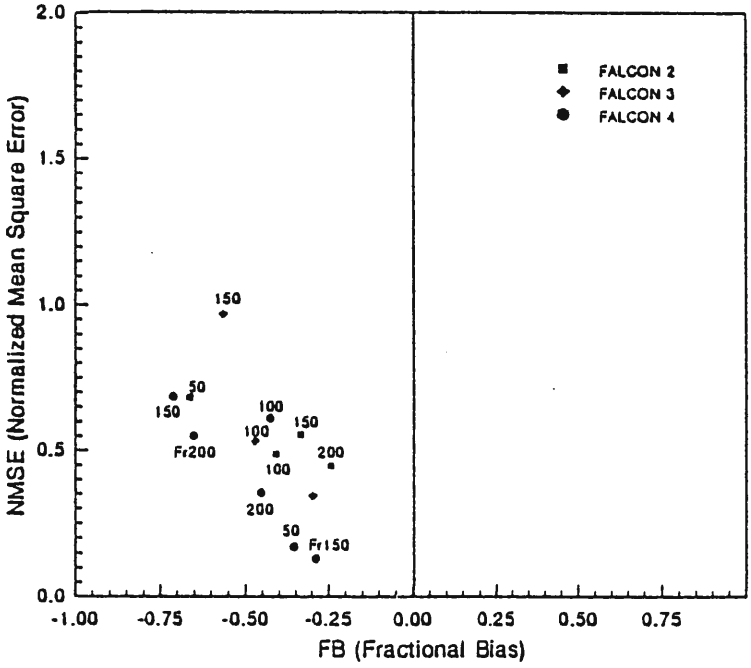

Figure 25 Weighted average Fractional Bias, FB, and Normalized Mean Square Error, NMSE, for peak concentration predictions fot Falcon Experiments 2 to 4

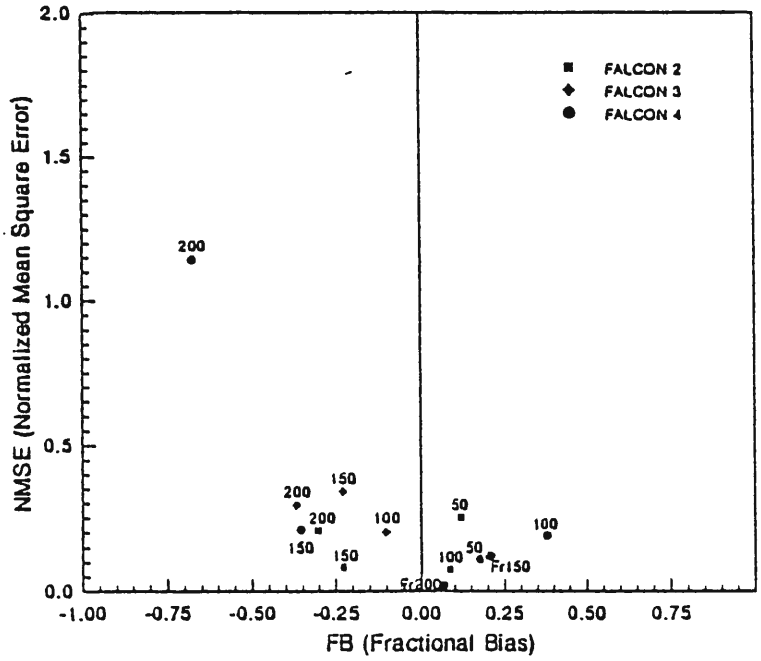

Figure 26 Weighted average Fractional Bias, FB, and Normalized Mean Square Error, NMSE, for arrival time of $0.2C_{MAX}$ for Falcon experiments 2 to 4

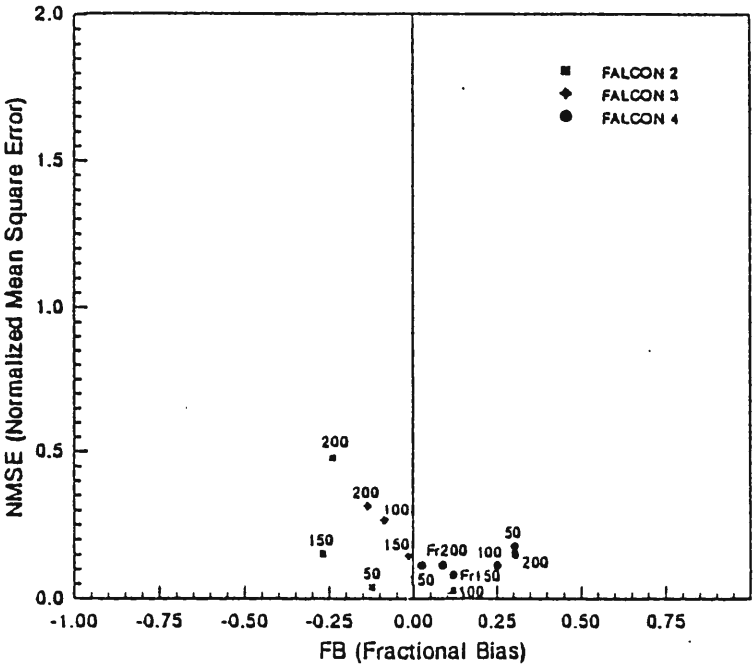

Figure 27 Weighted average Fractional Bias, FB, and Normalized Mean Square Error, NMSE, for arrival time of max. concentration predictions for Falcon experiments 2 to 4

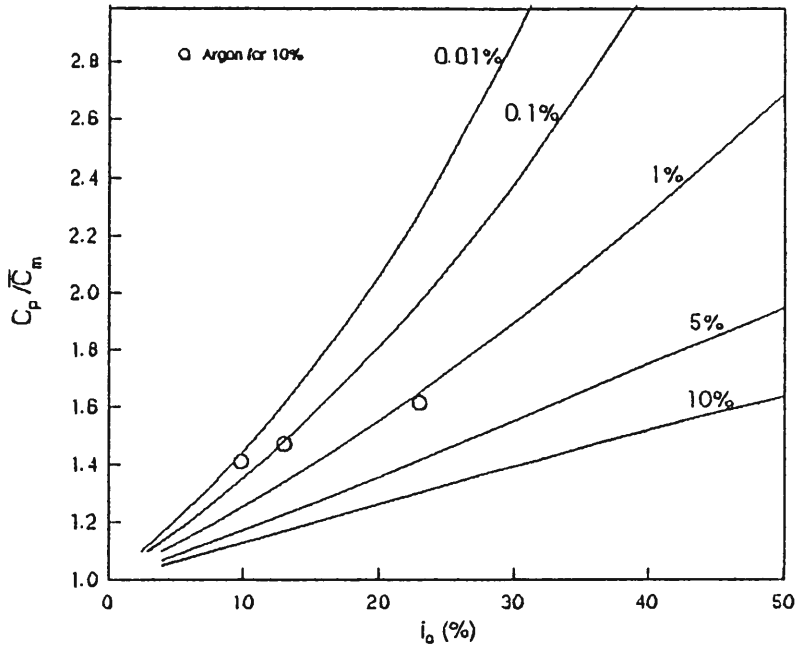

Figure 28 Peak-to-mean concentration ratio versus concentration intensity for several probability levels

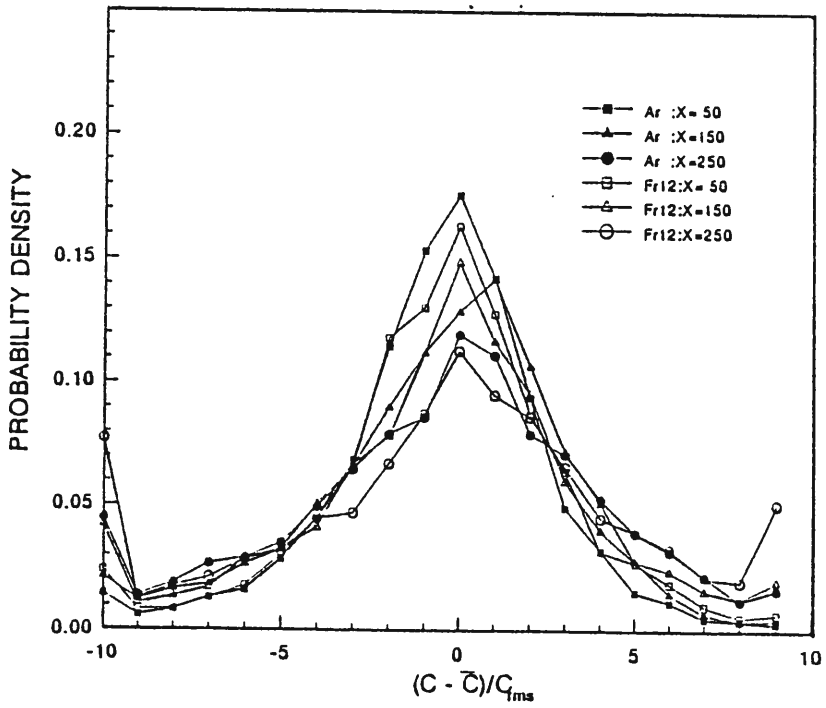

Figure 29 Probability density plot from Argon gas and Freon-12 gas from the first method

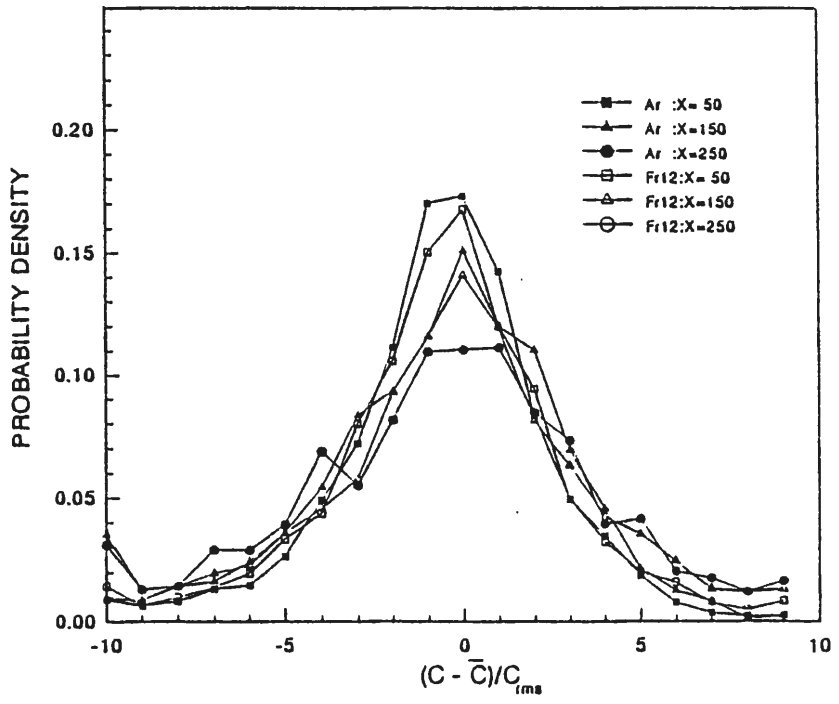

Figure 30 Probability density plot from Argon gas and Freon-12 gas from the second method

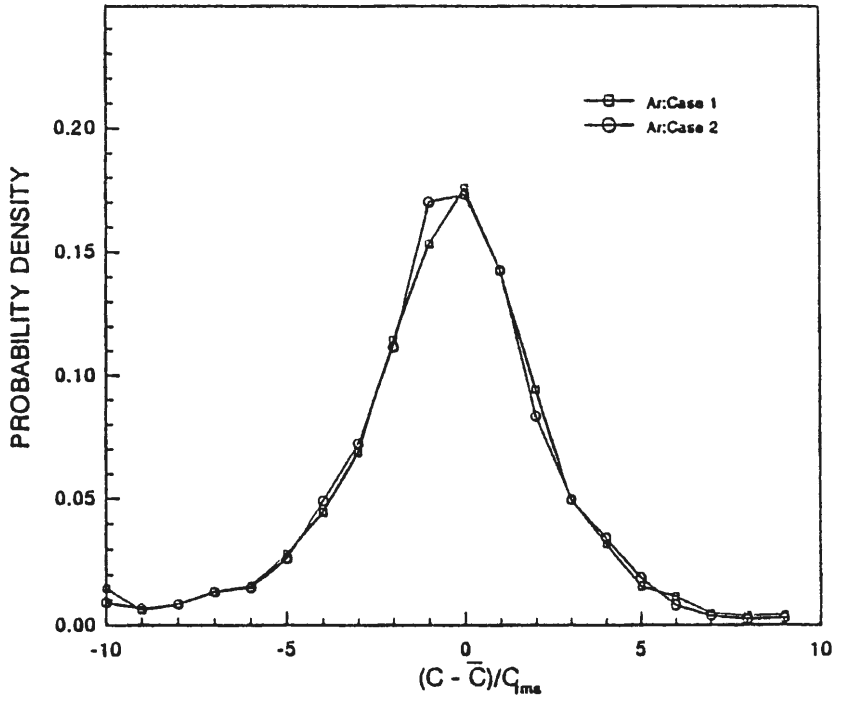

Figure 31 Comparison of probability distribution curves from the first and the second method : Argon gas

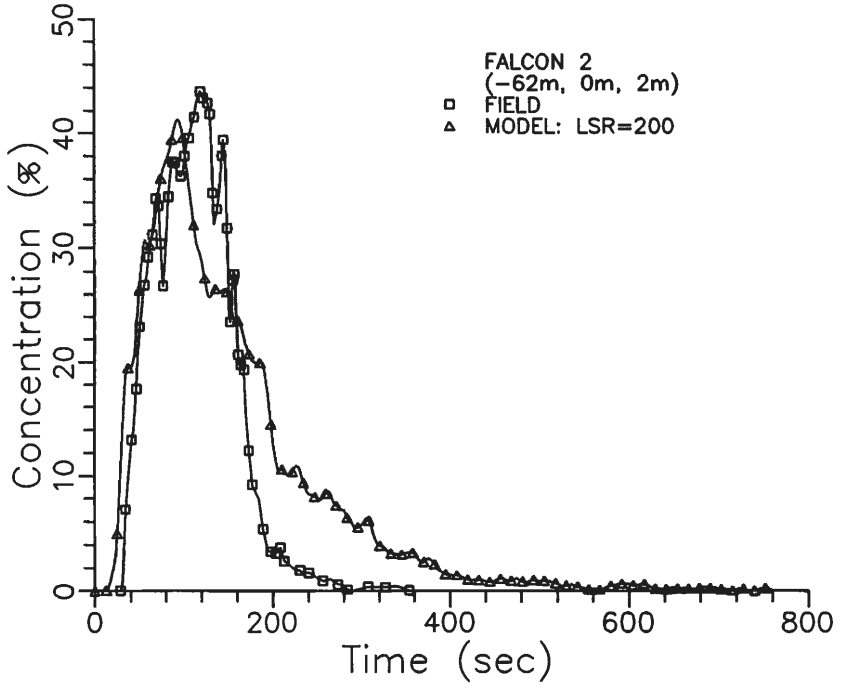

Figure 32 Concentration time history comparison at (-62 m, 0 m, 2 m) for Falcon 2 test

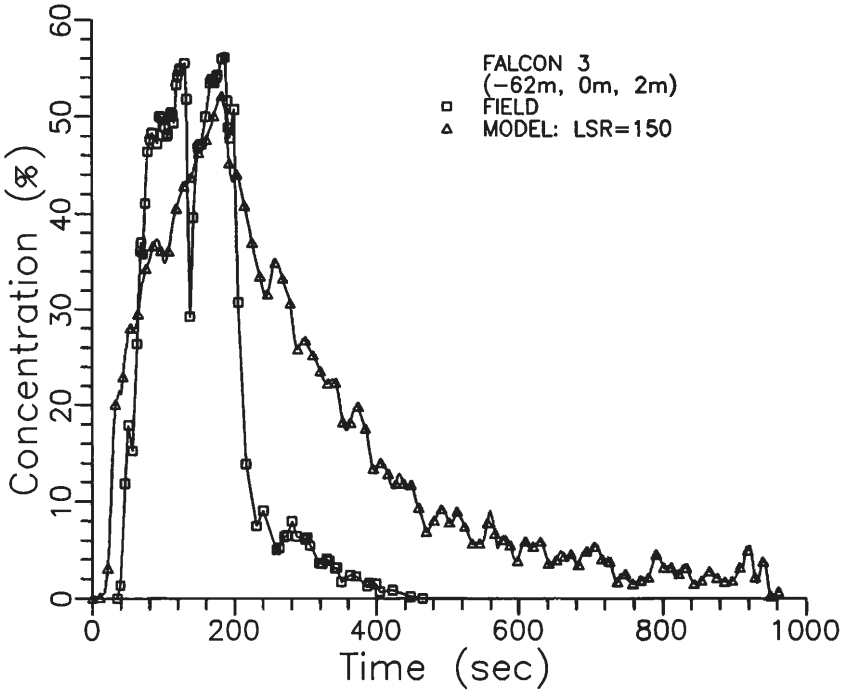

Figure 33 Concentration time history comparison at (-62 m, 0 m, 2 m) for Falcon 3 test

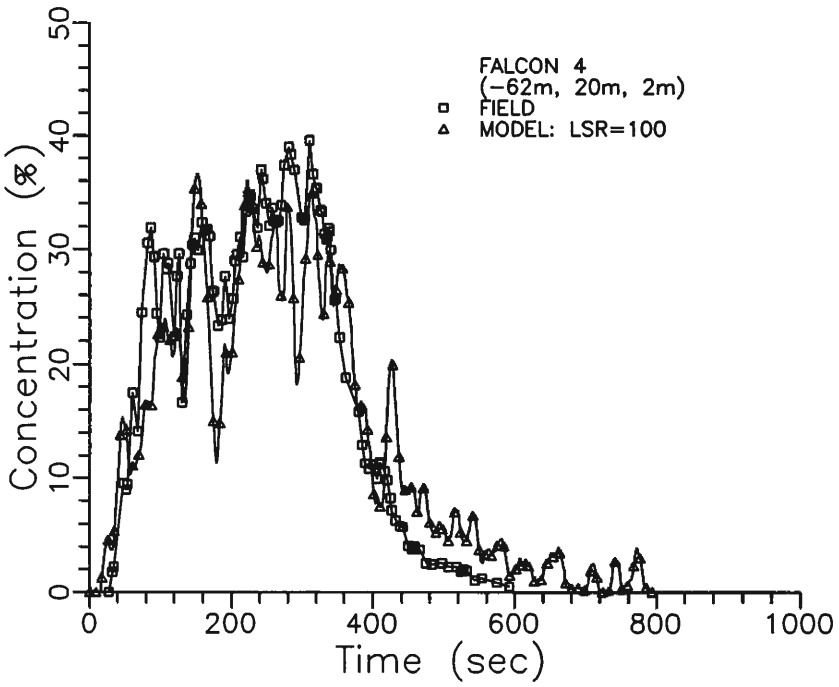

Figure 34 Concentration time history comparison at (-62 m, 20 m, 2 m) for Falcon 4 test

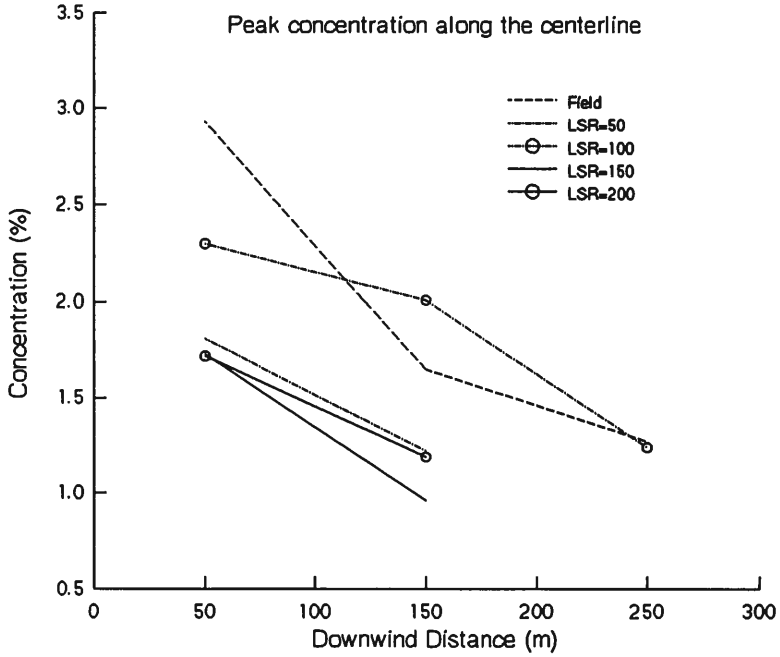

Figure 35 Peak concentration comparison along the centerline for all model scales for Falcon 4 simulations at Z = 5 m

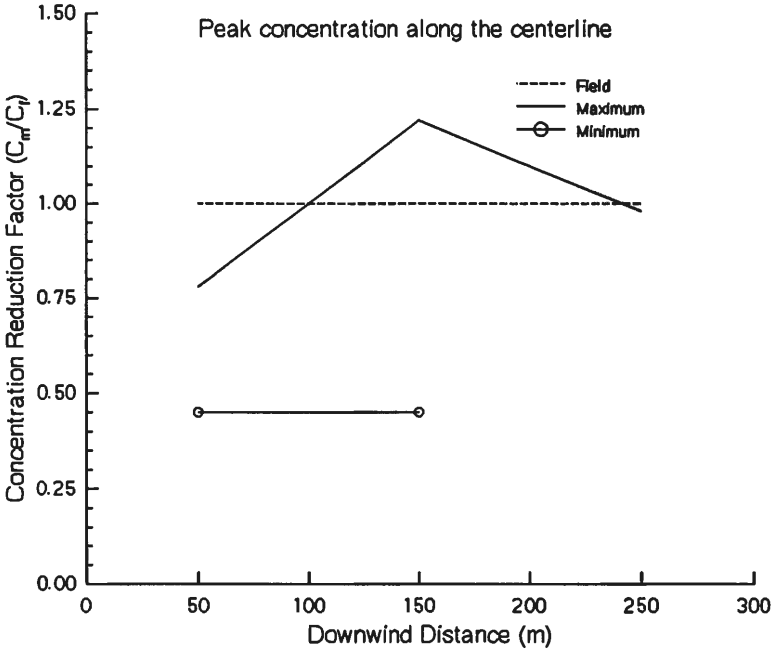

Figure 36 Peak concentration reduction factor comparison for all model scales of Falcon 4 simulations along the centerline at Z = 5 m

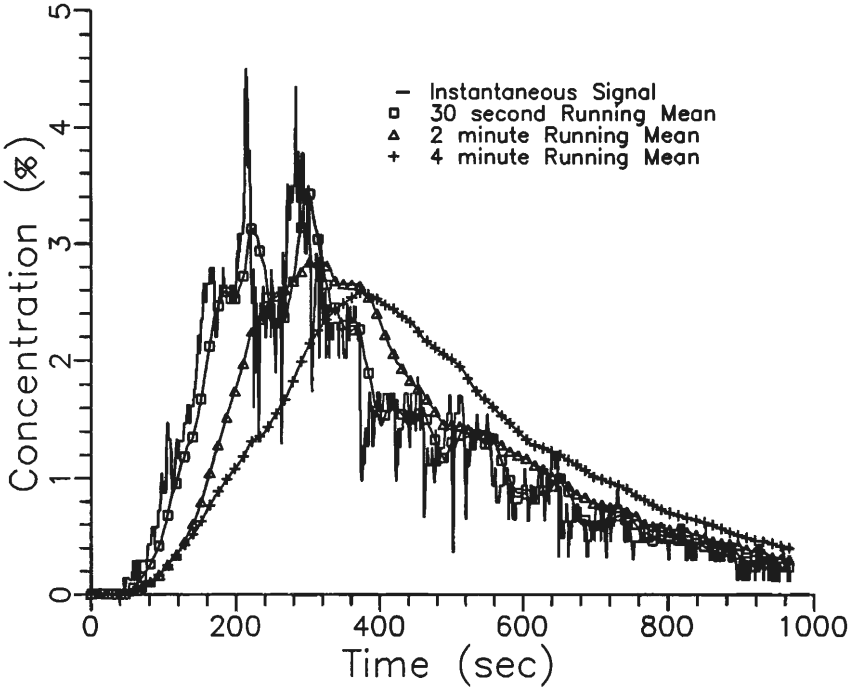

Figure 37 Concentration time history comparison between 30 sec, 2 min, and 4 min averaging times

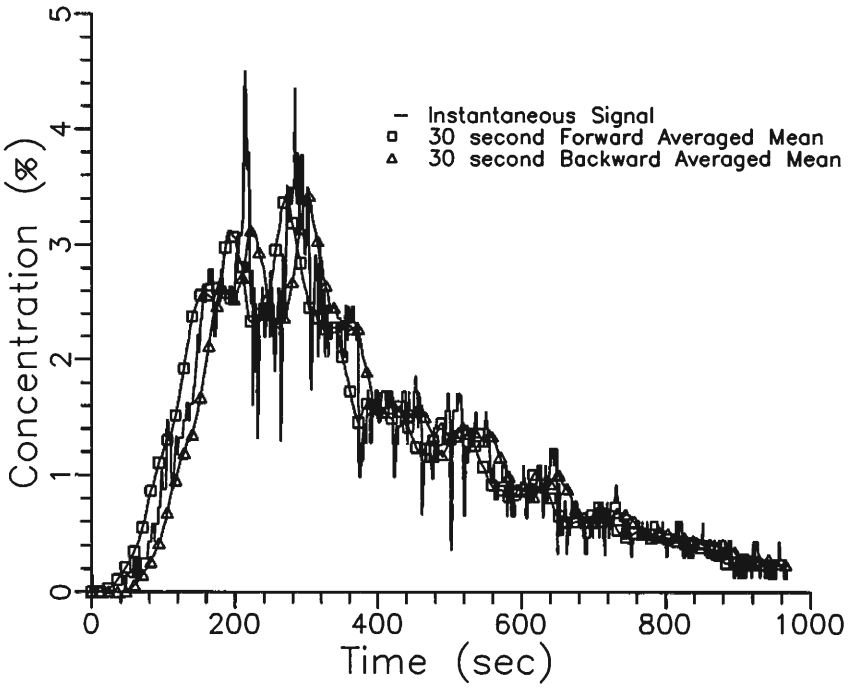

Figure 38 Concentration time history comparison between 30 sec forward and 30 sec backward averaging schemes

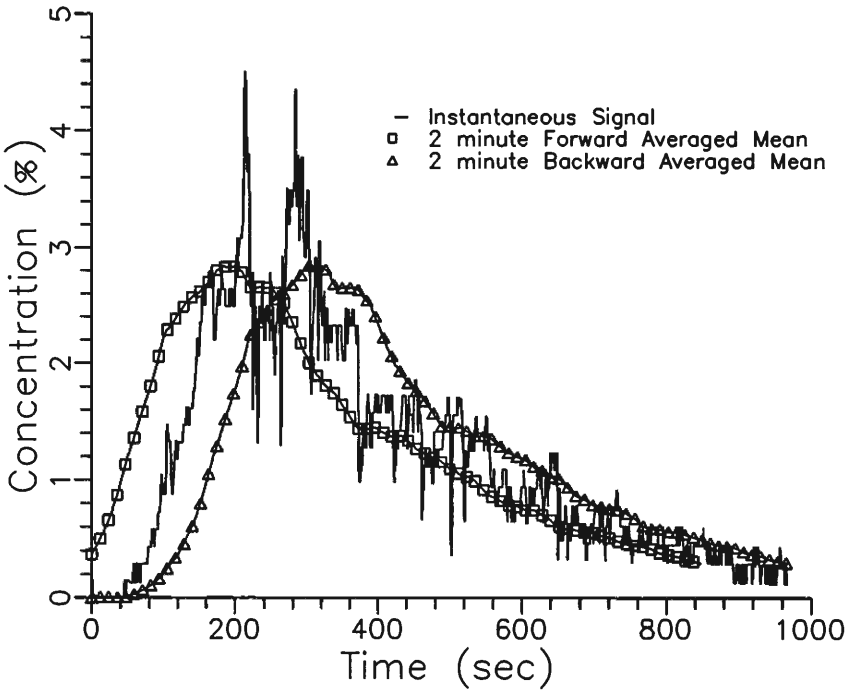

Figure 39 Concentration time history comparison between 2 min forward and 2 min backward averaging scheme

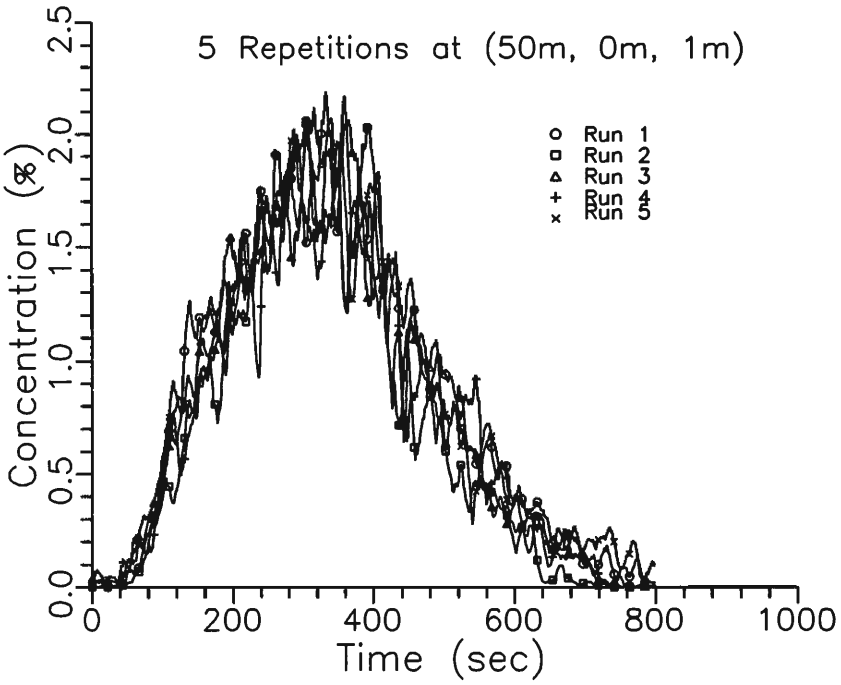

Figure 40 Concentration time history comparison between five repetitions at (50 m, 0 m, 1 m): Falcon 4, LSR=100

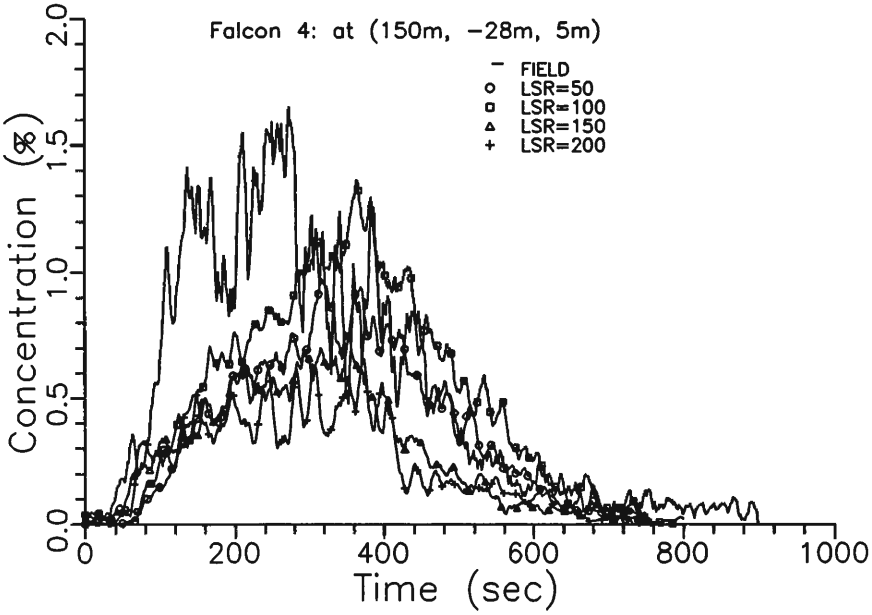

Figure 41 Concentration time history comparison between all model scales for Falcon 4 simulations

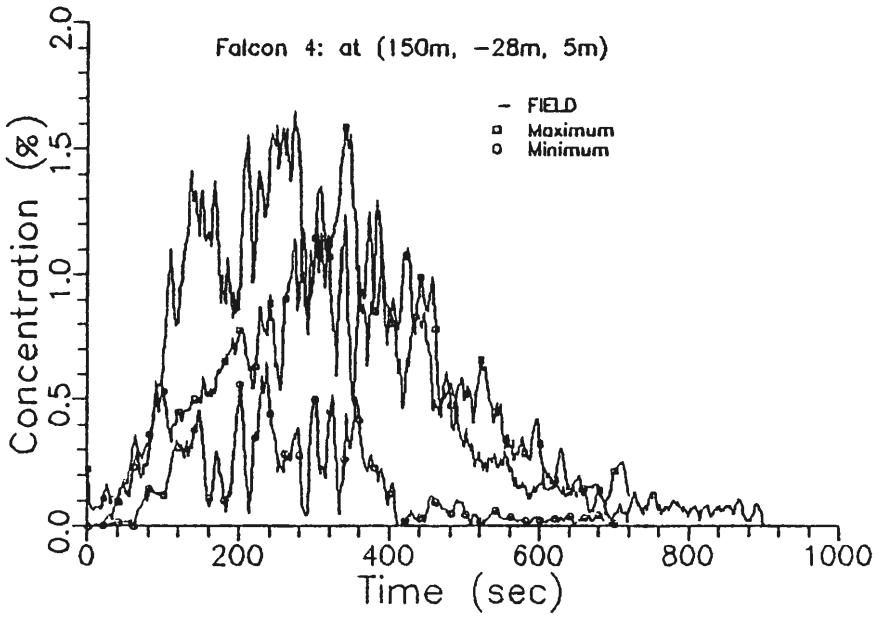

Figure 42 Concentration time history comparison of maximum and minimum for all model scales and all repetitions for Falcon 4 simulations

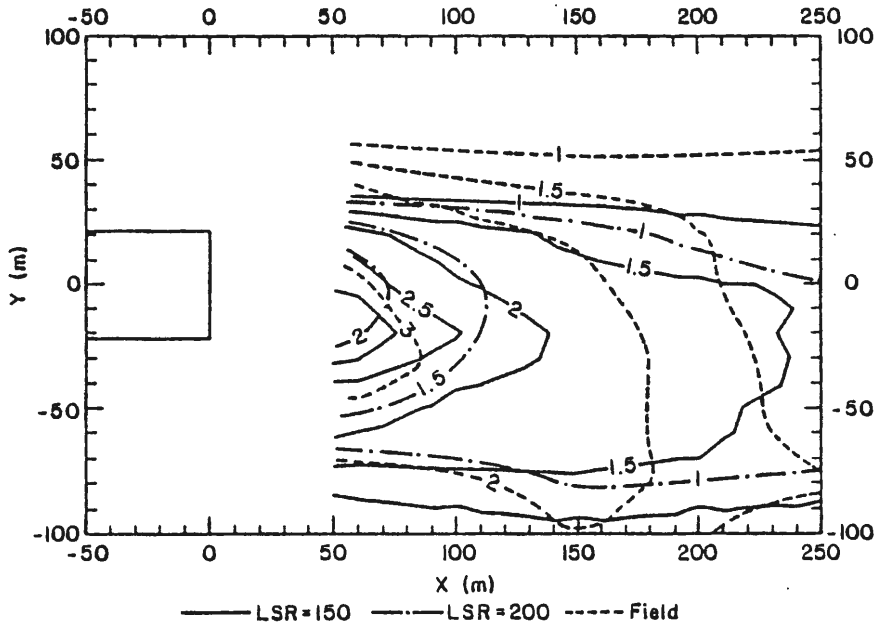

Figure 43 Concentration contour comparison between LSR=150 and LSR=200 at Z=5 m for Falcon 4 simulations with Freon-12 gas

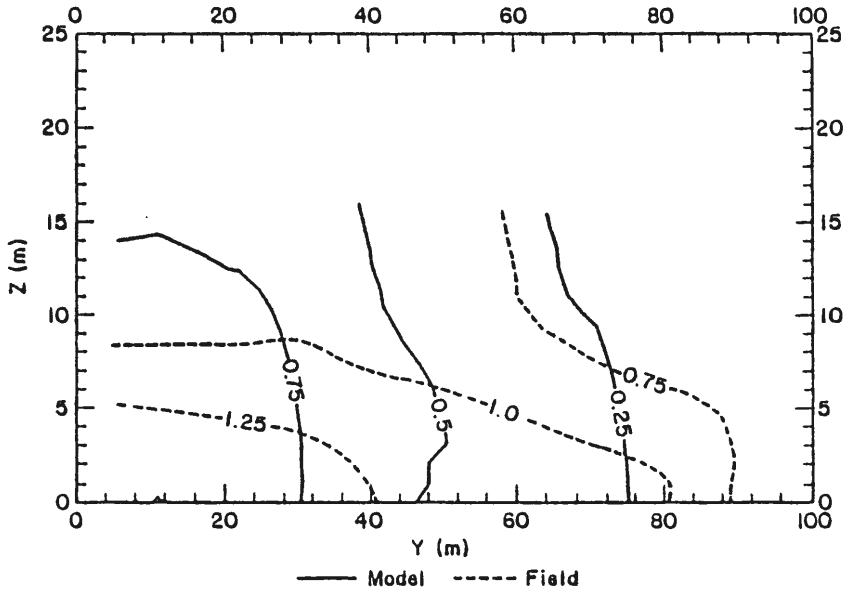

Figure 44 Verticel concentration contour comparison between the model data with LSR=100 and field data for Falcon 2 test at X=250m

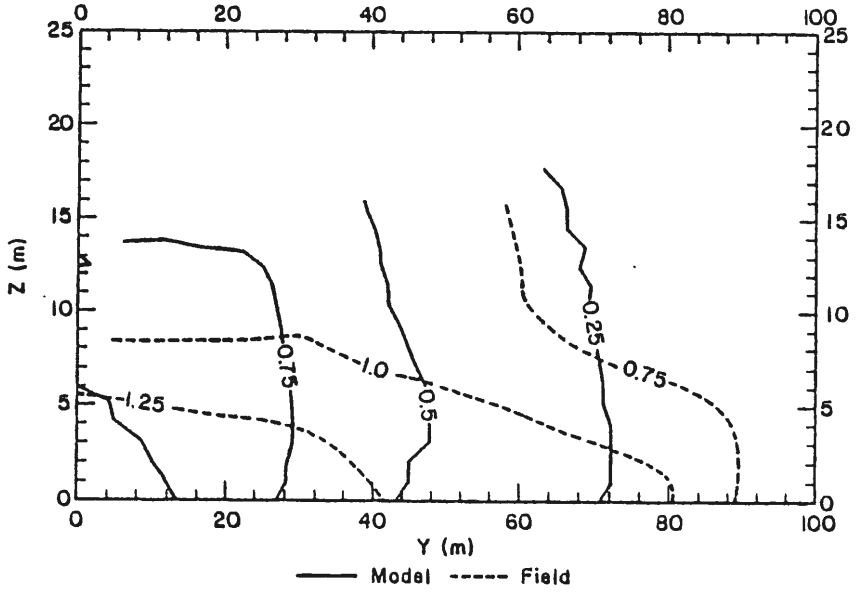

Figure 45 Vertical concentration contour comparison between the model data with LSR=150 and field data for Falcon 2 test at X=250 m

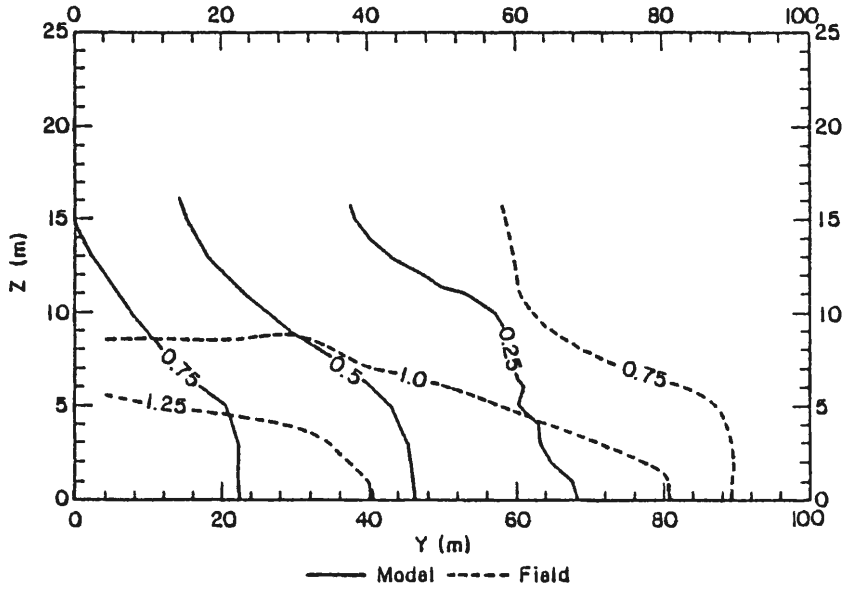

Figure 46 Vertical concentration contour comparison between the model data with LSR=200 and field data for Falocon 2 test at X=250 m

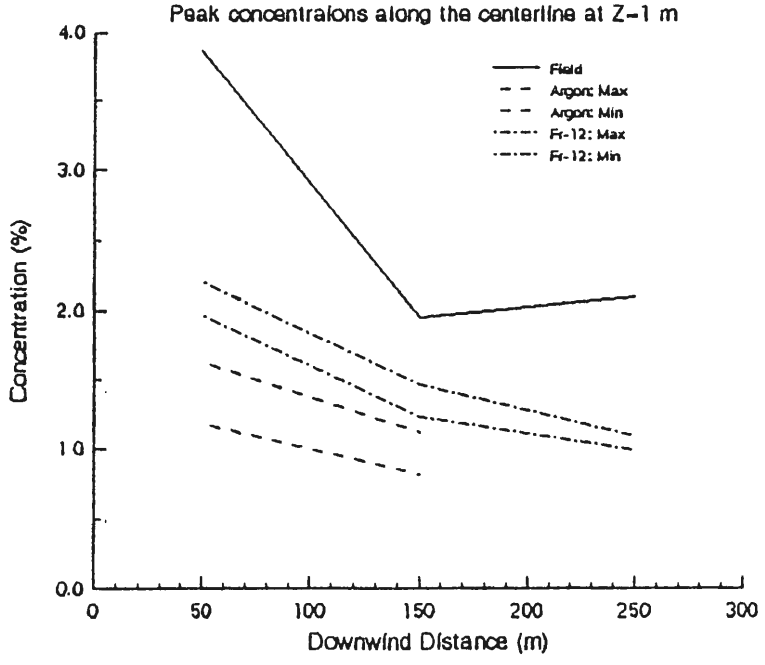

Figure 47 Peak concentration comparison along the centerline at Z=1 m between Argon gas and Freon-12 gas with LSR=150

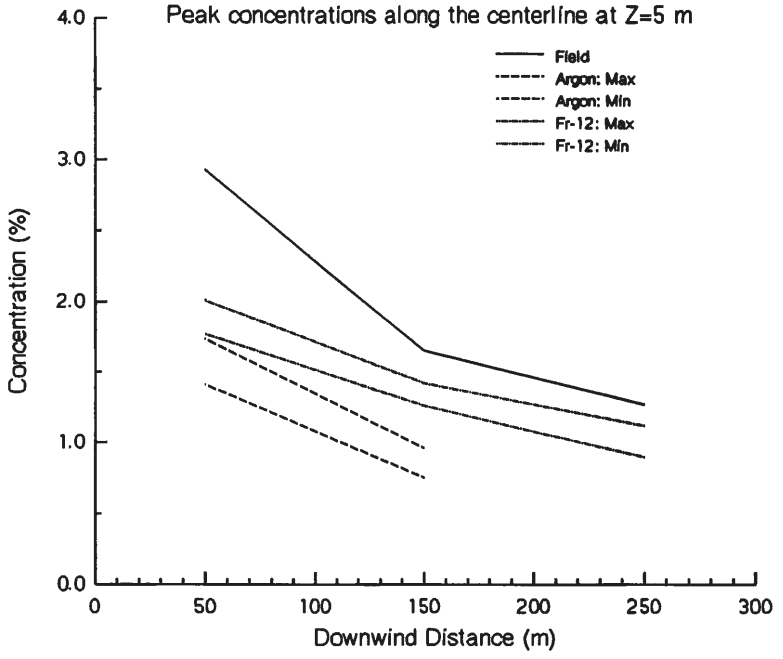

Figure 48 Peak concentration comparison along the centerline at Z=5 m between Argon gas and Freon-12 gas with LSR=150

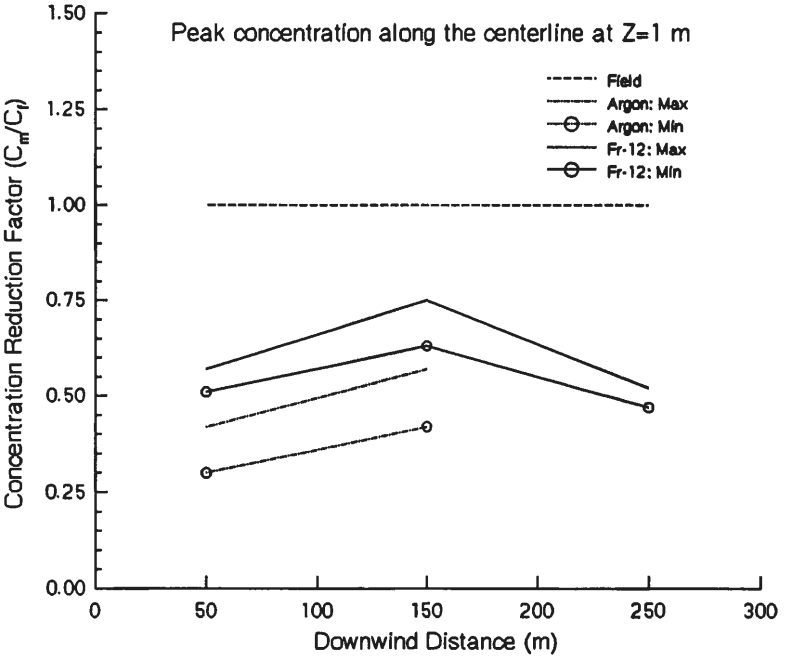

Figure 49 Peak concentration reduction factor comparison along the centerline at Z=1 m between Argon gas and Freon-12 gas with LSR=150

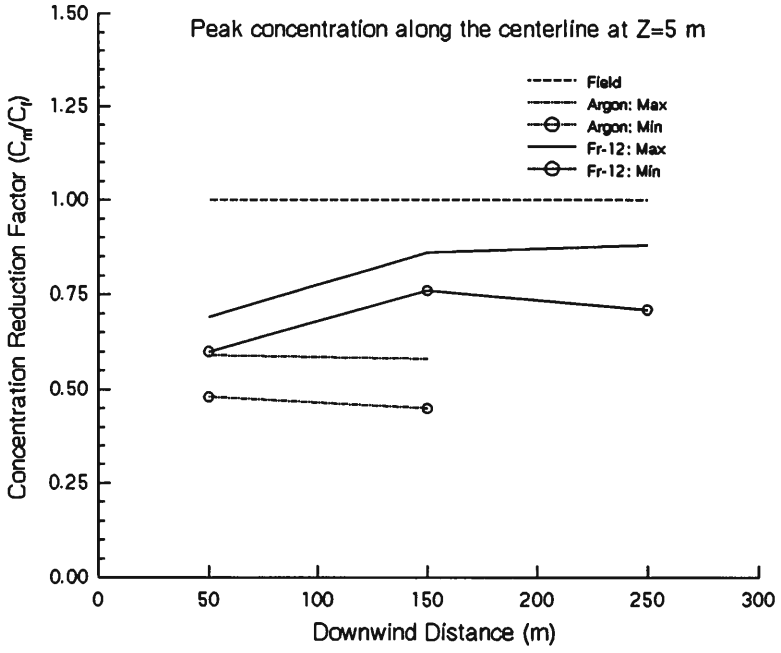

Figure 50 Peak concentration reduction factor comparison along the centerline at Z=5 m between Argon gas and Freon-12 gas with LSR=150

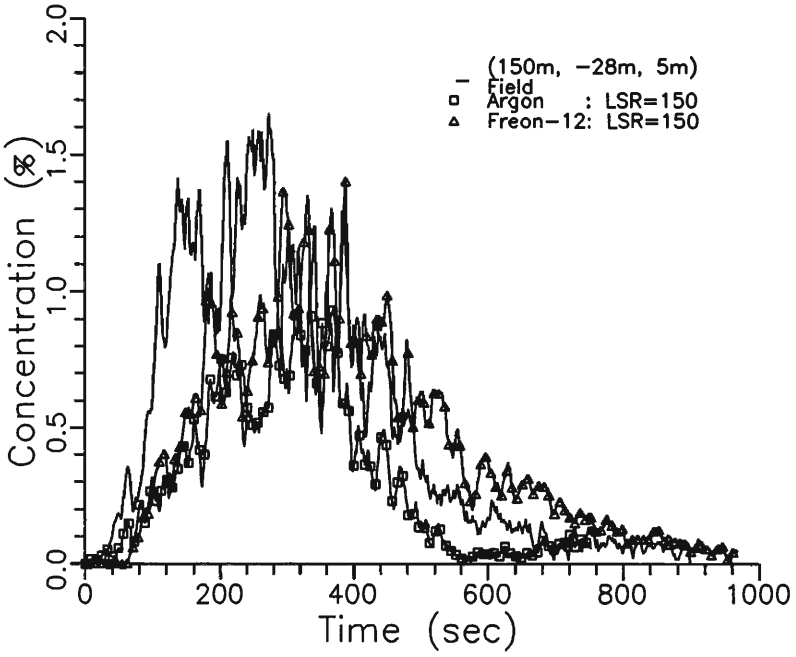

Figure 51 Concentration time history comparison for Argon gas and Freon-12 gas at (150 m, -28 m, 5 m) with LSR=150

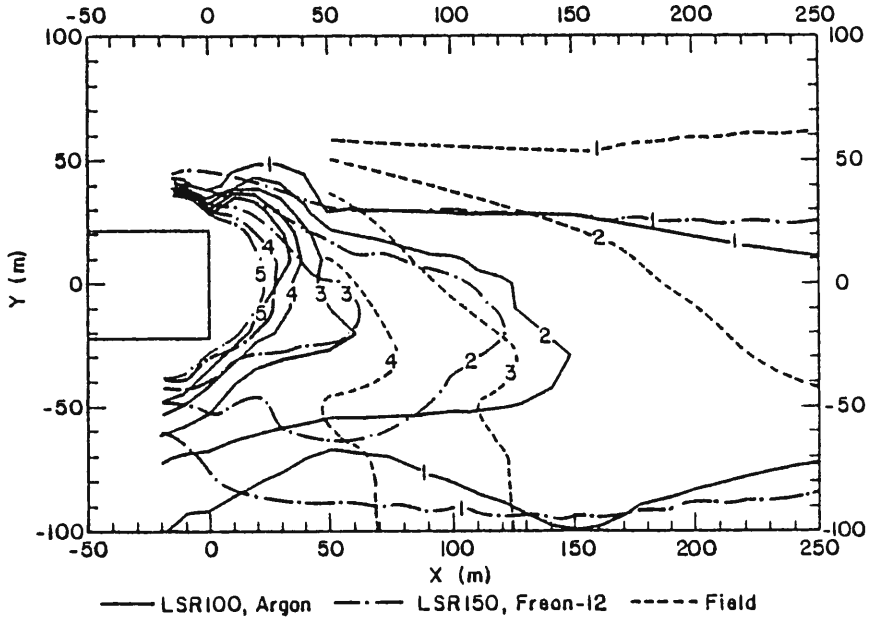

Figure 52 Concentration contour comparison between Argon gas data with LSR=100, Freon-12 gas data with LSR=150, and the field data at Z=1 m for Falcon 4 test

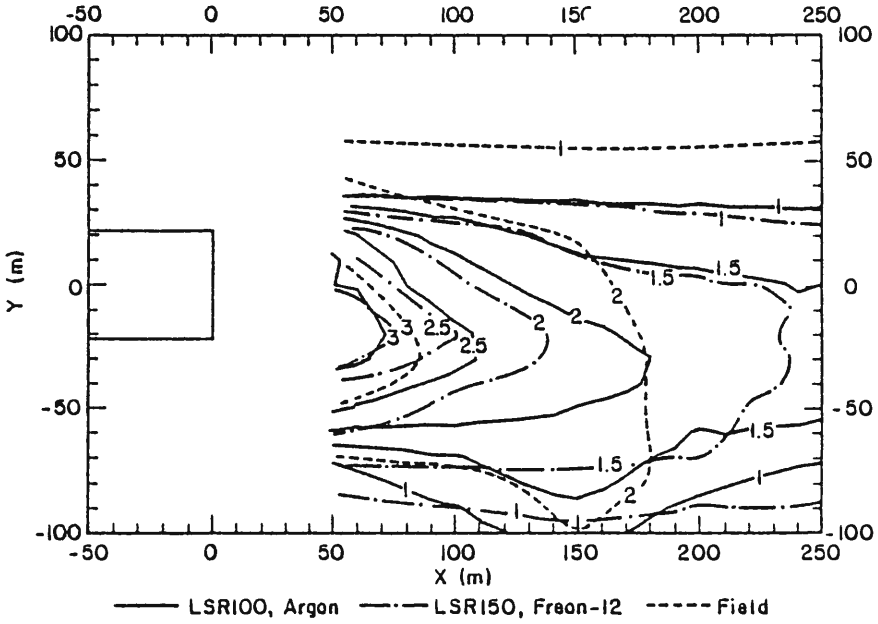

Figure 53 Concentration contour comparison between Argon gas data with LSR=100, Freon-12 gas data with LSR=150, and the field data at z=5 m for Falcon 4 test

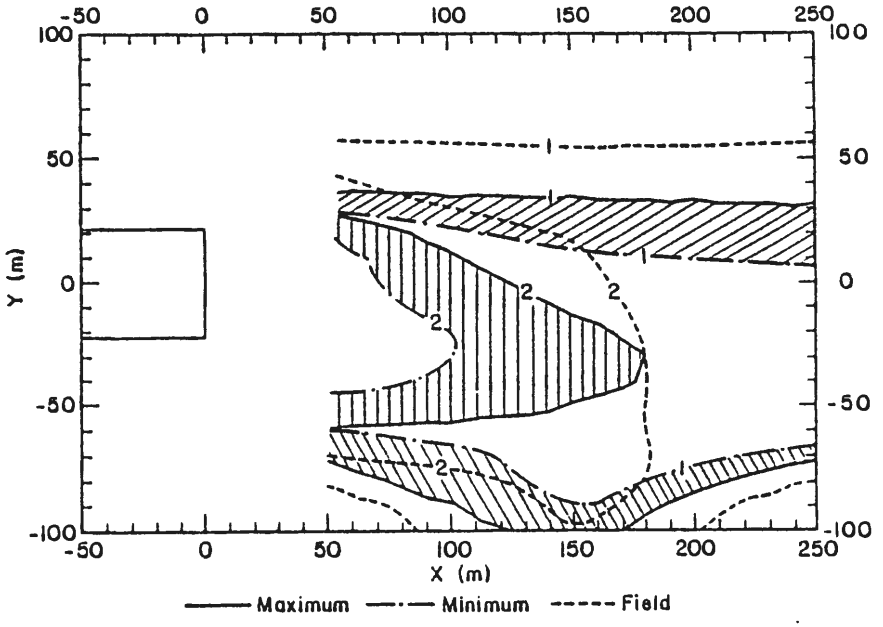

Figure 54 Concentration contour comparison between the max. and the min. peak concentrations from five repetitions with Freon-12 gas with LSR=150 at z=5 m

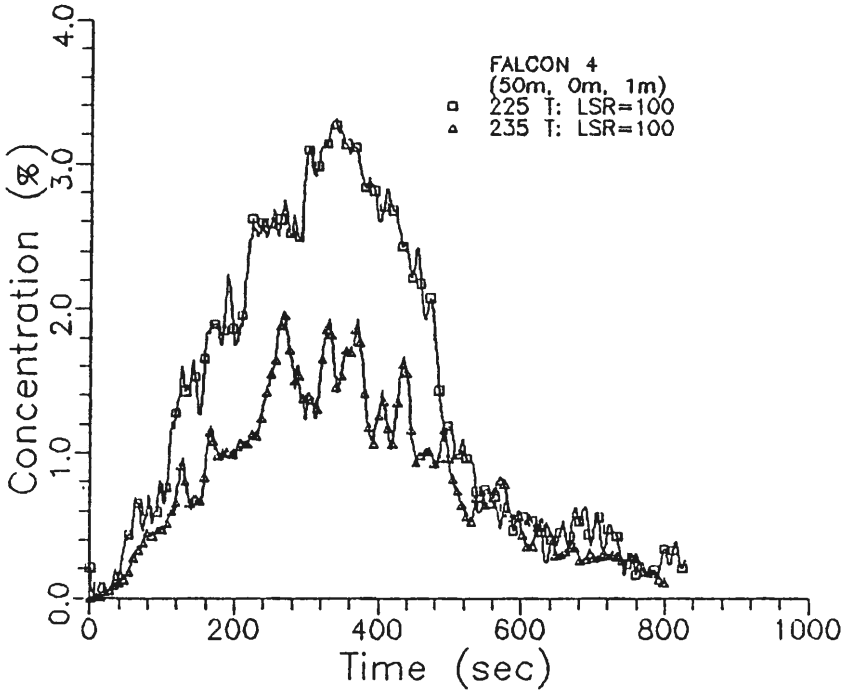

Figure 55 Concentration time history comparison between 225°T and 235°T array angles at (50 m, 0 m, 1 m) with LSR=100 for Falcon 4 test

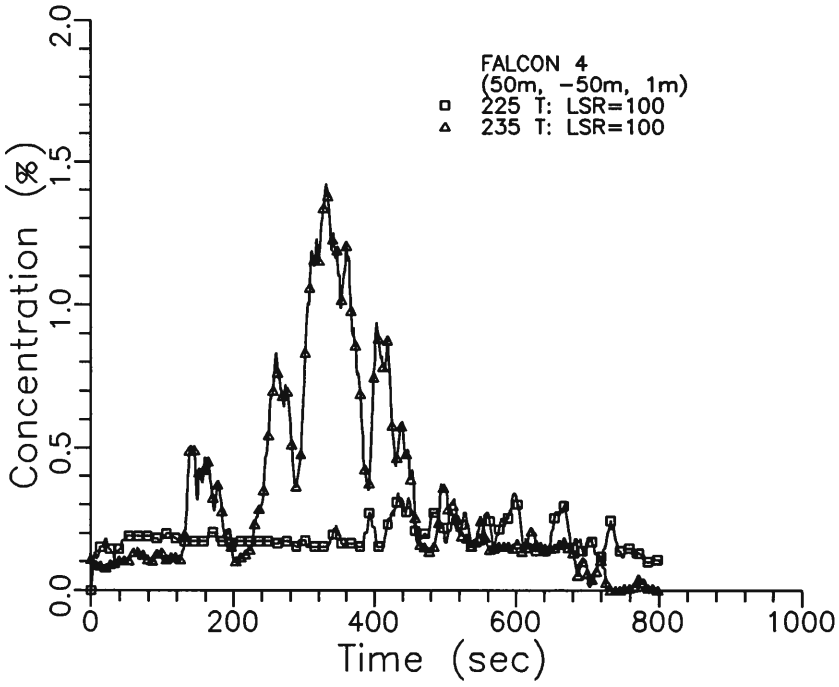

Figure 56 Concentration time history comparison between 225°T and 235°T array angles at (50 m, -50 m, 1 m) with LSR=100 for Falcon 4 test

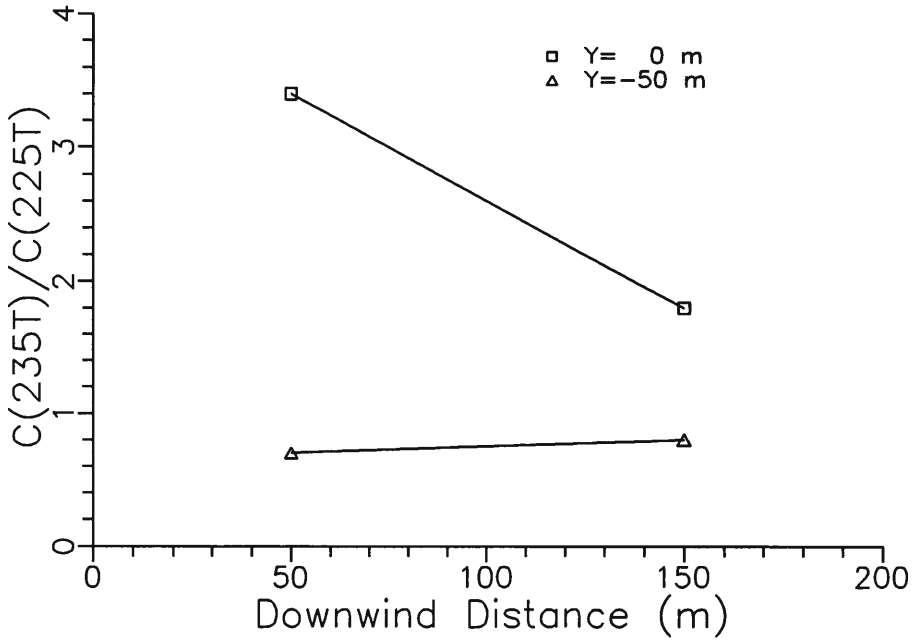

Figure 57 Peak concentration reduction factor comparison between 225°T and 235°T array angles

REFERENCES

American Gas Association, LNG Safety Program, Interim Report on Phase II Work, Report on American Gas Association Project IS-3-1, Battelle Columbus Laboratories, 1974.

Blackmore, D. R., Herman, M. N., and Woodward, J. L., "Heavy Gas Dispersion Model, J. of Hazardous Materials," Vol. 6, Nos. a and 2, pp. 107-128, 1982.

Bodurtha, F. T., Jr., The Behavior of Dense Stach Gases, J. of APCA, Vol. II, No. 9, pp. 431-437, 1961.

Boyle, G. J. and Kneebone, A., Laboratory Investigation into the Characteristics of LNG Spills on Water, Evaporation, Spreading and Vapor Dispersion, Shell Research Ltd., Report to API, March 1973.

Brown, T. C., Cederwall, R. T., Ermak, D. L., Koopman, R. P., McClure, J. W., and Morris, L. K., Falcon Series Data Report: 1987 LNG Vapor Barrier Verification Field Trials, May 1988.

Cermak, J. E., "Applications of Fluid Mechanics to Wind Engineering, A Freeman Scholar Lecture," J. of Fluid Engineering, Vol. 97, Ser. 1> No. 1, pp. 9-38, 1975.

Chatwin, P. C., The Statistical Description of the Dispersion of Heavy Gas Clouds, Report for Health and Safety Executive, Contract No. 1189/01.01, Department of Applied Mathematics and Theoretical Physics, University of Liverpool, U. K., 1981.

Chatwin, P. C., "The Use of Statistics in Describing and Predicting the Effects of Dispersing Gas Clouds," J. of Hazardous Materials, Vol. 2, Nos. 1 and 2, pp. 213-230, 1982.

Counihan, J., "Adiabatic Atmospheric Boundary Layers: A Review and Analysis of Data from the Period 1880-1972," Atmospheric Environment, Vol. 9, pp. 871-905, 1975.

Csanady, G. T., Turbulent Diffusion in the Environment, D. Reidel Publishing Company, 248 p., 1973

Davis, M. E. and Inman, P. N., Wind Tunnel Modeling of the Thorney Island Heavy Gas Dispersion Trials, Final Report for Gas Research Institute, Contract No. 5084-252-1016, 1986.

Eidsvik, K. J., "A Model for Heavy Gas Dispersion in the Atmosphere," Atmospheric Environment, Vol. 14, pp. 767-777, 1980.

Engineering Science Data Item, "Characteristic of Atmospheric Turbulence near the Ground," Engineering Science Data Item Number 74030 and 74031, October 1974.

Ermak, D. L., Chan, S. T., Morgan, D. L., and Morris, L. K., "A Comparison of Dense Gas Dispersion Model Simulations with Barrier Series LNG Spill Test Results," J. of Hazardous Materials, Vol. 2, Nos. 1 and 2, pp. 129-160, 1982.

Ermak, D. L. and Merry, M. H., A Methodology for Evaluating Heavy Gas Dispersion Models, UCRL-21015, Lawrence Livermore National Laboratory, CA, September 1988.

Fackwell, J. E. and Robins, A. G., Concentration Fields Associated with Emissions from Point Sources in Turbulent Boundary Layers: Part III., Concentration Fluctuations and Fluxes, Central Electricity Generating Board, Memorandum MM/MECH/TF 260, Marchwood Engineering Laboratories, Southhampton, U. K., 1980.

Fay, J. A., Gravitational Spread and Dilution of Heavy Vapor Clouds, Second International Symposium on Stratified Flows, the Norwegian Institute of Technology, Trondheim, Norway, 24-27 June 1980.

Halitsky, J., Validation of Scaling Procedures for Wind Tunnel Model Testing of Diffusion Near Buildings, Geophysical Sciences Laboratory, Report No. TR-69-8, New York University, New York., 1969.

Hall, D. J., Further Experiments on a Model of an Escape of Heavy Gas, Warren Springs Laboratory Report CR 1341 (AP), Department of Industry, United Kingdom, 1977.

Hanna, S. R., Strimaitis, D. G., and Chang, J. C., "Evaluation of 14 Hazardous Gas Models with Ammonia and Hydrogen Fluoride Field Data," Sigma Research Corporation, Westfors, MA, 1990.

Hinze, J. O., Turbulence, McGraw-Hill, 1975.

Hoot, T. G., Meroney, R. N., and Peterka, J. A., Wind Tunnel Tests of Negatively Buoyant Plumes, Fluid Dynamics and Diffusion Laboratory Report CER73-74TGH-RNM-JAP-13, Colorado State University, Fort Collins, Colorado, October 1974.

Isyumov, N., Jandali, T., and Davenport, A. G., "Model Studies and the Prediction of Full Scale Levels of Stack Gas Concentration," presented at 67th Annual Meeting of APCA, Denver, Colorado and published in APCA Journal, Vol. 26, No. 10, October 1976.

Kline, S. J., Similitude and Approximation Theory,McGraw-Hill, 1965.

Li, W. W. and Meroney, R. N., "Gas Dispersion Near a Cubical Model Building, Part II: Concentration Fluctuation Measurements," J. of Wind Engineering and Industrial Aerodynamics, Vol. 12, No. 1, pp. 35-47, 1983.

Mercer, A., Methods of Validating Models of Dense Gas Dispersion: A Review, Health and Safety Executive, Research and Laboratory Services Division, Safety Engineering Laboratory, Sheffield, England, 1986.

Meroney, R. N., Cermak, J. E., Garrison, J. A., Yang, B. T., and Nayak, S. K., Wind Tunnel Study of Stack Gas Dispersal at the Avon Lake Power Plant, Fluid Dynamics and Diffusion Laboratory Report CER73-74RNM-JEC-BTY-SKN35, Colorado State University, Fort Collins, Colorado, April 1974.

Meroney, R. N., Cermak, J. E., Neff, D. E., and Megahed, M., Dispersion of Vapor from LNG Spills - Simulation in a Meteorological Wind Tunnel, Colorado State University, CER76-77RNM-JEC-DEN-MM57, 1977.

Meroney, R. N., "Transient Characteristics of Dense Gas Dispersion; Part I: A Depth-Averaged Numerical Model," J. of Hazardous Materials, Vol. 9, pp. 139-157, 1984.

Meroney, R. N., Guideline for Fluid Modeling of Liquified Natural Gas Cloud Dispersion - Vol. II: Technical Support Document, Final Report for Gas Research Institute, Report GRI86/0102.2, 1986.

Meroney, R. N., Neff, D. E., Shin, S. H., Steidle, T. C., Tan, T. Z., and Wu, G., Analysis of Vapor Barrier Experiments to Evaluate their Effect as a Means to Mitigate the HF Cloud Concentration, for Exxon Research and Engineering, Florham Park, New Jersey, CSU Contract No. 29-7330, CER88-89RNM-DEN-SHS-TCS-TZT-GW-1, 1988.

Neff, D. E., Meroney, R. N., and Cermak, J. E., Wind Tunnel Study of Negatively Buoyant Plume Due to an LNG Spill, Report prepared for R & D Associates, California, Fluid Dynamics and Diffusion Laboratory Report CER76-77DEN-RNM-JEC22, Colorado State University, Fort Collins, Colorado, 1976.

Neff, D. E. and Meroney, R. N., The Behavior of LNG Vapor Clouds: Wind-Tunnel Simulations of 40 m^3 LNG Spill Tests at China Lake Naval Weapons Center, California, Colorado State University Report CER81-82DEN-RNM1 for Gas Research Institute, GRI Report No. 80/0094, 1981.

Neff, D. E. and Meroney, R. N., The Behavior of LNG Vapor Clouds: Wind-Tunnel Tests on the Modeling of Heavy Plume Dispersion, Fluid Dynamics and Diffusion Laboratory Report CER81-82DEN-RNM25, Colorado State University, Fort Collins, Colorado, March 1982.

Neff, D. E. and Meroney, R. N., LNG Vapor Barrier and Obstacle Evaluation: Wind-Tunnel Pre-Field Test Results, for Lawrence Livermore National Laboratory, Contract No. 8432705, FMWEP85-86RNM3, 1986.

Neff, D. E., Physical Modeling of Heavy Plume Dispersion, Ph.D. Dissertation, Colorado State University, Fort Collins, Colorado, 1989.

Netterville, D. D. J., Concentration Fluctuations in Plumes, Syncrude Environmental Research Monograph 1979-4, 1979.

Sandborn, V. A., Resistance Temperature Transducers, Metrology Press, 1972.

Schatzman, M., Konig, G., and Lohmeyer, A., Dispersion Modeling of Hazardous Materials in the Wind Tunnel, 15th Int. Meeting on Air Pollution Modeling and Its Applications, 15-18 April, St. Louis, MO., 1985.

Schlichting, H., Boundary Layer Theory, McGraw-Hill, New York, 1968.

Shin, S. H. and Meroney, R. N., "Surface Pattern Comparability of Wind-Tunnel Simulations of the Thorney Island Dense Gas Dispersion Trials," Air Pollution Modeling and Its Application VII, pp. 77-88, 1989.

Shin, S. H., Meroney, R. N., and Neff, D. E., LNG Vapor Barrier and Obstacle Evaluation: Wind-Tunnel Simulation of 1987 Falcon Series, Data Report, prepared for Gas Research Institute, Contract No. N00014-88-K-0029, CER89-90SHS-RNM-DEN-18, 1989.

Skinner, G. T. and Ludwig, G. R., Physical Modeling of Dispersion in the Atmospheric Boundary Layer, Calspan Advanced Technology Center, Calspan Report No. 201, May 1978.

Snyder, W. H., Guideline for Fluid Modeling of Atmospheric Diffusion, United States Environment Protection Agency Report EPA-600/8-81-009, 1981.

van Ulden, A. P., On the Spreading of a Heavy Gas Released Near the Ground, Loss Prevention and Safety Promotion Seminar, Delft, Netherlands, 1974.

Wilson, D. J. and Netterville, D. D. J., "A Fast-Response, Heated-Element Concentration Detector for Wind-Tunnel Applications," J. of Wind Engineering and Industrial Aerodynamics, Vol. 7, pp. 55-64, 1981.

APPENDIX A: SURFACE PATTERN COMPARABILITY APPROACH

For most model performance measurements, the predicted values are directly compared to observed values. The precise pairing in time and space introduces too strong a penalty on small misalignments in wind direction, while pairing in time alone provides no information on spatial variability. Lewellen and Sykes [1985] proposed a measure of the spatial comparison between observed and predicted patterns, which compares data over increments of decreasing spatial resolution. It estimates how much the predicted pattern must be shifted in space to cover all of the observed values.

This method considers the segment of area $A(x_o, \delta\theta)$ sketched in Figure 17 centered on the observation point and bounded by an angular displacement, $\delta\theta$, relative to the source point. The area is bounded by $\theta_i+\delta\theta$, $\theta_i-\delta\theta$, $r_i(1+\delta\theta)$, and $r_i(1-\delta\theta)$. Within this area the predicted concentration is bounded by lower and upper values defined as $C_p^{\,l}(A)$ and $C_p^{\,u}(A)$, respectively. Given observed concentrations $C_o(x_i)$ at a number of points i = 1, 2, 3,..., M, the effective predicted concentrations for the area A is defined in terms of the two limiting values, $C_p^{\,l}$ and $C_p^{\,u}$, and the observed concentration $C_o(x_i)$ as the following:

$$C_p(x_i, \delta\theta) = \begin{cases} C_p^{\,l}(A) & \text{if } C_o(x_i) < C_p^{\,l}(A) \\ C_o(x_i) & \text{if } C_p^{\,l}(A) < C_o(x_i) < C_p^{\,u}(A) \\ C_c^{\,u}(A) & \text{if } C_o(x_i) > C_c^{\,u}(A) \end{cases} \qquad (1)$$

The ratio used for comparison is defined as

$$N_i = C_p(x_i,\delta\theta)/C_o(x_i) \quad \text{if } C_p(x_i,\delta\theta) \geq C_o(x_i) \text{ or}$$

$$C_o(x_i)/C_p(x_i,\delta\theta) \quad \text{if } C_p(x_i,\delta\theta) < C_o(x_i)$$

Thus, the comparison is not between the observed and predicted concentration at a point, but rather between the observed concentration at a point and the calculated concentration for the area A.

One can now calculate the fraction of the test points, $f_N(\delta\theta,N)$, which yields predicted concentrations within a specified ratio N of the observed values within the areas defined by δA.

$$f_N(\delta\theta,N) = \frac{1}{M} \sum_{i=1}^{M} H\{ N - N_i \} \qquad (2)$$

where $H\{f\} = 1 \quad \text{if } f \geq 0$

$$0 \quad \text{if } f < 0.$$

A plot of $f_N(\delta\theta,N)$ gives a direct measure of how well the laboratory-predicted spatial distribution compares with the observations. Thus, one can plot the sequence of curves $f_N(\delta\theta,N)$ as a function of $\delta\theta$ for a various values of N.

It is noted that the sum in the Equation (2) should include all points where either the calculated or the observed concentrations are greater than background; however, it can only be applied at points where observed values are available.

When this technique is used to evaluate model performance with a given data base, one often tends to focus on the range of agreement for an acceptable percentage of the test points. For example, using $f_N(M)$, one might evaluate the model by determining the factor N that includes one standard deviation of the test points (i.e. $f_N = 0.68$). In this case, N

becomes the measure of model performance and is such that a lower value of N implies better model performance. Thus, the performance of different models can be compared in a quantitative manner in this way.

If the data base is sufficiently large, this technique can also be viewed as providing an estimate of the confidence level with which the model can be expected to perform. Thus, the value f_N, derived from one or more data bases, can be taken as an estimate of the probability (applicable to the set of all cases) that the predicted value will be within the specified range of the observed value. Using $f_N(M)$ as an example, one might estimate the probability $f_2(\infty)$ that the predicted value will agree with the observed value to within a factor N = 2 by using f_2. Thus, $f_2(\infty) \approx f_2$ or in general

$$f_N(\infty) \approx f_N.$$

The value of $f_N(\infty)$ is a measure of the confidence with which the model can be expected to agree with observation within the factor of N. A larger number of $f_N(\infty)$ implies greater confidence.